DEVELOPMENT AND INVESTIGATION OF AN AMMONIA SYNTHESIS REACTOR

By
Ghassan Chehade

A Thesis Submitted in Partial Fulfillment
of the Requirements for the degree of Master of Applied Science
in
Mechanical Engineering

University of Ontario Institute of Technology
Faculty of Engineering and Applied Science

Oshawa, Ontario, Canada
August, 2018

ABSTRACT

Ammonia production has gained increasing attention in the last decade due to its importance as a feedstock and an energy carrier. In the present thesis study, two novel ammonia production systems are presented. The first experimental system is a lab scale electromagnetic induced ammonia synthesis reactor. The reactor is designed, built and tested under various conditions. The Faraday efficiency of the reactor is 5.4 % and the ammonia production capacity is 1.2×10^{-10} mol/cm^2.s. Furthermore, the experiments on ammonia synthesis are performed with EMF and without EMF on the reactor and the change in potential is recorded to be 1.7 V and 1.1 V respectively. The second theoretical system is a new integrated energy system for power, steam and ammonia production developed, simulated through Aspen Plus and assessed thermodynamically through energy and exergy approaches. The present system employs a novel ammonia production loop to potentially replace the conventional Haber-Bosch process by integrating an expander/turbine in the ammonia loop. The ammonia production system produces 2310 kmol/h of liquid ammonia and steam as a by-product. Although having optimum conversion rate is attained by controlling/shifting the volume of synthesized ammonia, interestingly the exergetic assessment shows that the best output ammonia product is attained by the performance of each independent cycle. Hence, the overall exergy efficiency of the integrated system is 83 % and turbine exergy efficiency of 91 % for optimal operating conditions with a total power of 6000 kW and ammonia conversion rate of 38 % respectively.

Keywords: Ammonia, efficiency, electrochemical, electromagnetic, energy, exergy, power.

ACKNOWLEDGEMENTS

The satisfaction that accompanies the successful completion of this thesis study would be incomplete without the honorable mention of sincere gratitude, and greatest respect to my supervisor professor Dr. Ibrahim Dincer, who has provided me with heart full encouragement support, guidance and academic expertise throughout this thesis; without his motivation and sensible approach I would not be a committed researcher.

I whole heartedly thank Burak Yuzer and Murat Demir for their consistent support, and guidance throughout the thesis and research work done at Clean Energy Research Laboratory. Without their patience, support and ideas, it would have been impossible.

I am much thankful to Calin Zamfirescu and Osama Siddiqui for their help and guidance throughout this thesis.

My greatest thanks goes to my parents, Ahmed Chehade and Ranada Basma for supporting me emotionally and financially through some of the toughest times. I express my outmost appreciation to my sister Rania Chehade; I would not have been as successful as I am now without her encouragement. I warmly thank to my brothers, Khodr Chehade and Hassan Chehade for their nonstop support at all times.

TABLE OF CONTENTS

LIST OF FIGURES

LIST OF TABLES

NOMENCLATURE

A	Area (cm^2)
A_c	Catalyst activity
C	Concentration (M)
E	Potential (V)
EMF	Electromagnetic field (Mt)
En	Energy (kJ)
Ex	Exergy (kJ)
ex	Specific exergy (kJ/kg)
$\dot{E}n$	Energy rate (kW)
$\dot{E}x$	Exergy rate (kW)
F	Faraday constant (96500 C/mol)
G	Gibbs free energy (J)
h	Specific enthalpy (kJ/kg)
J	Current density (mA/cm^2)
K	Kinetic constant
K_{HT}	High temperature kinetic constant
K_{LT}	Low temperature kinetic constant
K_{LT}	Standard LT catalyst activity
LHV	Lower heating value (J or kJ)
m	Mass (kg)
$\dot{m}$	Mass flow rate (kg/s)
$\dot{n}$	Molar flow rate (mol/s)
t	Time (min or S)
T	Temperature (^oC)
V	Voltage (mV or V)
$\dot{V}$	Volume flow rate (m^3/s)
P	Pressure (Pa or kPa)
R	Universal gas constant (8.314 kJ/kmol K)
s	Specific entropy (kJ/kgK)

$\dot{S}$	Entropy rate (kW/K)

Greek letters

Δ	Change
η	Efficiency
ρ	Density (kg/m^3)
α	Transfer coefficient
δ	Nernst diffusion layer thickness
Δ	Change
η	Efficiency
π	Pi number
ξ	Reaction rate

Subscripts

a	Anode
c	Cathode
conc	Concentration
EMF	Electromagnetic field
en	Energy
ex	Exergy
ohm	Ohmic
ZVS	Zero voltage switching

Acronyms

$(CH_3)_2CHOH$	Isopropyl alcohol
Al_2O_3	Alumina
Ar	Argon
$C_{15}H_{15}N_3O_2$	Methyl red
$C_{16}H_{18}CIN_3S.xH_2O$	Methylene blue
C_2H_6	Ethane
C_3H_8	Propane
CH_4	Methane
CO	Carbon monoxide
CO_2	Carbon dioxide

CO_3MO_3N	Bimetallic molybdenum nitride
$CoFe_2O_4$	Cobalt iron oxide
CsCl	Caesium chloride
Fe_3MO_3N	Iron molybdenum nitride
Fe_3O_4	Iron (III) oxide
Fe_3O_4	Iron (III) oxide
H_2	Hydrogen
H_2O	Water
H_3BO_3	Boric acid
KCl	Potassium chloride
$La_{0.6}Sr_{0.4}FeO_3$	Peroveskite oxide
Li_3N	Lithium nitride
$LiAlO_2$	Lithium aluminate
LiCl	Lithium chloride
N_2	Nitrogen
NH_3	Ammonia
NH_3	Ammonia
NH_4HCO_3	Ammonium hydrogen carbonate
O_2	Oxygen
OCV	Open circuit voltage

CHAPTER 1 : INTRODUCTION

This chapter provides introduction on ammonia (NH_3), a renewable energy transportation media and chemical fertilizer accountable for nourishing of living systems and population on earth. Ammonia and hydrogen (H_2) as sustainable forms of energy are examined. In addition, the objectives of this thesis study are provided.

1.1 Prominence of renewable energy transportation media

Energy measured in joules (J) is a key element in world economic development and serves as the intrinsic currency of the earth. On the other hand, increasing energy demands across the globe have unwillingly changed the world's climate through accumulating the waste products of its civilization [1]. The burning of non-renewable energy sources such as coal and oil is releasing carbon dioxide (CO_2) into the atmosphere causing extraordinarily extreme weather patterns and warming of the globe. Figure 1.1 shows the global energy consumption from 2016. Petroleum, natural gas, and coal constitute most of the energy consumption (75 %). Furthermore, hydro and nuclear power put together form 15 % of utilized energy resources while renewable energy makes up 5 % of the total global energy. The increase in energy demands is due to the massive urbanization and industrialization [2] powered by fossil fuel. In order to move towards a sustainable and environmentally benign world, it is essential to replace carbon-based fuels with sustainable green energy. However, renewable energy sources are discontinuous and are difficult to store because of their inconsistent characteristics. For instance, electricity is exploited to store energy, but also chemicals such as hydrogen and ammonia are considered energy carriers and are produced from renewable sources, such as solar, geothermal, wind, ocean, biomass and hydro, which are granted as primary solutions to battle environmental pollution and global warming [3–8]. On that premise, energy storing methods have to be more efficient and more affordable than they currently are but also have to be safe. If the existing methods are improved, then, the usage of renewables can grow worldwide. Hence, there will be wider participation in the transition to a green energy economy.

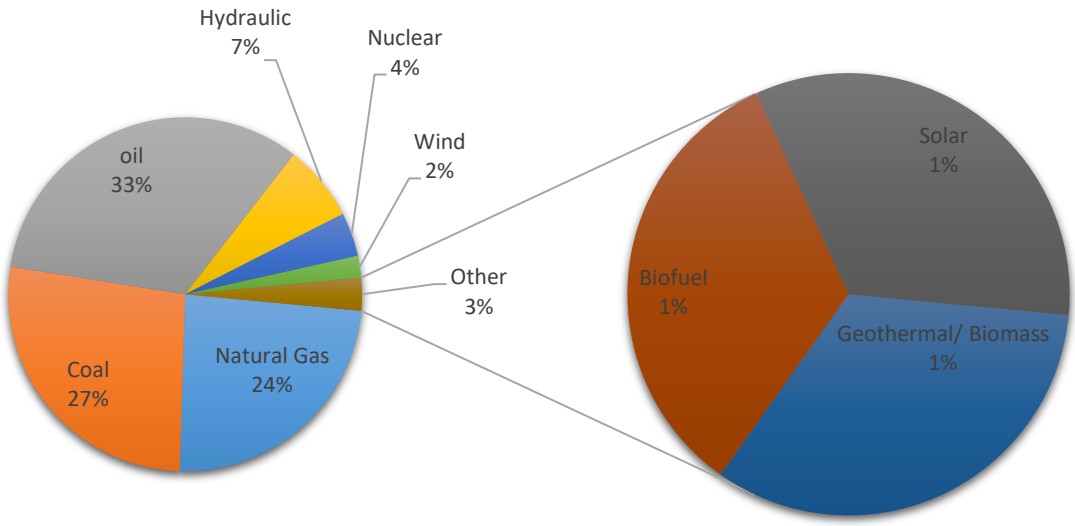

Figure 1.1 World energy production for 2016 [data from 10]

1.2 Hydrogen fuel

Hydrogen, the simplest element in the periodic table, consists of a large proton and a single electron charge on its valence shell; it is considered an energy efficient low polluting fuel [9]. In view of this, hydrogen does not occur naturally; it is found in water (H_2O) and in many organic compounds, notably the hydrocarbons that make up fuels such as gasoline natural gas methanol and propane. Thus, hydrogen can only be extracted chemically. The most recognized processes of extracting hydrogen are through steam reforming (96 %) and electrolysis (4 %). Other methods, such as renewable and nuclear energy, photo-assisted electrolysis, biochemical, photonic, electro-thermal, photo-thermal and thermochemical water splitting are primarily carbon-free, thus are considered promising candidates for a diversified energy supply [10–16]. In steam reforming, hydrocarbon fuels (natural gas, renewable liquid fuels, gasified coal, and biomass) react with steam in the presence of high temperature to produce hydrogen. While in electrolysis, water is split to hydrogen and oxygen using an electric current. For all of the above, hydrogen is considered an energy carrier, not an energy source. It is an efficient way to store and transport energy. Thus, hydrogen has a unique role in the global energy system and its future role for an environmentally sustainable friendly world.

1.3 Ammonia as a hydrogen carrier

The low volumetric energy density of hydrogen limits its applications both as an energy carrier and feedstock. Even the applications as compressed gas or cryogenic liquefaction forms are not enough to overcome these issues. These restrictions over practical applications of hydrogen are mostly felt in the onboard storage applications; it is also challenging to deliver and distribute hydrogen [17]. Ammonia appears to be a promising candidate to overcome the aforementioned issues due to its features such as the high capacity of H2 (17/6 wt %), the ability to be liquefied under mild conditions, and less vapor pressure at room temperature (9.2 bar) which is quite similar to propane. Ammonia is considered both as a feedstock and an energy carrier. Due to its physical features, it can be a used as a medium to store hydrogen or can be directly burned in an internal combustion engine without any carbon emission [18]. Due to the above reasons, research and development processes are focussed towards ammonia production in recent years. Even though there are several pathways for ammonia synthesis, Haber-Bosch process and solid state ammonia synthesis process are the most commonly used methods. Currently, over 90 % of the global ammonia production is attained via the Haber-Bosch process which is combines hydrogen and nitrogen over an iron oxide catalyst at high temperature and pressures [19]. The ammonia production routes via Haber-Bosch processes is depicted in Figure 1.2 (a). The required amount of N2 is delivered via air separation process where the cryogenic separation of air to O_2 ,N_2 and Ar is considered the most cost-efficient and cost-effective method for bulk productions [19,20]. For the hydrogen production arm of the ammonia synthesis, hydrogen can be manufactured via hydrocarbon-based processes (catalytic decomposition of natural gas, partial oxidation of heavy oil, steam-methane reforming, steam-iron coal gasification and coal gasification), non-hydrocarbon-based processes (water splitting via electrochemical, photochemical, photoelectrochemical, thermochemical, biological, photobiological, electrobiological processes), or via integrated processes which combines several technologies as using wastes energy from the prior one to be used for the another one to enhance the overall system efficiency. Steam- methane reforming (SMR) is considered one of the most significant industrial methods for H_2 production today [21,22]. Therefore steam reforming is considered the most optimal way

of producing ammonia, with about 77 % of world ammonia capacity being based on natural gas [23].

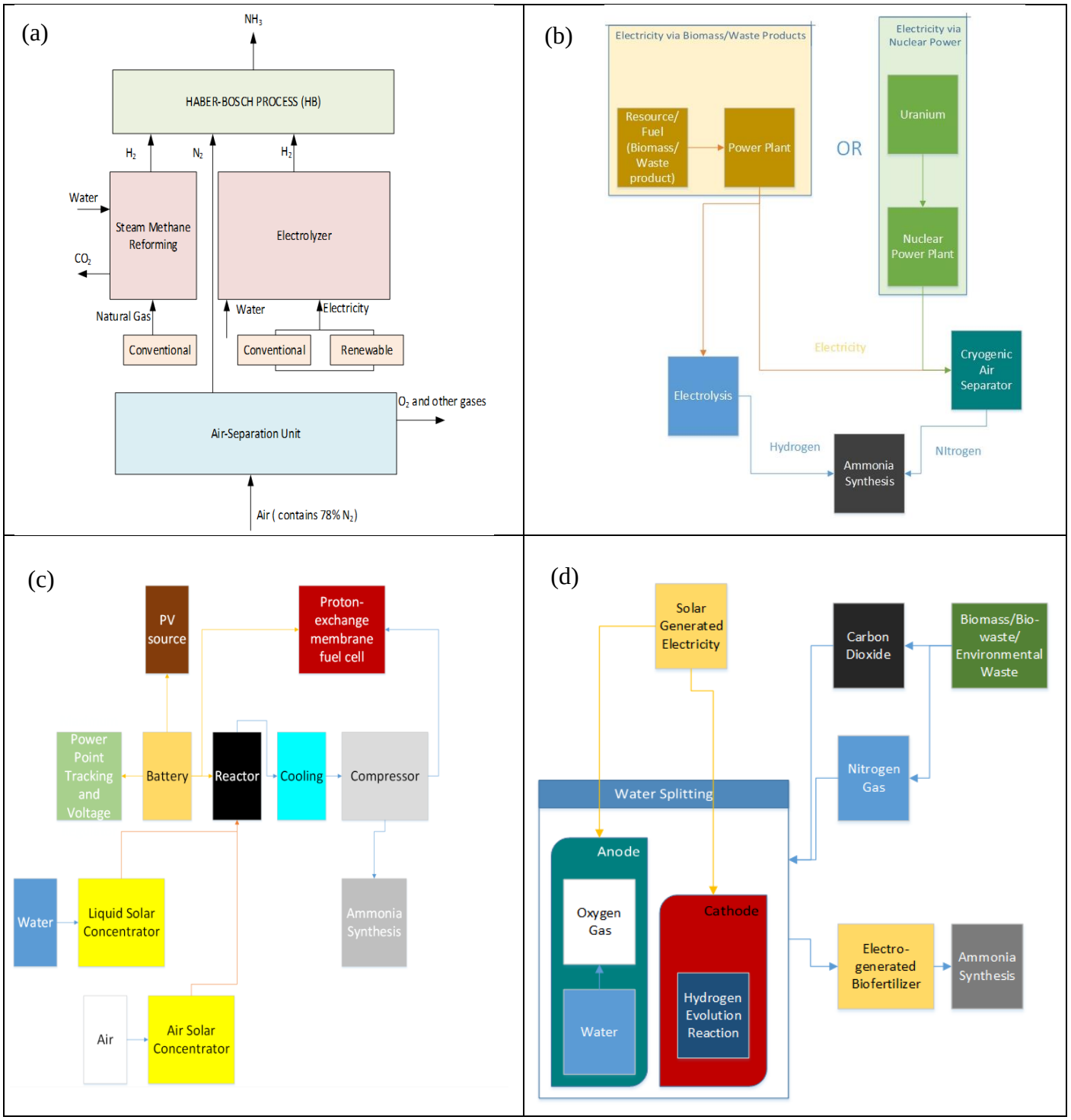

Figure 1.2 Different ammonia production methods. a) Haber-Bosch Process requires high temperature and pressure to synthesize ammonia. b) Ammonia production vial nuclear and biomass. c) Solar assisted fuel reactor used in electrochemical ammonia synthesis. d) Biochemical ammonia synthesis [24–31].

1.4 Electrochemical ammonia synthesis

Ammonia containing hydrogen (17.8 wt.%) with a high energy density (4.3 kW), is considered one of the most vitally produced chemical in the globe, with an annual production of 131 million tons [32]. Ammonia provides most of the fertilizers that we use, and the importance is not an exaggeration as illustrated in Figure 1.3 which shows that the development in the world population and the ability to produce ammonia are closely coordinated.

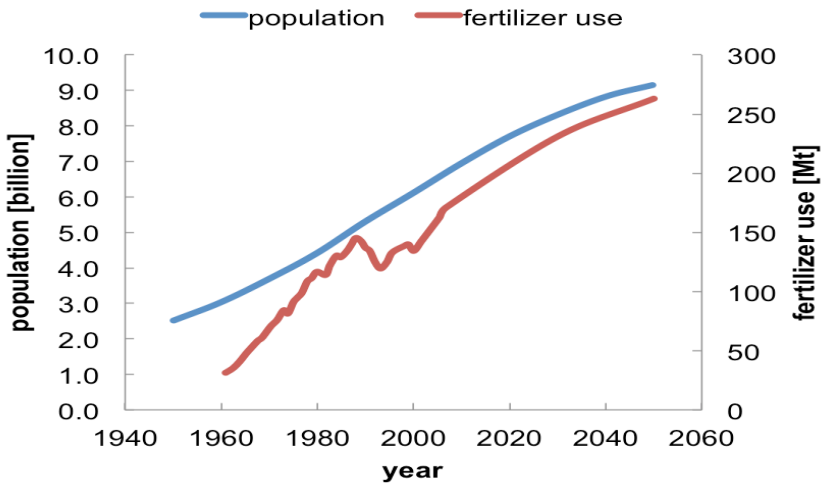

Figure 1.3 Fertilizers and human population projection [data from 45].

Thus, the need to feed the growing population while reducing carbon emissions necessitates finding a better method of producing ammonia. Electrochemical path of synthesizing ammonia shows a promising technology in the future. In an electrochemical reactor, chemical reactions are driven by the electric field which drives the overpotential of the electrodes. Conventionally, the electrodes are solid metals or semiconductors. An electrolyte (solid or liquid) is introduced to the reactor to complete the internal (ionic) and external (electronic) circuit. Thus, the "electro" part in electrochemical is the driver that supplies the minimum free energy (Gibbs energy) to drive the "chemical" reaction to occur [34]. Taking this into account, in an electrochemical reactor, ammonia is produced in the presence of hydrogen and nitrogen precursors with a metal catalyst at atmospheric pressure, when the applied potential is greater than the electrode potential measured at open circuit, and the reaction between hydrogen and nitrogen is spontaneous at a temperature below 175 ^{o}C [35]. However, when the reactions reach the equilibrium state, reversibility starts to occur and the reaction shifts towards the reactant; this is due to Le Chatelier's principle

[36]. Alternatively, when hydrogen is substituted with water, the reaction between hydrogen and nitrogen in not spontaneous and the required potential to drive the reaction is above 1.17 V as illustrated in Figure 1.4. The potential for electrochemical ammonia synthesis has attracted a lot of attention in the 21st century since the conditions for the synthesis require atmospheric temperature and pressure with no carbon emission. However, the Faraday efficiency is much lower than the efficiency of the Haber-Bosch process.

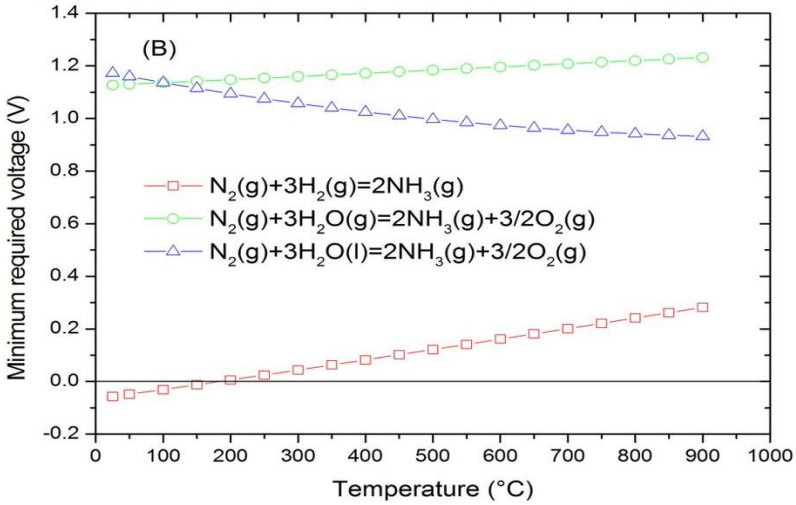

Figure 1.4 The minimum required voltage based on Gibbs free energy for electrochemical ammonia synthesis at atmospheric pressure [modified from 47].

1.5 Bioelectrochemical ammonia synthesis

For an animate system to morph into life, it requires appropriate nutrients to grow, flourish and procreate to ensure that continuity of the species. Nitrogen is one such nutrient, an element that is important component of photosynthesis, genetic material such as DNA, RNA, and protein. Nitrogen is available in the air (78 %), but in order to be beneficial for living organism, a nitrogen atom must be bonded to hydrogen atoms to form ammonia. In nature, this bonding form is noted as nitrogen fixation. However, the nitrogen atom in the air prefers to bond to each other to form dinitrogen, due to its lone pairs electron in its valance shell, the bond between nitrogen atoms is considered an extremely strong bond to break and thus renders the nitrogen in the air; useless to living things. Naturally, nitrogen fixation occurs by either lighting, combustion, and bacteria where the products are in the form of nitrogen radicals (NO_2^-, NO_3^-); this process only yields 10 % of the available

nitrogen. The natural process of ammonia production relies on prokaryotes that have the enzyme nitrogenase which converts elemental N_2 to ammonia. These prokaryotes range from aquatic bacteria to soil and plant associated bacteria. Some plants can use N_2 from the air to incorporate it into their systems by forming a symbiotic relationship with microorganisms, for example rhizobia [49–54].

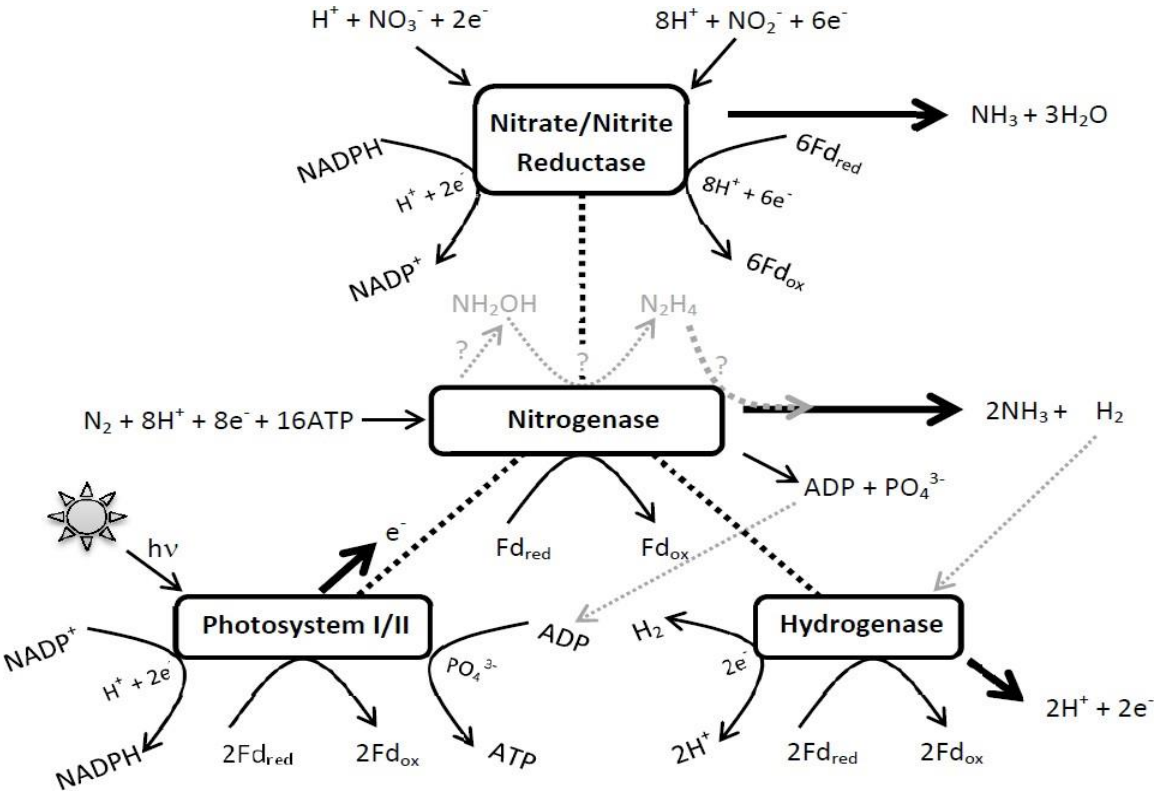

Figure 1.5 Representation of the reciprocal reaction centers in a nitrogenase enzyme to produce NH_3 from N_2 by nitrogen fixation [modified from 55].

Also, bacteria such as cyanobacteria (blue-green algae) produce enzymes; nitrogenases (EC1.18.6.1EC 1.19.6.1)[44–46] as show Figure 1.5, which are responsible for nitrogen fixation. As a result, ammonia is produced. Withal, these enzymes can be combined with a chemical process, react and evolve electron transfer in the presence of low potential as the driving force in a biochemical reactor. In an electrochemical reactor, electrodes (cathode, and anode) are impregnated with enzymes that inhabit the ability to reduce nitrogen. The immobilization of enzymes on the electrode surface increases the biocatalytic potential for nitrogen fixation and ammonia synthesis [59–61]. The biochemical, electrocatalysis of ammonia synthesis shows promising technology not only

for ammonia production but also for treating contaminated water and hazardous material waste that contains ammonia nitrates. However, the efficiency of the reactor is low, and need for improvement is required to make sustainable and scalable ammonia production system.

1.6 Ammonia synthesis via Haber-Bosch

The Haber-Bosch revolution in the past centuries is considered the catalyst for economic prosperity but, with every revolution comes long-term consequences. Such consequences are arguably the main reason for global warming. For every 100 million ton of ammonia produced, comes along 245 million tons of CO_2 emitted into the atmosphere [50]. The chemical reaction of nitrogen gas and hydrogen gas at elevated temperature and pressure in the presence of iron catalyst produces ammonia, without this reaction, farmers would be capable of producing food for only third of the earth population. In order to produce ammonia via the Haber-Bosh process, hydrogen and nitrogen gas need to be presented. Hydrogen in the form of methane is mixed with superheated steam and is feed to the primary reformer; the steam-gas mixture is then heated further between 500 and 600 ^oC since the process of reforming is highly endothermic, additional heat is required, so the temperature is raised to up to 830 ^oC. The iron-containing reforming catalyst has no effect on the position of chemical equilibrium rather it provides an alternative pathway with lower activation energy and hence increase the reaction rate. However, 30 to 40 % of the hydrocarbon react in the primary reformer. Thus the products are blended with air before flowing into the secondary reformer for an additional yield of hydrogen. In the high-temperature shift conversion process, undesired carbon monoxide is removed; the gas is passed to a bed of iron oxide and chromium oxide catalyst at a temperature of 400 ^oC and is converted to carbon dioxide (CO_2) which is then removed by absorption in aqueous ethanol or maintenance solutions. Withal, a small amount of carbon monoxide and carbon dioxide remaining in the process are converted to methane in the methanation process at around 300 ^oC. Finally, hydrogen is then catalytically reacted with nitrogen a drive from process aid to form nitrous liquid ammonia, this step is known as the ammonia synthesis loop; two important factors are layering in this process. First one is Chatelier principle for higher yield of ammonia and then the effect of pressure on the rate of reaction. At high pressure, the rate of reaction increase according to the collision theory; the high-pressure

cause more successful collisions, therefore the rate of reaction is increased consequently. Ammonia then is separated due to its low boiling point, and the unreacted gas is recycled thus making the Haber process as the most efficient but non-conventional way to produce ammonia due to its carbon footprint [51–59].

1.7 Motivation

One of the biggest challenges of the 21st century is energy demand and supply, and the problem is compounded by the fact that demand for energy grows globally by about 2 % each year forcing perplexities in the 4-prisms; economic, health, environmental sustainability, and leadership. In fact, 85 % of the global energy consumed comes from coal, oil and fossil fuel which are depleting at a fast rate. It is well known that burning of fossil fuel releases carbon dioxide thus, forcing a significant risk of manmade climate change. Consequently, alternative green energy such as hydrogen and ammonia show a promising energy carrier but they need to be assessed for global conditions and sustainability. The need to shift from a hydrogen economy to meet energy demand and environmental sustainability has received lots of attention. On the other side, ammonia with its low energy density and the ability to be liquefied under mild conditions, such as less vapor pressure at room temperature is considered the best candidate for hydrogen storage. Ammonia, the most consumed compound in fertilizers, is considered as both as a feedstock an energy carrier. Hence, this thesis is concerned with exploring the potential of ammonia synthesis and understanding the advantages and limitations of this technology.

1.8 Objectives

Numerous studies have been conducted on the electrochemical process for synthesizing ammonia. The conditions vary from high temperature and pressure depending on the electrolyte (solid or liquid) used. The chemical reaction between hydrogen and nitrogen is exothermic and reversible. Thus, the need to find a balance between temperature, pressure and maximum ammonia yield is important. Solid oxide fuel cells operate at high temperature and use rare metals as its electrolyte. However, ammonia tends to decompose at an elevated temperature around 500 ^{o}C yielding too low ammonia synthesis. Electrochemical reduction of nitrogen in alkaline medium at anode side exhibits low current density and ammonia production because of low proton conductivity. In this thesis, an electromagnetic field is induced in an electrochemical reactor for ammonia synthesis at

ambient pressure and low temperature to study the proton conductivity and its effect on current density and ammonia production. Also, another separate study on a new integrated energy system for power, steam and ammonia production based on steam methane reforming is developed in Aspen Plus. The system employs a novel ammonia production loop to potentially replace the conventional Haber-Bosch process by integrating an expander/turbine in the ammonia loop.

The specific objectives of this thesis study are listed below:

- To build a lab scale ammonia synthesis reactor that operates with gaseous nitrogen as cathode input and gaseous hydrogen as anode input in an alkaline electrolyte.
- To assess the performance of the lab scale ammonia synthesis reactor at ambient pressure and low temperature.
- To test and analyze the effect of the electromagnetic field by varying the temperature, applied current density, and volume flow rate on the performance of the lab scale ammonia synthesis reactor.
- To develop and investigate a new theoretical integrated energy system for power, steam and ammonia production unit in Aspen plus.
- To perform exergy and energy study, and assessment on the theoretical integrated energy system for power, steam, and ammonia production.

CHAPTER 2 : LITERATURE REVIEW

The natural fixation of nitrogen has opened multiple avenues for scientists to explore electrochemical synthesis of ammonia in mild conditions. In this chapter, the progress of electrochemical ammonia synthesis in aqueous and solid electrolytes is reported. The latest experimental techniques are compared and discussed as well as their practical applications.

2.1 Low-temperature electrochemical ammonia synthesis in aqueous electrolyte

Recent experimental studies for electrochemical ammonia synthesis in aqueous electrolyte used molten salt due to its high ionic conductivity. Bicer and Dincer [60] developed and assessed an electrochemical ammonia synthesis unit utilizing photoelectrochemically produced hydrogen. A molten salt electrolyte consisting of a eutectic mixture of NaOH/KOH was utilized as an electrolyte for the electrochemical reactor (Figure 2.1). In addition, Nano-sized Fe_3O_4 particles acted as catalysts in the reaction process. The hydrogen required was produced from a photoelectrochemical (PEC) reactor. The PEC reactor was developed by electrodeposition of copper oxide on the electrodes [61]. Copper oxide was utilized due to its photosensitive material properties. The developed system used nitrogen and hydrogen as reactants. A columbic efficiency of 14.2 % was found for the electrochemical ammonia synthesis.

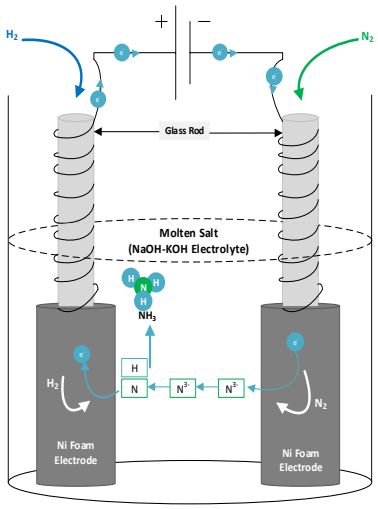

Figure 2.1 Electrochemical reactor utilizing molten salt as an electrolyte with porous nickel meshing at cathode and anode.

Several other studies have been conducted on ammonia synthesis technologies. Licht et al. [62] developed and investigated a molten salt ammonia synthesis reactor. The molten salt reactor utilized air and water as reactant inputs. Moreover, Li and Licht [63]

conducted a subsequent study in which they observed the formation of hydrogen due to the utilization of water in the reactor. They found that nearly 90 % of the current supplied was utilized to generate hydrogen. Furthermore, several methods have been proposed for ammonia synthesis reactors. Kim et al. [64] investigated ammonia synthesis via a molten electrolyte based reactor comprising of LiCl-KCl-CsCl electrolyte. Catalysts used included Fe_2O_3 and $CoFe_2O_4$ nano-particles. The ammonia production capacity was found to be 3×10^{-10} mol/s cm^2. The reactants utilized comprised of nitrogen and water. Serizawa et al. [64]investigated a LiCl-KCl-CsCl molten electrolyte based ammonia synthesis reactor. The higher level conversion ratio was observed to be nearly 70 % conversion of Li_3N to NH_3. The operating temperatures utilized included 360 ^oC to 390 ^oC. Another way of producing ammonia electrochemically is by reducing nitrate in aqueous solutions. Murakami al.[65] proposed an electrochemical ammonia reactor in a eutectic mixture of LiCl, KCL, and CsCl in porous nickel electrode. The source of nitrogen radical (N_3^-) was Li_3N (0.5 mol %) added to the molten salt. The nitrogen fixation occurs on the cathode while hydrogen at the anode the overall chemical reaction:

$$N_3^- + \frac{3}{2}2H_2 \rightarrow NH_3 + 3e^-$$

which yields 3.33×10^{-9} mol s^{-1} cm^{-2} at 0.7 applied potential with a Faraday efficiency of 72 %. Also different gases like hydrogen carrier such as methane [66], Hydrogen sulfide[67] and hydrogen chloride[68] were used as hydrogen source at the anode electrode. Also, Casallas et al. [69] suggested the use of steam instead of hydrogen at the anode electrode. The optimum system conditions were attained at an applied potential of 1.7 V and overall reaction:

$$N^{3-} + \frac{3}{2}2H_2O \rightarrow NH_3 + \frac{3}{2}O^{2-}$$

In the last few years, the composite electrolyte has been investigated in a eutectic mixture of alkali electrolyte in a means to enhance proton conductivity. Amar al.[70–72] used a mixture of $(Li/Na/K)_2CO_3$ mixed with LiAlO2 with mole rate 1:1. To increase the reaction rate, different catalysts were used, including Fe_3MO_3N, CO_3MO_3N, and $COFe_2O_4$. The maximum ammonia yielded 3.27×10^{-10} mol s^{-1} cm^{-2} with an applied potential of 0.8 V vs. counter electrode. Also, water vapor and nitrogen was investigated using an electrolytic reactor based on $CoFe_2O_4$–$Ce0_{.8}Gd_{0.18}Ca_{0.02}O_{2-\delta}$, CGDC-ternary carbonate composite, and

$Sm_{0.5}Sr_{0.5}CoO_{3-\delta}$–$Ce_{0.8}Gd_{0.18}Ca_{0.02}O_{2-\delta}$ as cathode, electrolyte and anode respectively under atmospheric pressure and the maximum rate of ammonia production was found to be 6.5 × 10^{-11} mol s^{-1} cm^{-2} at 400 °C and 1.6 V [73]. Ammonia from wet nitrogen in an electrolytic reactor using a $La_{0.6}Sr_{0.4}FeO_{3-\delta}$–$Ce_{0.8}Gd_{0.18}Ca_{0.02}O_{2-\delta}$ composite cathode and an oxide–carbonate composite electrolyte yielded an ammonia formation rate of 7 × 10^{-11} mol s^{-1} cm^{-2} at 400 °C when a voltage of 1.4 V was applied[74]. Low-temperature ammonia synthesis was firstly reported by Kordali el al. using alkaline solution combined with Nafion membrane where ammonia synthesis occurred at a temperature below 100 °C. Nitrogen was introduced at the cathode and hydrogen at the anode [75–77] or water[78,79] with an overall reaction:

$$N_2 + 3H_2O \rightarrow 2NH_3 + 3/2O_2$$

The Faraday efficiency of 90.4 % was achieved and 10^{-8} mol s^{-1} cm^{-2}. By far, Lan et al. produced ammonia directly from air and water electrochemically at ambient temperature and pressure with a Faraday efficiency of 55 % and reaction rate of 1.14× 10^{-11} mol s^{-1} cm^{-2} [75].

2.2 High-temperature solid state ammonia synthesis

A solid-state electrochemical reactor consists of a porous anode and cathode that are separated by an ion conductive solid electrolyte. The oxidation-reduction reaction takes place at the anode and cathode respectively. This is possible as electrons move by a supplied potential in the outer circuit of the reactor as shown in Figure 2.2.

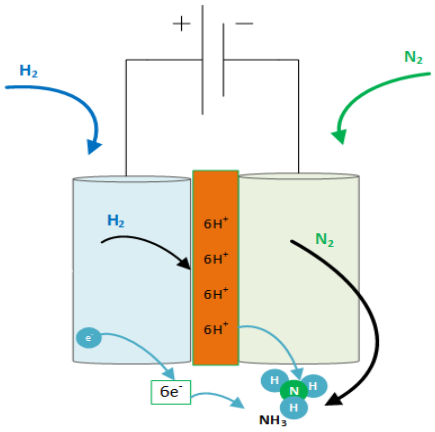

Figure 2.2 Schematic diagram of an SSAS reactor.

Skodra and Stoukides [80] investigated a solid-electrolyte based ammonia synthesis route. A proton-conducting electrolyte was utilized at operating temperatures of 450 °C to 700 °C and a ruthenium-based catalyst. Kordali et al.[81] conducted a study on

ammonia synthesis utilizing a ruthenium catalyst comprising cathode and a Nafion membrane electrolyte. The developed system was capable of producing ammonia from nitrogen and water at a production capacity of 2.8×10^{-12} mol/s cm^2 at ambient operating temperature. Further, the production capacity was observed to increase to 2.1×10^{-11} mol/s.cm^2 at a higher temperature of 90 ºC obtaining a columbic efficiency of 0.2 %. Lan et al. [82] developed and investigated a Nafion electrolyte based ammonia synthesis reactor utilizing platinum on carbon gas diffusion layers. An ammonia production rate of 1.1×10^{-9} mol/s.cm^2 was observed at ambient conditions. The columbic efficiency was found to be 0.6 %. Li et al [83] achieved a high reaction rate of 5.82×10^{-9} mol/s.cm^2 by using barium cerate as an electrolyte. Others[84–86] used lanthanum hallate and lanthanum zirconate electrolyte with a Faraday efficiency ranging between 70 and 80 %. It is noted, most of the studies [87–90] on SSAS reactor used perovskite an electrolyte where gaseous H_2 and N_2 were introduced at the anode and cathode respectively. In order to increase the protonic conductivity of the electrolyte for higher current density and ammonia reaction rate, steam as a hydrogen source was used at the anode tested along with various earth metals. When barium cerate-based electrolytes used over the anode, higher reaction rate and Faraday efficiency were achieved up to 50 % [89–91].

2.3 Integrated steam reforming ammonia production

Steam- methane reforming (SMR) is considered one of the most significant industrial methods for H_2 production today [21,22]. Therefore steam reforming is considered the most optimal way of producing ammonia, with about 77 % of world ammonia capacity being based on natural gas[23]. Wang et al. [92] investigated the integrated the endothermic methane reforming applications with selective removal of H_2 through H_2 permeation membrane which allows almost a complete conversion of CH_4 at the temperatures around 400 °C or below by shifting the equilibrium of reforming reaction. The researchers built a mathematical model of solar-driven CH_4 reforming reaction in a palladium membrane reactor. As a result of the study, an optimal conversion rate range of CH_4 for efficient solar methane membrane reforming is calculated, and the net solar-to-fuel efficiency is obtained at over 38 % at 400 ℃. Rosen [21] did a thermodynamic assessment based on energy and exergy analysis of an SMR process for hydrogen production from natural gas. A mathematical code is developed by the author to identify state properties and system

characteristics such as exergy losses and destruction through the proposed layout. The results revealed that the main exergy losses took place in the reformer, and are due to the irreversibilities associated with combustion process and the places where heat transfer occurred at greater temperatures. Hwangbo et al. [92] built a network for hydrogen production by combining conventional steam methane reforming and a cascade of waste biogas treatment processes. A cascade of four-associated technologies (COFAT) is developed and modeled as biomethane is converted into H_2 via the steam-biomethane reforming process. Unlike the conventional reforming systems, the (COFAT) system is not dependent on fossil fuels and integrated with conventional stem methane for a bulk amount of hydrogen yield. All the steam methane reforming applications mentioned above can be integrated with an air separation unit, and under convenient temperature and pressure, ammonia can be synthesized via the Haber-Bosch process. Orrego and Junior [93], modeled, analyzed and optimized an industrial scale ammonia synthesis via integrated SMR-Haber Bosch processes. Based on the study results, primary exergy destruction rates are coming from ammonia conversion and the cooling system which corresponds to 71-82 % of the overall exergy destruction in the ammonia loop.

2.4 Gaps in the literature

Synthetic ammonia production has become more of a commodity as the population of the planet increase. With the increasing population, there is a demand for an increase of production, where ammonia is a key compound in fertilizers for crops and farms. Synthetic ammonia production was developed by Fritz Haber and Carl Bosch, where the process of present-day ammonia plants base their engineering and chemistry upon. Most present-day ammonia plants follow a similar process that includes:

- Natural Gas desulfurization
- Catalytic steam reforming
- Carbon Monoxide shift
- Carbon dioxide removal
- Methanation
- Ammonia synthesis

Studies in the open literature show ammonia synthesis electrochemically from hydrogen and nitrogen as a precursor; others show ammonia synthesis from air and water in an aqueous or solid electrolyte. Most of the literature based their findings on studying the effect of electrode material and electrolyte on nitrogen reduction/fixation. However, there is no study showing the effect of the electromagnetic field on ammonia synthesis. Here, we present how ammonia can be synthesized/enhanced by introducing an electromagnetic field rather than the conventional electric field at low temperature and atmospheric pressure. Also, the flow of nitrogen and hydrogen was not fully explored in the literature, though, ammonia synthesis is highly reversible. When the amount of reactant and products reaches equilibrium the reaction shift toward the reactant, and thus ammonia decomposes. In this study, we show the effect of the volume flow of hydrogen and nitrogen on the rate of reaction at different temperatures. Ammonia synthesis via Haber-Bosch process is considered highly exothermic; although studies show the feasibility of waste heat recycling into the reformer, there is no study around integrating expander type turbine in the ammonia loop. In second part of this thesis, an investigation is made to assess the feasibility of integrating a two-stage expander in an integrated industrial ammonia synthesis plant for supplying all the power required to operate the compressors and pumps to run the system.

CHAPTER 3 : EXPERIMENTAL PROCEDURE AND MODELING

In this chapter, the experimental setup a procedure for the lab scale ammonia synthesis reactor are explained. Moreover, thermodynamic assessment is performed on the proposed system.

3.1 Reactor design and measurement devices

The electromagnetic induced ammonia reactor is made from a highly corrosive resistant material, chemically stable Alumina (Al_2O_3) and high temperature resistant up to 1750 K. The body and cap are made of ceramic materials and are dimensioned as seen in Figure 3.1. The Cap is threaded with holes of various sizes for the thermocouples, and tubes for input and output of gas. The ceramic composition is to maintain the integrity of the reactor at high temperatures during molten salt electrolysis process (approx. 250 ℃). To maintain pressure and temperature within the reactor, an O-ring is inserted in the slot of the cap. The T fittings are used for feeding hydrogen and nitrogen gas into the reactor. The single fitting is used to transport the ammonia and unreacted gas within the reactor. The alumina crucible is made of 99.7 % pure aluminum oxide.

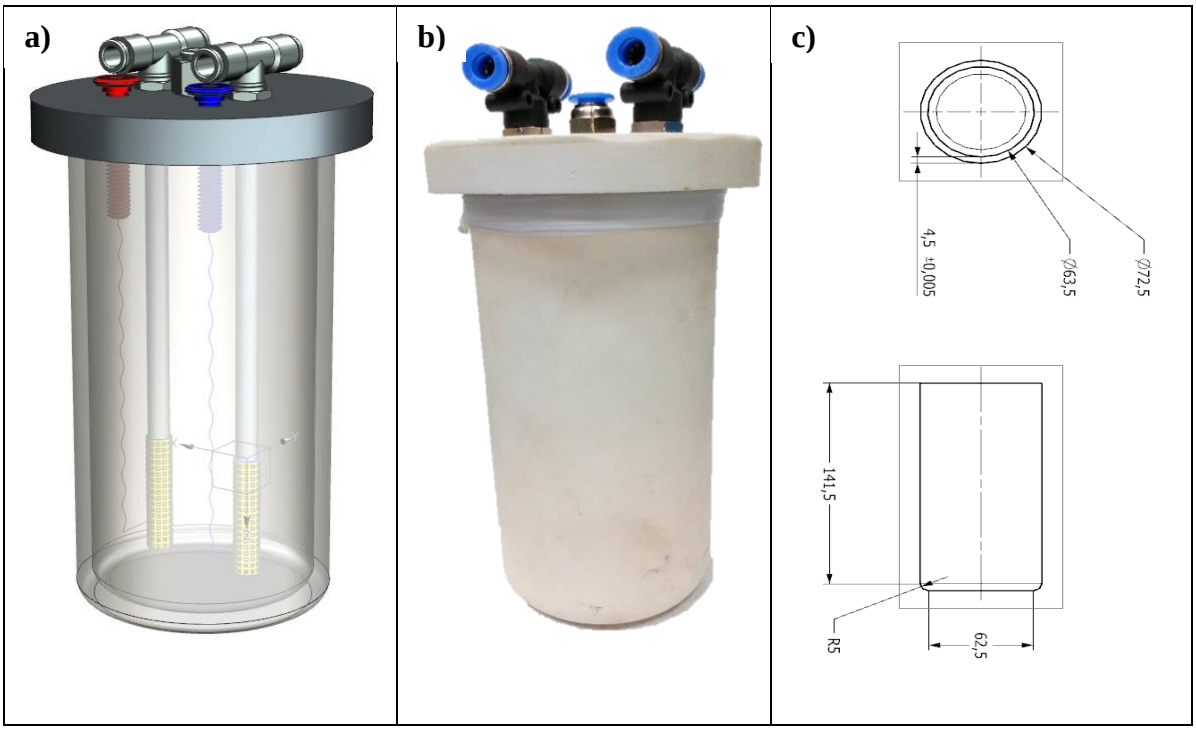

Figure 3.1 Ammonia reactor illustrations; (a) electrochemical reactor 3d design, (b) the actual reactor made from the Al_2O_3 ceramic body and PTFE cap (c) shows the dimension of the reactor in mm.

The low profile titanium screws as shown in Figure 3.2 (a, b) are used to supply the current to drive the anodic and cathodic reactions. At the cathode, the nickel wire is attached to a porous nickel foam. This allows for nitrogen to be reduced to nitride:

$$N_2 + 6e^- \rightarrow 2N^3$$

At the anode, the hydrogen combines with the nitrides and synthesize ammonia:

$$2N^3 + 3H_2 \rightarrow 2NH_3 + 6e^-$$

The reactor lid is fabricated out of Polytetrafluoroethylene (PTFE). The cap is designed with a press fit, so the reactor is sealed from air while this material is chemically stable at high temperature. It is important to note air humidifies the molten salt, thus the ionic conductıvıty of the electrolyte is affected by humidity.

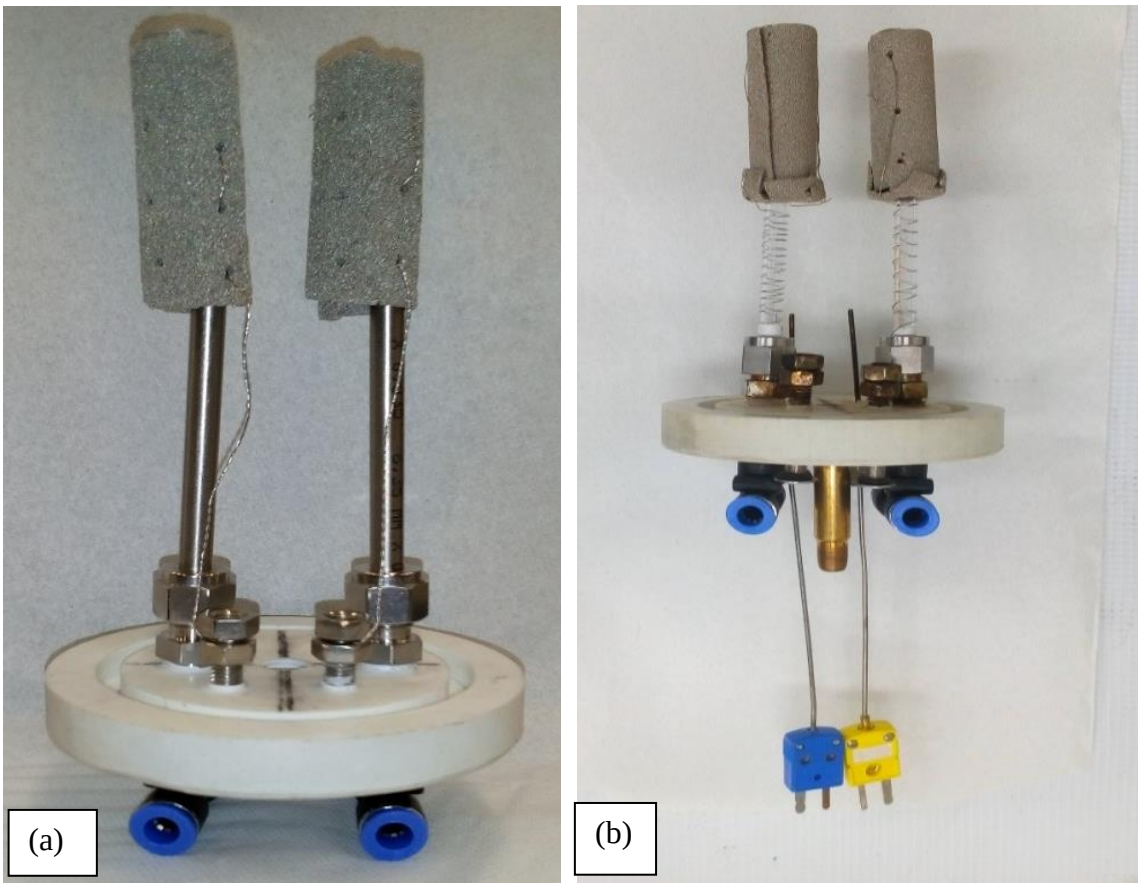

Figure 3.2 (a) Electrode assembly with stainless steel for gas transport. The nickel mesh has an overall area of 55 cm^2 (b) electrode assembly with quartz glass as gas transport and thermocouple assembly for temperature measurements.

The electromagnetic inductor integrates a frequency generator for inducing a current through electromagnetic induction. When AC current is applied to the copper coil

as shown in Figure 3.3 (b) and (a), a magnetic field is generated around the coil causing eddy current. At the same time, the current flowing in the coil is lost due to hysteresis loss. When the alternating current energizes the coil, it creates a time-varying magnetic field. The magnetic lines of flux tend to be concentrated at the center of the coil. Eddy current inspection is based on Faraday's electromagnetic induction [94].

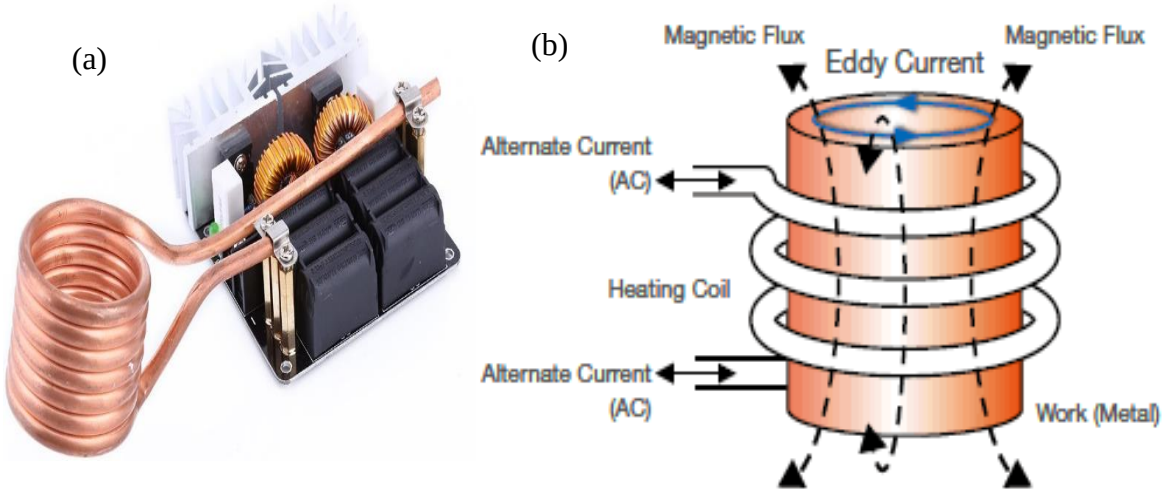

Figure 3.3 Illustration of electromagnetic induction; (a) ZVS DC to AC electromagnetic inductor (b) Eddy current in electromagnetic induction.

The zero voltage switching device (ZVS) is DC to AC voltage converter. When a DC voltage is applied at the positive pole, the current start to flow through two MOSFETs causing them to turn on. Since there are no components that are exactly the same. One MOSFET tend to turn on slightly faster than the other MOSFET causing more current to pass through. The effect causes one of the MOSFET to turn off (Zero switching) when the voltage reaches zero. The capacitors on each side of the MOSFET allow the voltage to go up and down causing a sinusoidal wave and an AC current is generated [97].

The electrolyte used in the electrochemical reactor is composed of a mixture of sodium hydroxide (NaOH) and potassium hydroxide (KOH). When NaOH is exposed to air, it reacts with carbon to produce sodium bicarbonate and lose its protonic conductivity strength as well as for KOH. Thus, a cap made from PTFE is specifically designed to fit on the reactor and seal the top. In the presence of NaOH and KOH, nitrogen is purged into and out of the reactor ensuring there is no contamination occurring. As shown in Figure

3.4 the cap has a thermocouple and a parallel “U” fitting. One inlet is used for nitrogen, and the other is for an outlet for undesired gas whıle the thermocouple is used to maintain the desired temperature.

Figure 3.4 PTFE cap for melting the electrolyte and cycling nitrogen gas (inert) to purge out undesired gas.

Electrochemical ammonia synthesis system consists of an electrochemical reactor, heat source, and an electromagnetic source. In order to ensure the functionality of the reactor, design for the experiment is implemented and discussed in this section. The ALICAT MC (0 to 5 slpm) presented in Figure 3.5, is a volume flow controller which determines the volumetric flow rate by measuring the pressure drop along a fixed distance within a laminar flow field. The pressure drop is linearly related to the volumetric flow rate as stated by the Hagen-Poiseuille equation. In order for the equation to work, the gas mixture dynamic viscosity has to be known. Thus, it is recommended that the flue gas composition is determined to get accurate results. The gas composition is then entered into the device to determine the “true” volumetric flow rate of the gas mixture. The device contains separate absolute temperature and pressure sensors which are used to correct the volumetric flow rate to a set of standard conditions. This standardized flow rate is commonly called the mass flow rate and is reported in units such as standard cubic feet per

minute (SCFM) or standard liters per minute (SLM) as shown in table 3.1. The device has a signal output of 0-5 V (4-20 mA) and RS232 communications.

Table 3.1 Performance data sheet for the volume flow controller.

Performance	**MCS & MCRS Mass Flow Controller**
Accuracy at calibration conditions after tare	± (0.8 % of Reading + 0.2 % of Full Scale)
High Accuracy at calibration conditions after tare	± (0.4 % of Reading + 0.2 % of Full Scale) High Accuracy option not available for units ranged under 5 sccm or over 500 slpm.
Repeatability	± 0.2 % Full Scale
Zero Shift and Span Shift	0.02 % Full Scale / ºCelsius / Atm
Operating Range / Turndown Ratio	1 % to 100 % Full Scale / 100:1 Turndown
Maximum Controllable Flow Rate	102.4 % Full Scale

Figure 3.5 Volume flow controller used in the experimental setup.

The potentiostat/galvanostat depicted in Figure 3.6 suited for studying physical electrochemistry experiments requiring voltages and currents. The performance of the device is given in Table 3.2. When connected in galvanostatic mode the device measures the potential across the working electrode. The potentiostat/galvanostat used in this research in the GAMRY 300 high performance [98]. In order to assess the ammonia electrochemical reactor, the device is set in a galvanostatic mode to measure voltage, apply current polarization and provide electrochemical impedance spectroscopy (EIS). Galvanic open circuit voltage (OCP) is applied at the start of the experiment where the voltage across the working electrode and counter electrode is measured without applying power. The reading represents the potential across the electrodes. Furthermore, application of electrode

polarization (I-V) provides essential information about the electrochemical reactor performance. The Gamry Reference 3000 in galvanostatic mode draws different output voltage values from the ammonia reactor and measures the corresponding current at these voltages. The obtained I-V curve provides information about the activation, ohmic and concentration losses occurring across the working electrode.

Table 3.2 Gamry reference 3000 performance table.

Maximum Current	±3 A or ±1.5 A @ 32V
Current Ranges	11 (300 pA – 3 A)
Current Ranges	13
Minimum Current Resolution	92 aA
Maximum Applied Potential	±32 V
Rise Time	<250 ns
Minimum Time Base	3.333 μs
Noise and Ripple (typical)	<2 μV arms

Figure 3.6 Gamry reference 3000 used in the experiment to perform electrochemistry studies.

The national instrument shown in Figure 3.7 is a Compact DAQ USB chassis designed for small, portable sensor measurement that includes a time stamp, and a data synchronizer between C Series I/O modules and an external host. It is used to measure the temperature change inside the electrochemical ammonia reactor and log the data in Labview 2017 [98].

Figure 3.7 The national instrument USB device used in the experimental setup.

The analog input system from national instruments shown in Figure 3.8 is used for monitoring the temperature across the electrochemical reactor by use of a thermocouple. It features programmable input ranges and variable connectivity options.

Figure 3.8 The analog input system for measuring the temperature across the ammonia reactor.

The thermocouple consists of two distinct metal wires, joined at one end. It is a robust way to measure a wide range of temperature. In this study, Omega, K type thermocouple shown in Figure 3.8 is used by connecting it to the NI9203, and it is controlled through LabVIEW software to control and measure the temperature inside the

electrochemical reactor. The accuracy and performance of the thermocouple are provided in Table 3.3 where the maximum operating temperature is up to 1250 °C.

Table 3.3 Performance table for omega K type thermocouple.

Calibration	**Temperature Range**	**Standard Limits of Error**	**Special Limits of Error**
K type thermocouple	-200° to 1250°C	Greater of 2.2°C	Greater of 1.1°C
	(-328° to 2282°F)	or 0.75 %	or 0.4 %

Fast-acting pressure-relief valves as shown in Figure 3.9, provides instantaneous pressure relief. The spring fully open at a set pressure and remains open until the system pressure is recovered below the set pressure. It is normal for these valves to eject small amounts of gas as the system pressure approaches the set pressure. In this research, two pressure relief valve are installed to maintain the pressure inside the reactor at atmospheric [101].

Figure 3.9 Pressure relief valve set to 5 psi to maintain atmospheric pressure across the electrochemical reactor.

The automatic temperature controller shown in Figure 3.10 is used to supply the required temperature to the electrochemical reactor with an output power of 1800 W. The load is protected by a fuse, and the set point for the proportional integral is 20 °C increment

Figure 3.10 Temperature controller for the lab scale reactor.

Figure 3.11 Corning 450 PH benchtop ionic meter used in the experimental setup.

The pH meter presented in Figure 3.11, is used to measure the hydrogen ion concentration of a solution to determine how acidic or basic the solution is. PH is the unit of measurement of hydrogen ion concentration and can be used to determine the alkalinity or the acidity of a solution. The measuring device is connected to a sensing electrode with a calibrated pH value, when testing a solution, a potential is produced, this is caused by the activity of the hydrogen ion in the solution The Model 450 which performance and accuracy data are given in Table 3.4, measures and converts the resulting electrode voltages into a pH reading [103].

Table 3.4 Performance and accuracy table of the benchtop ionic meter.

accuracy: 0.5 %	accuracy: 0.001 pH	accuracy: 0.2 mV	accuracy: 0.5 °C	resolution: 0.001 pH	resolution: 0.1 mV	resolution: 0.1 °C

The DC voltage control dissipated in Figure 3.12 is a power supply that is used to control the voltage, and current supplied to the ZVS control for inducing the electromagnetic field [103].

Figure 3.12 DV voltage control used to control the electromagnetic field power for the electrochemical reactor.

Thermal imaging is used to perform temperature measurements across the reactor. The infrared camera Optris PI 160 shown in Figure 3.13 is employed whenever temperature measurement of areas is required, and single-spot measurement is not enough. Due to the chemical composition of the molten salt, it is important to scan a thermal image across the reactor to determine the temperature gradient and maximum thermal expansion across the electrochemical reactor. The performance and measurement accuracy of the device is presented in Table 3.5.

Figure 3.13 The infrared camera used for thermal imaging of the reactor for the electrochemical reactor.

Table 3.5 Performance and accuracy range of the PI 160 infrared camera.

Optical resolution	160 x 120 pixels
Detector	FPA, uncooled (25 µm x 25 µm)
Spectral range	7.5 – 13 µm
Temperature ranges	–20 ... 100 °C, 0 ... 250 °C, (20) 150 ... 900 °C)
Frame rate	120 Hz
Thermal sensitivity (NETD)	0.08 K with 23° x 17° FOV / F = 0.8
	0.3 K with 6° x 5° FOV / F = 1.6
	0.1 K with 41° x 31° FOV and 72° x 52° FOV / F = 1
Accuracy	±2 °C or ±2 % (±3.6 °F or ±2 %), whichever is greater

3.2 Experimental setup for the lab scale electromagnetic induced ammonia reactor

The reagent grade NaOH (Sigma-Aldrich Ltd., ≥97.0 %), KOH (Sigma-Aldrich Ltd., 90 %) are dried to remove any water residual. The mixture of NaOH and KOH (50:50 mol %) is used as the electrolyte due to its high protonic conductivity at elevated temperatures and is melted in high purity alumina crucible (99.95 % Al_2O_3) under inert gas (N_2) and atmospheric pressure. Thermal imaging is performed prior to melting of the electrolyte to see any thermal imperfection in the crucible as shown in Figure 3.14 Thermal imaging of the alumina reactor.

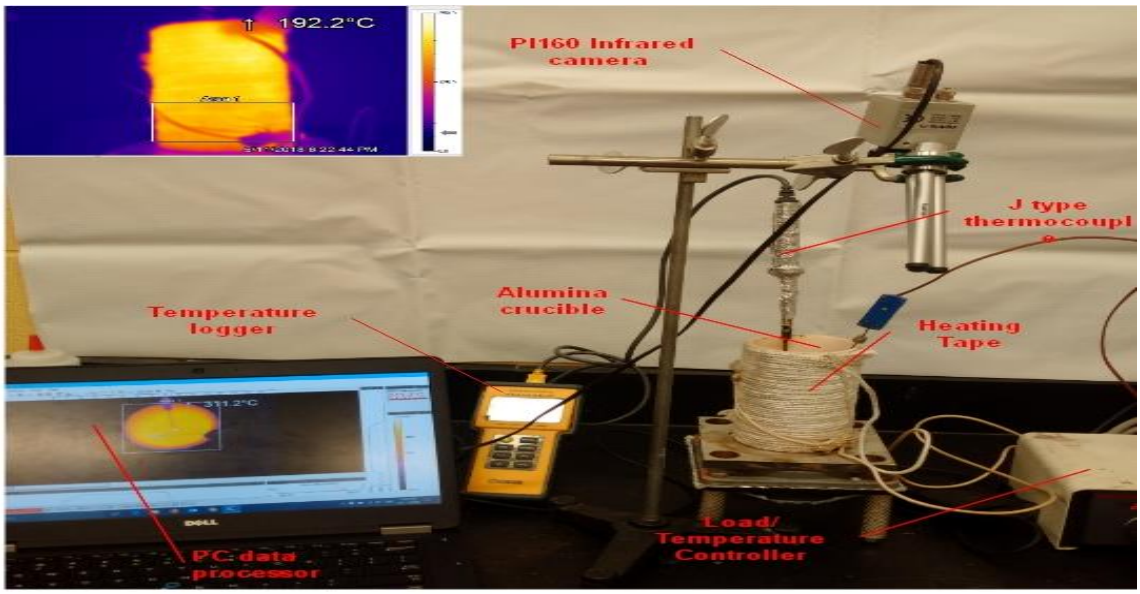

Figure 3.14 Thermal imaging of the alumina reactor.

The eutectic mixture has a melting point of 170 °C which is desirable for the ammonia synthesis. The cycling of nitrogen purges any undesired gas or water in the reactor as presented in Figure 3.15. The melting time is achieved in 1 h. Hydrogen (99.99 %) and nitrogen (99.5 %) prosecutors are used as the source of gas inlets connected to Alicat (MC-series) volume flow controllers. Since the hydrogen and nitrogen cylinder are operated with 1 stage regulator, needle valves are installed at the inlets of the volume flow controllers. To ensure the safety of the experiment, the system is developed in hydrogen sensitive room with hydrogen sensor installed for measuring hydrogen ppm in air.

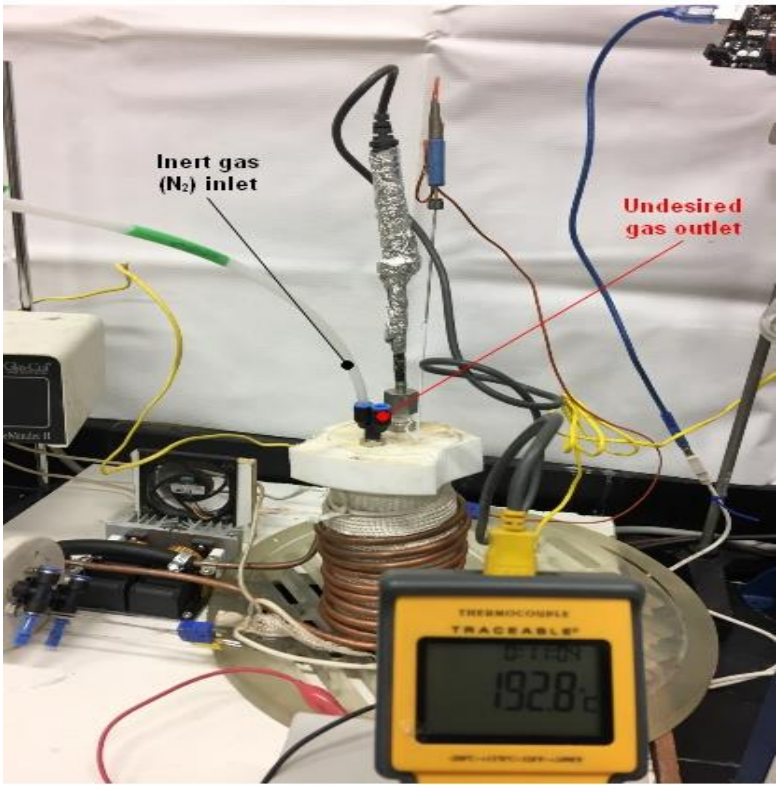

Figure 3.15 Nitrogen gas flow into the reactor and purges out undesired gas for the melting of KOH and NaOH to occur at 170 °C.

The design for experiment as illustrated in Figure 3.16, includes two safety pressure relief valves which are installed in series with the volume flow controller using a T connection. If the pressure in the reactor suddenly increases above atmospheric, the pressure relief valve will open releasing excess gas. After the melting process, a custom designed PTFE cap is fitted onto the reactor to seal the reactor prior to the beginning of the ammonia synthesis experiment. The working electrode is hydrogen gas, and the counter electrode is nitrogen gas. Nickel foam with a surface area of 55 cm^2 is connected to the end

of the gas carrier glass tube with nickel wire (99.9 % pure) on both electrodes. The gas carriers (tube with 6.36 mm OD) inside the reactor are made from quartz glass which is chemically stable in alkaline electrolyte and high temperature. In order to examine the effect of electromagnetic field, the reactor is placed around the copper coil. The electromagnetic field is induced into the copper coil by a ZVS circuit connected to a DC voltage supply. To maintain better eddy current generated by the coil, a water pump is connected at the end of the copper coil to circulate water and keep the temperature of the coil low. The flow rate of nitrogen and hydrogen at the beginning of the experiment is set to 0.14 L/min and 0.05 L/min respectively. The gamry reference 3000 is set in a galvanostatic mode with a constant current of 0.35 A and testing time of 30 min at the beginning at the experiment, and the electromagnetic field is turned on with a constant voltage of 15-volt. It is noted that the voltage is not supplied into the reactor rather than consumed by the ZVS circuit when a current is generated. The outlet of the reactor is connected by a tube (3.175 OD) to a funnel separator.

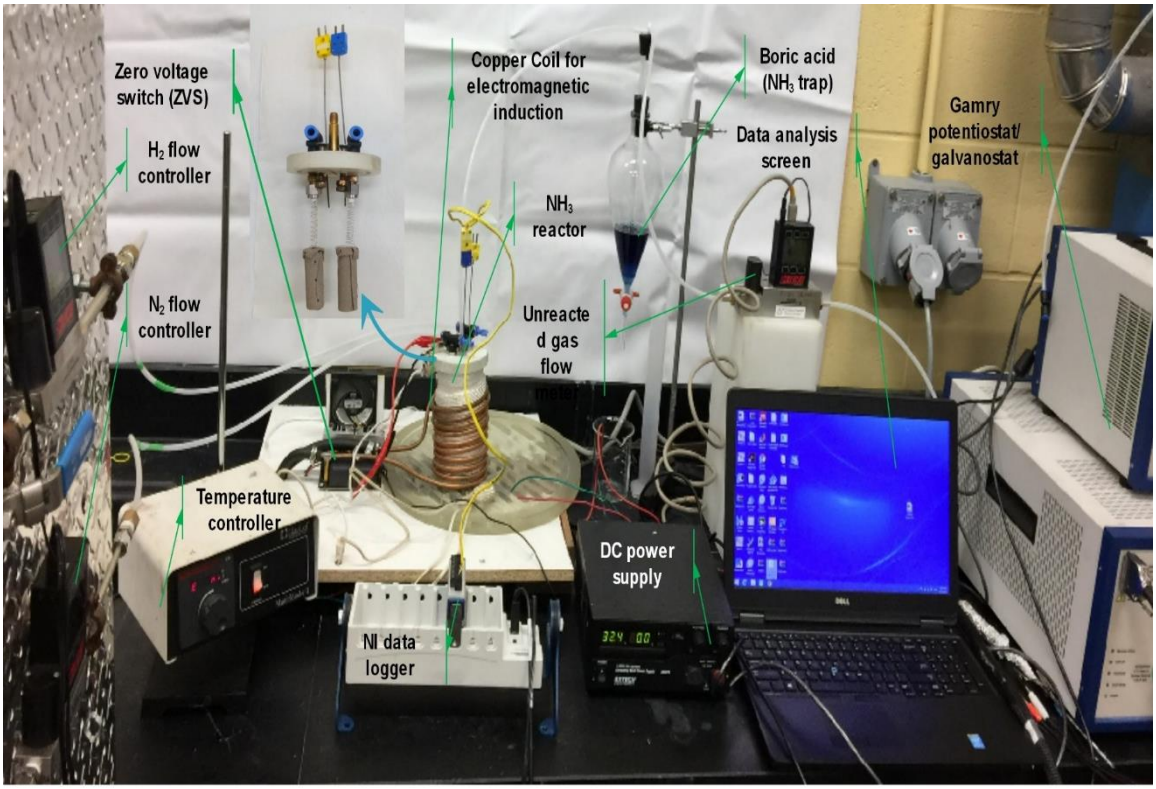

Figure 3.16 Experimental setup to test electromagnetic/electrochemical reactor.

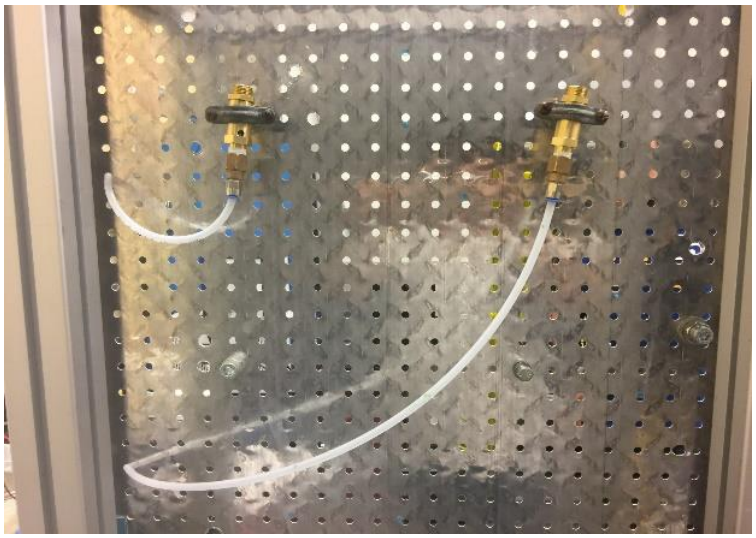

Figure 3.17 Pressure relief valve installed in series with volume flow controller to avoid any over pressurizing in the reactor.

The sampled ammonia in 100 ml of boric acid follows standard methods for test water and wastewater [105]. 200 mg methyl red indicator is dissolved in 100 ml of isopropyl alcohol and then mixed with 100 mg of methylene blue premixed with 50 ml of isopropyl alcohol. The solution is stirred for 15 min. Then, the boric acid solution is prepared by mixing 20 g of H_3BO_3 in 1 L of distilled water. Finally, 10 ml of the prepared indicator is added to the boric acid solution to give a purple color. To determine the rate of reaction, standard sulfuric acid titrant 0.02 M is titrated with the sampled gas as shown in Figure 3.18 (a) and (b).

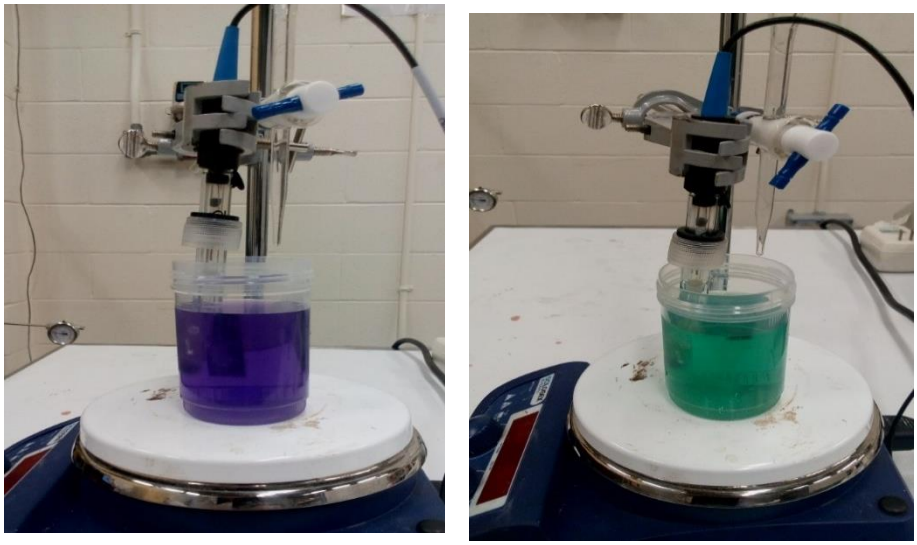

Figure 3.18 (a) The ammonia trap (boric acid and mixed indicator) has a purple color indicating no ammonia presence (b) post experiment; the green color shows the presence of ammonia.

Table 3.6 Applied set of experiments on the ammonia reactor.

Exp #	Reactor type	Current (A)	Time (min)	Flow rate (L/min)		Temperature (°C)
				N_2	H_2	
1	Galvano	0.35	30	0.14	0.05	197
2	Galvano	0.5	30	0.14	0.05	197
3	Galvano	0.65	30	0.14	0.05	197
4	Galvano	0.8	30	0.14	0.05	197
5	Galvano	0.35	30	0.14	0.05	210
6	Galvano	0.35	30	0.14	0.05	230
7	Galvano	0.2	30	0.07	0.05	197
8	Galvano	0.1	30	0.14	0.0025	197

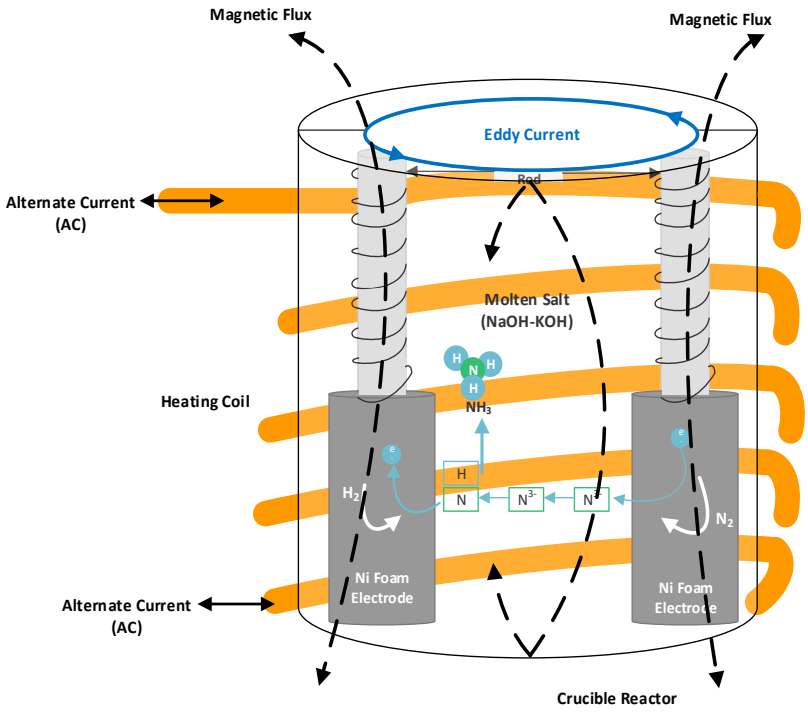

Figure 3.19 Ammonia synthesis driven by electromagnetic field and eddy current in the molten salt electrolyte.

In order to investigate the effect of the electromagnetic field on ammonia synthesis reactor as shown in Figure 3.19, an experimental procedure is derived based on changing temperature, flow rate, and applied constant current as decipated in Table 3.6.The

experiments are repeated multiple time to eliminate any errors and disturbance and to assure the forgiven results.

3.3 Thermodynamic modeling of the lab scale ammonia synthesis reactor

Any system that consumes or provides energy can be assed thermodynamically. In this research, the general energy balance equation of the system is analyzed following the principle of the first law of thermodynamics.

The general energy balance equation of the system is analyzed

$$\Delta\dot{E} = \Delta\dot{E}_{phsical} + \Delta\dot{E}_{chemical} \tag{3.1}$$

Expanding the chemical and physical energy results in

$$\dot{Q}_i + \dot{W}_i + \sum \dot{n}_r(\bar{h}_f^0 + \bar{h} - \bar{h}^0)_r = \dot{Q}_e + \dot{W}_e + \sum \dot{n}_p(\bar{h}_f^0 + \bar{h} - \bar{h}^0)_p \tag{3.2}$$

The entropy balance equation for the physical and chemical energy can be defined as the following:

$$\frac{\dot{Q}_i}{T} + \dot{m}_i s_i + \dot{S}_{gen} = \frac{\dot{Q}_e}{T} + \dot{m}_e s_e \tag{3.3}$$

Assuming ideal gas law for all the gas mixture at inlets and exits, the component of the gas is expressed as the following:

$$s_i = \bar{s}^0(T, P_0) - R_u \, ln\frac{y_i \, p}{p_0} \tag{3.4}$$

The exergy balance equation of a general system disregarding any potential or kinetic change is expressed as the following [106]:

$$\Delta\dot{E}_x = \Delta\dot{E}_{x,physical} + \Delta\dot{E}_{x,chemical} \tag{3.5}$$

$$\dot{m}_i ex_i + \sum \dot{Q}_i\left(1 - \frac{T_0}{T}\right) + \left(\dot{E}_{x_i}^{physical}\right) + \sum \dot{W}_i + \sum \dot{E}_{x_i}^{chemical} = \dot{m}_e ex_e + \sum \dot{Q}_f\left(1 - \frac{T_0}{T}\right) + \left(\dot{E}_{x_f}^{physical}\right) + \sum \dot{W}_f + \sum \dot{E}_x^{chemical} + \sum \dot{E}_{x\,destruction} \tag{3.6}$$

Considering ideal gases are flowing in and out of the system, the chemical exergy per mole of the mixture is expressed as the following:

$$\overline{ex}_{chemical} = \sum n_g \overline{ex}_{chemical}^{g} + RT_0 \sum n_g \ln(n_g) \tag{3.7}$$

The thermodynamic analysis of the system is conducted based on the following assumptions:

- The control volume is stationary and steady state is assumed across the system.
- The state of the mass within the control volume (CV) does not vary with time.
- The volume flow rate into and out of the control volume does not vary with time.
- The reference temperature and pressure are 25 °C and 1 atmospheric respectively.

When applying thermodynamic analysis for the electrochemical ammonia synthesis, the electrochemical potential is referred to assess the reversible potential for the half-reaction taking place at the anode and the cathode respectively. When the applied potential on the outer circuit of the reactor is greater the Gibbs free energy of the reaction, nitrogen gets reduced, and ammonia is formed. The reversible potential of the reactor is defined as follows:

$$E_{rev} = \frac{\Delta G}{zF} \tag{3.8}$$

where E_{rev} represents the minimum potential and z and F represent the number of electric charges and Faraday number respectively. One can make a note the rate of formation is equivalent to the current density.

The Gibbs function for the overall reaction of ammonia synthesis follows:

$$\Delta G = \Delta H - T\Delta S \tag{3.9}$$

where ΔG denotes the change in Gibbs function between the ammonia and reactants H_2 and N_2

The total electric power in the electrochemical reactor is denoted by the following equation:

$$W_e = V \times I \tag{3.10}$$

The electrochemical ammonia synthesis reversible reaction is shown:

$$N^{3-} + \frac{3}{2}H_2 \rightarrow NH_3 + 3e^- \tag{3.11}$$

The nitrogen fixation/reduction occurs at the cathode where nitrogen is reduced to nitride ion as follows:

$$\frac{1}{2}N_2 + 3e^- \rightarrow +N^{3-} \tag{3.12}$$

The synthesis of ammonia follows the overall reaction:

$$\frac{1}{2N_2} + \frac{3}{2H_2} \rightarrow NH_3 \tag{3.13}$$

As mentioned earlier, the ammonia synthesis reaction is highly reversible and is driven by pressure, temperature and volume. Withal, one can note that the force of attractive for N_2 and H_2 are highly repulsive (due to their electron valance and bond); hydrogen atom will always attract only a hydrogen atom and same for nitrogen. However, the attraction force for ammonia is dominate. Thus, ammonia synthesis will experience a decrease in enthalpy and is found by:

$$\Delta h_R(T,P) = h^0_{NH_3} - \frac{1}{2}C - \frac{3}{2h^0_{H_2}} \tag{3.14}$$

where Δh_R describes the enthalpy of formation and h^0 represents the residual enthalpy of gas (deviation from the ideal state) at specific temperature and pressure.

The entropy is driven by temperature and pressure thus it follows:

$$\Delta S_R(T,P) = s^0_{NH_3} - \frac{1}{2}s^0_{N_2} - \frac{3}{2}s^0_{H_2} \tag{3.15}$$

where ΔS_R describes the enthalpy of formation and S^0 represents the residual enthalpy of gas (deviation from the ideal state) at specific temperature and pressure.

The chemical equilibrium constant K is found form Gibbs free energy as follows:

$$\Delta g^0_R = -RT\sum ln\left(\frac{f_i}{f_{i_0}}\right)^{v_i} = -RTlnK \tag{3.16}$$

The change in Gibbs energy is caused by the change in fugacity evaluated at reference temperature and pressure where the fugacity are found at state f_i and standard f_{i_0}

To obtain the equilibrium constant the enthalpy of reaction is assumed to be taken at standard conditions (reference temperature and pressure) and the equation follows:

$$lnK_T = lnK_{T_0} - \frac{\Delta h^0_R}{R}\left(\frac{1}{T} - \frac{1}{T_0}\right) \tag{3.17}$$

where lnK_T represents the equilibrium constant at the desired temperature.

To evaluate the rate of maximum conversion of ammonia. Mole balance of the overall reaction is applied as follows:

$$X = \frac{n_{A_0} - n_A}{n_{A_0}} \tag{3.18}$$

It is noted that the basis of the conversion rate is always evaluated by the limiting reactant which is N_2 in the case of ammonia synthesis. Thus, Eq. (3.18), the conversion of N_2 is equal to the number of moles of reacted N_2 per mole of N_2 fed into the reactor. Since

the overall experiment in a run in batch mode, the number of unreacted N_2 after specific time can be expressed in terms of the number of moles of N_2 fed by the following equation:

$$nN_2 = n_{N_{2_0}}\left(4 - 2X_{N_2}\right) \tag{3.19}$$

Thus the equilibrium constant K can be expressed as follows:

$$K = \frac{n_{N_{2_0}}\left(4 - 2X_{N_2}\right)}{3^{1.5}(1 - X_{N_2})^2 p} \tag{3.20}$$

where p denotes to the pressure at a time (t) of the experiment.

In cells or reactors involving electrochemical reactions, several irreversibilities, as well as electrochemical impedances, prevent the reactor from reaching its ideal operation levels. Electrochemical impedance spectroscopy (EIS) is a technique that aids in estimating the various impedances present across the electrochemical reactor. Various components contribute to different types of impedances. In the case of a resistor operating in an ideal condition, the relation between the voltage, current, and resistance can be expressed as

$$I = \frac{V}{R} \tag{3.21}$$

As it can be observed from the equation above, the resistance in the case of a resistor operating in ideal condition, frequency does not affect the parameters, and the Ohm's law is obeyed. Nevertheless, several circuit components including capacitors and inductors are determined according to the frequencies. The impedance of a capacitor circuit element can be determined from the frequency and capacitance as

$$Z_{capa} = \frac{1}{jwC} \tag{3.22}$$

where C represents the component capacitance. The frequency is denoted by w. For an inductor circuit element, the impedance can be determined as

$$Z_{indc} = jwL \tag{3.23}$$

Here, component inductance is represented by L. The inductor impedance increases with rising frequencies and the capacitor impedance decreases with rising frequencies.

When an electrochemical reactor is operating, charges with opposite polarities accumulate forming layers or areas that are similar to a capacitor circuit element owing to the organized segregation of charges. In addition, the electrically conductive reactor components result in the presence of an inductance resembling an inductor circuit element that discharges energy or stores due to the presence of magnetic fields arising from the

flow of current. Furthermore, there are other types of resistances present in an electrochemical reactor including mass and charge transfer resistances. These hinder the movement of charges and electrons within the reactor.

To investigate electrochemical impedances, present in the ammonia synthesis reactor, EIS technique is utilized. The GAMRY Ref-3000 potentiostat is utilized for this purpose. In an experimental EIS study, signals of sinusoidal voltages fluctuate across the reactor and the alternating currents are logged. To investigate the various types of impedances present, an EIS modelling is performed in the present study. The overall impedance can be obtained as the resultant of the imaginary and real components and can be expressed as

$$|Z| = \sqrt{Z_{real}^2 + Z_{imag}^2} \tag{3.24}$$

The associated phase angle can be determined as

$$\phi = tan^{-1}\left[\frac{Z_{imag}}{Z_{real}}\right] \tag{3.25}$$

To perform the EIS modelling, an equivalent circuit model is developed for the ammonia synthesis reactor that is depicted in Figure5.15.

The modeled equivalent circuit also includes a constant phase element. It is essential to include this element when modelling an electrochemical reactor as the observed behavior may not resemble an ideal capacitor that obeys the equation described earlier. Hence, a constant phase element allows modeling the capacitance circuit element of an electrochemical reactor. The impedance of this type of element can be determined as

$$Z = \frac{\frac{1}{Y_o}}{(jw)^a} \tag{3.26}$$

The above equation would describe the behavior of a capacitor when the exponent a equals one and parameter Y_0 would represent the element capacitance. Experimental results obtained in the form of a Bode plot are utilized to determine the impedances included in the equivalent circuit. The simplex method is used for this purpose. The Gamry Echem Analyst software is utilized to perform this operation. The simplex method includes an algorithm to fit a model with the experimental results by repeatedly testing values and obtaining the parameters that provide a satisfactory fit.

3.4 Uncertainty analysis

In order to confirm the accuracy of the results presented in the experimental part it is essential to perform uncertainty analysis. For that, the accuracy of the devices that are illustrated in this thesis are used the calculation to compute the total uncertainty measure. The standard method is applied to the device uncertainty using the following equation:

$$U_y = \sqrt{\sum_x (\frac{\partial y}{\partial x}) \times U_x^2} \tag{3.27}$$

where U stands for the uncertainty of the variable.

Table 3.7 Uncertainty calculations.

Device	Measurement	Ref. Value	Absolute Bias Error	Relative Bias Error (%)	Relative Precision Error (%)	U (%)
Gamry Reference 3000	Voltage	2 V	0.006 V	0.3	2.2	2.2
Gamry Reference 3000	Current	4 A	0.012 A	0.3	1.3	1.4
Thermocouple J	Temperature	200°C	1°C	0.5	0.7	0.9
Alicat Flowmeter (hydrogen)	Volume flow rate	15 SLPM	0.12 SLPM	0.8	3.1	3.2
Alicat Flowmeter (ammonia)	Volume flow rate	30 SLPM	0.45 SLPM	1.5	3.1	3.5
Alicat Flowmeter (nitrogen)	Volume flow rate	45 SLPM	0.36 SLPM	0.8	3.0	3.1
PH103A Meter	pH	10 pH	0.02 pH	0.2	1.5	1.6

CHAPTER 4 : CONCEPTUAL INTEGRATED SYSTEM DEVELOPMENT

In this chapter, the theoretical setup and approach for the integrated energy system for power, steam and ammonia production are explained. Moreover, thermodynamic assessment is performed on the proposed system.

4.1 System Description

A new integrated energy system for power, steam, and ammonia production is developed and simulated in Aspen Plus. The ammonia process is considered exothermic thus higher conversion rates at an industrial scale size achieved when multiple catalyst beds are introduced. The system employs a novel ammonia production loop to potentially replace the conventional Haber-Bosch process by integrating an expander/turbine in the ammonia loop.

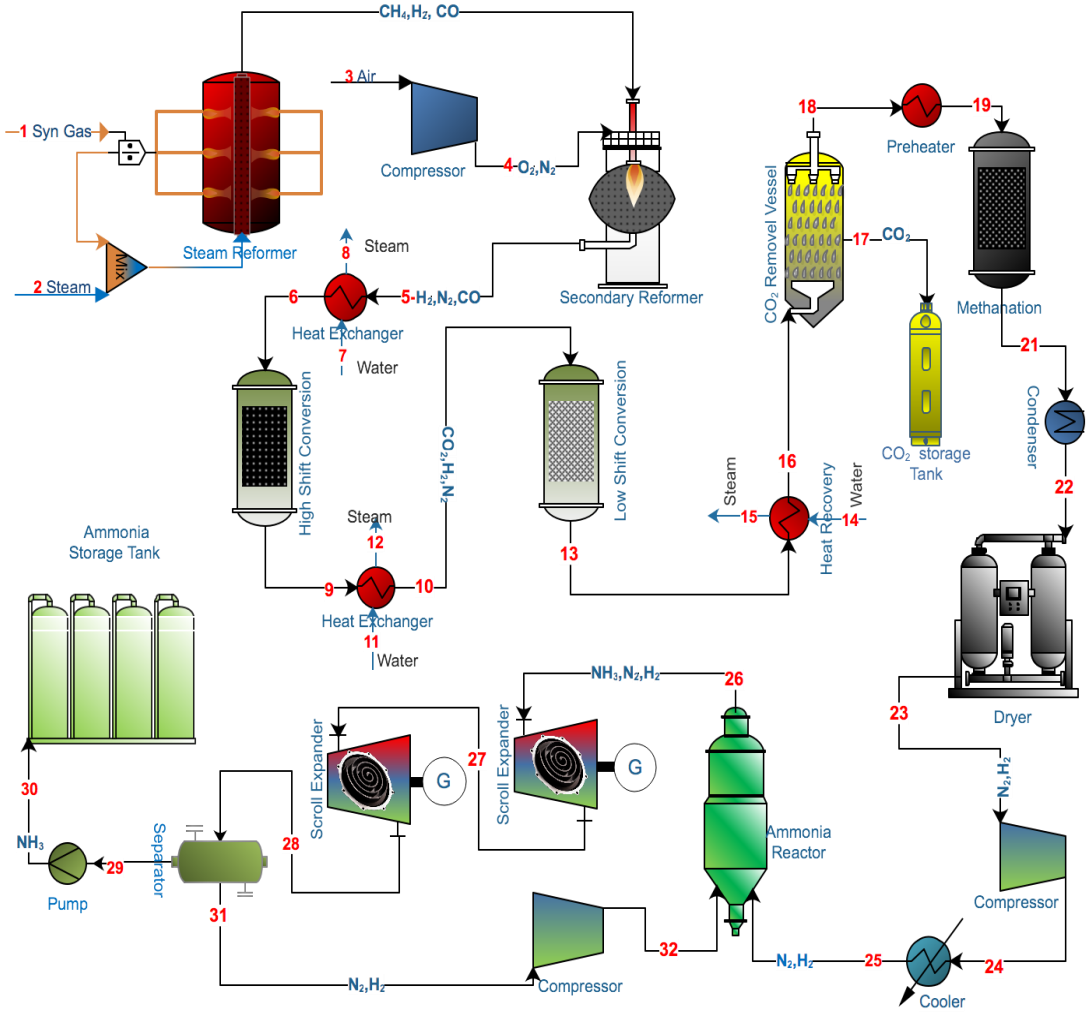

Figure 4.1 The overall schematic representation of the system.

The overall schematic diagram shown in Figure 4.1 consists of 5 subsystems, the reformer unit which consists of primary and secondary reforming, the CO conversion unit which consists of a high-temperature-shift reactor and a low temperature-shift reactor, the CO_2 removal unit, Methanation, dryer, the ammonia synthesizer, and the integrated 2 stage expander.

Hydrogen in the form of methane is mixed with superheated steam and is feed to the primary reformer; the steam-gas mixture is then heated further between 500 and 600 ^oC since the process of reforming is highly endothermic, additional heat is required, so the temperature is raised to up to 830 ^oC. The iron-containing reforming catalyst has no effect on the position of chemical equilibrium rather it provides an alternative pathway with lower activation energy and hence increase the reaction rate. However, 30 to 40 % of the hydrocarbon react in the primary reformer. Thus the products are blended with air before flowing into the secondary reformer for an additional yield of hydrogen. In the high-temperature shift conversion process, undesired carbon monoxide is removed; the gas is passed to a bed of iron oxide and chromium oxide catalyst at a temperature of 400 ^oC and is conversed to carbon dioxide (CO_2) which is then removed by absorption in aqueous ethanol or maintenance solutions. Withal, a small amount of carbon monoxide and carbon dioxide remaining in the process are converted to methane in the methanation process. The reaction takes place at around 300 ^oC. Finally, hydrogen is then catalytically reacted with nitrogen a drive from process aid to form nitrous liquid ammonia this step is known as the ammonia synthesis loop; two important factors are layering in this process. First one is effect of pressure on the rate of reaction and then Chatelier principle for higher yield of ammonia. At high pressure, the rate of reaction increases according to the collision theory; the high-pressure cause more successful collisions, therefore the rate of reaction is increased consequently. Then, the density of ammonia produced is considerably larger than that of hydrogen and nitrogen, thus the volume is larger, shifting the equilibrium reaction toward the products. Being said, nitrogen and hydrogen pass to the ammonia synthesis unit. In the ammonia synthesizer, the chemical reactions are highly exothermic; it releases energy, so that the sum of the enthalpies of N_2 and H_2 (the reactants) is higher than the enthalpy of NH_3. The reaction is affected by temperature, pressure, and catalyst on the composition of the equilibrium mixture, the rate of the reaction and the economics of the

process. The catalyst is slightly more complicated than pure iron. The synthesis of ammonia takes place in an iron based catalyst at high pressure and temperature of 246.7 atm and 550 ^{o}C respectively, only 20 to 30 % of hydrogen and ammonia are reacted due to the unfavorable equilibrium conditions. Since the reaction of hydrogen and nitrogen is considered highly exothermic and reversible the need to find more efficient ways to extract ammonia from the synthesis loop is important. In the integrated ammonia loop the reaction heat of the exothermic reaction is used to produce power in the expander. The hot reaction products are expanded directly thus resulting in low exergy loss and consumption and better conversion rate across the synthesis loop. Furthermore, the power generated by the turbine/expander is used to power the compressors and lower the energy consumption across the system. Finally, unreacted gas of hydrogen and nitrogen and produced ammonia are separated by a liquid-vapor separator. The extracted ammonia can be pumped to a storage tank while the excess hydrogen and nitrogen are compressed and then introduced back to the synthesis reactor.

4.2 Thermodynamic modelling

The performance of the integrated energy system is modeled using exergy method. Mass, energy, entropy, and exergy balance equations are defined for all the sub processes and are implemented in Aspen Plus software. To provide accurate results for the thermodynamic properties of the high temperature, high pressure conditions, Redlich-Kwong modification RKS-BM is selected for the ammonia production system. Henry-components are selected for the compound NH_3. Also, RK equation of state and Electrolyte NRTL method is used to calculate both liquid and vapor properties in the carbon dioxide removal subsystem. The overall system design is presented in Figure 3 with temperature and pressure showed at main inlets and outlets of the sub processes.

The general energy balance equation of the system is analyzed following the principle of the first and second law of thermodynamics.

$$\Delta\dot{E} = \Delta\dot{E}_{phsical} + \Delta\dot{E}_{chemical} \tag{4.1}$$

Expanding the chemical and physical energy results in

$$\dot{Q}_i + \dot{W}_i + \sum \dot{n}_r(\bar{h}_f^0 + \bar{h} - \bar{h}^0)_r = \dot{Q}_e + \dot{W}_e + \sum \dot{n}_p(\bar{h}_f^0 + \bar{h} - \bar{h}^0)_p \tag{4.2}$$

The entropy balance equation for the physical and chemical energy can be defined as follows:

$$\frac{\dot{Q}_i}{T} + \dot{m}_i s_i + \dot{S}_{gen} = \frac{\dot{Q}_e}{T} + \dot{m}_e s_e \quad (4.3)$$

Assuming ideal gas law for all the gas mixture at inlets and exits, the component of the gas is expressed as follows:

$$s_i = \bar{s}^0(T, P_0) - R_u \, ln \frac{y_i \, p}{p_0} \quad (4.4)$$

The exergy balance equation of a general system disregarding any potential or kinetic change is expressed as follows [106]:

$$\Delta \dot{E}_x = \Delta \dot{E}_{x,physical} + \Delta \dot{E}_{x,chemical} \quad (4.5)$$

$$\dot{m}_i ex_i + \sum \dot{Q}_i \left(1 - \frac{T_0}{T}\right) + \left(\dot{E}_{x_i}^{physical}\right) + \sum \dot{W}_i + \sum \dot{E}_{x_i}^{chemical} = \dot{m}_e ex_e + \sum \dot{Q}_f \left(1 - \frac{T_0}{T}\right) + \left(\dot{E}_{x_f}^{physical}\right) + \sum \dot{W}_f + \sum \dot{E}_x^{chemical} + \sum \dot{E}_{x\ destruction} \quad (4.6)$$

Considering ideal gases are flowing in and out of the system, the chemical exergy per mole of the mixture is expressed as follows:

$$\overline{ex}_{chemical} = \sum n_g \overline{ex}_{chemical}^{g} + RT_0 \sum n_g \ln(n_g) \quad (4.7)$$

For hydrocarbons the chemical exergy is expressed in terms of Gibbs functions as follows [106]:

$$\overline{ex}_{chemical} = \left[\bar{g}_F + \left(x + \frac{1}{4}y\right) \bar{g}_{O_2} - x\bar{g}_{CO_2} - \frac{y}{2} \bar{g}_{H_2O} \right]_{(T_0, P_0)} + RT_0 \quad (4.8)$$

4.3 Aspen plus kinetic modeling for the theoretical integrated energy system

The chemical kinetic modeling of the integrated energy system is developed in Aspen plus. Each subsystem described is modelled based on chemical kinetic following pressure volume and reaction rate.

- **Reactor kinetic of the reformer unit**

The reformer unit consists of two stoichiometry reactors and two plug-flow reactors. The reaction that is taking place in the reformer is the conversion of methane to a mixture of $CO + H_2O + 3H_2$.

The reformer chemical kinetic expression [107] is written as follows:

$$R = \frac{k_2\left(K_2 P_{CH_4} P_{H_2O}^2 - P_{H_2}^4 P_{CO_2}\right)}{379} \frac{lb\ mole}{hr\ ft^3} \quad (4.9)$$

By assuming ideal gas law; the partial pressure is converted to a molar quantity as [108]:

$$R = \frac{k_2 P^3}{SS^3 379}\left[K_2(CH_4)(H_2O)^2 - \frac{(H_2)^4(CO_2)}{SS^2}P^2\right] \quad (4.10)$$

Since some of the properties are not taken with reference to environment, the reaction rate is expressed as follows:

$$k_2 = A_c e^{\left(\frac{31720}{T+460} - 7.912\right)} \quad (4.11)$$

where A_c represents the catalyst used in the reformer.

Also, K_2 is equivalent to K_1K_3 which gives:

$$K_1 = \exp\left(-\frac{49{,}435}{t+460} + 30.707\right) atm^2 \quad (4.12)$$

$$K_2 = \exp\left(\frac{8{,}240}{t+460} - 4.335\right) below\ 1{,}100\ °F \quad (4.13)$$

$$K_3 = \exp\left(\frac{7{,}351.24}{t+460} - 3.765\right) above\ 1{,}100\ °F \quad (4.14)$$

The chemical equilibrium is achieved if

$$K_3 = \frac{(H_2)(CO_2)}{(H_2O)(CO)} \quad (4.15)$$

The reformer reaction is highly endothermic. Thus the heat transfer rate is considered critical for the rate of the reaction. In the reformer, the heat transfer rate is determined by the inner tubes of the wall at the inside and occurs by convection. The pressure drop and heat flux in the reformer can be expressed as follows:

$$\frac{dP}{dz} = -P_{fact}(0.04183 + 0.003292Z - 0.0000395Z^2) \quad (4.16)$$

$$Flux = ht_{in}(T_W - T) = ht_{out}\left(T_f - T_W\right) \quad (4.17)$$

- **Reactor kinetic modeling for the CO-shift unit**

The reformer produces undesired gas; carbon monoxide, which is removed in the presence of the iron oxide catalyst. The kinetic expression is described as follows [109]:

$$r_{CO} = A_c \frac{T_{ref}}{T}\left[\frac{k_{LT} Y_{CO} Y_{H_2O}^{\frac{1}{2}}\left(1-\frac{K_F}{K_3}\right)}{\frac{1}{P}+k_A Y_{CO}+k_B Y_{CO_2}}\right] \quad (4.18)$$

$$K_F = \frac{\left(Y_{CO_2}\right)\left(Y_{H_2}\right)}{\left(Y_{CO}\right)\left(Y_{H_2O}\right)} \quad (4.19)$$

$$k_{LT} = \exp\left(\frac{3260}{T} - 4.32126\right) standard\ LT\ catalyst\ activity\ in\ lb-mol/hr/ft^3/atm \quad (4.20)$$

$$K_3 = \exp\left(\frac{820}{t+459.7} - 4.33\right) \quad k_A = \exp\left(\frac{4580}{T} - 7.4643\right) atm^{-1} \quad (4.21)$$

$$k_B = \exp\left(\frac{1500}{T} - 2.623\right) atm^{-1} \quad (4.22)$$

The high-temperature conversion plug reactor is modeled similarly as follows:

$$r_{CO} = A_c K_{HT} P^{\frac{1}{2}} Y_{CO}\left(1-\frac{K_f}{K_3}\right) \quad (4.23)$$

$$K_3 = \exp\left(\frac{8240}{t+459.7} - 4.33\right)\ below\ 1100\ °F \quad (4.24)$$

$$K_F = \frac{\left(Y_{CO}\right)\left(Y_{H_2}\right)}{\left(Y_{CO}\right)\left(Y_{H_2O}\right)} \quad (4.25)$$

$$k_{HT} = \exp\left(10.3375 - \frac{5787.62}{T}\right) \quad (4.26)$$

- **Electrolyte modelling for the CO_2 removal unit**

The carbon dioxide is then removed by absorption in the aqueous ammonia solution. The electrolyte solution chemistry is modeled in Aspen Plus, where chemical equilibrium is assumed with all the ionic reactions in salts.

The reaction rate of the CO_2 removal is modeled by power-law expression [107]:

$$r = k\left(\frac{T}{T_0}\right)^n exp\left[\left(\frac{-E}{R}\right)\left(\frac{1}{T}-\frac{1}{T_0}\right)\right]\prod_{i=1}^{N} C_i^{a_i} \quad (4.27)$$

$$r = kT^n \exp\left(-\frac{E}{RT}\right)\prod_{i=1}^{N} C_i^{a_i} \quad (4.28)$$

The built-in K_{eq} expression is used for the salt precipitation reaction of NH_4HCO_3 [110],

$$\ln K_{eq} = A + \frac{B}{T} + C\ln(T) + DT \quad (4.29)$$

- **Reactor chemical kinetics for the methanation unit**

In the methanator, excess carbon monoxide and carbon dioxide react to form hydrogen in a nickel catalyst. Langmuir-Hinshelwood mechanism is used as follows [109]:

$$r = A_c 0.314 e^{\left(1{,}300\left[\frac{1}{T}-\frac{1}{513}\right]\right)}\left\{\frac{P}{P_{H_2}^{0.5}}\right\}\left[y_{CO_2} - \frac{y_{CH_4} y_{H_2O}^2}{y_{H_2}^4 P^2 K_{CO_2}}\right] \quad (4.30)$$

The reaction rate for CO in methanation is expressed as follows [109]:

$$K_{CO_2} = e^{\left(-33.923+\frac{21{,}621}{T}\right)} \quad (4.31)$$

- **Chemical equilibrium and Kinetics for the ammonia synthesizer unit**

The reaction taking place in the ammonia synthesizer is highly exothermic reaction due to the Haber Bosh process; it releases energy so that the sum of the enthalpies of N_2 and H_2 (the reactants) is greater than the enthalpy of NH_3. The partial mole of the gas mixture of nitrogen and hydrogen in terms of reactor conversion ξ is expressed as follows [111]:

$$\xi = \frac{\mathrm{n}_{\mathrm{N}_2,i} - n_{N_{2,f}}}{n_{N_{2,i}}} = \frac{\mathrm{n}_{\mathrm{H}_2,i} - n_{H_{2,f}}}{n_{H_{2,i}}} = \frac{\mathrm{n}_{\mathrm{NH}_3,i} - n_{NH_{3,f}}}{n_{NH_{3,i}}} \quad (4.32)$$

The reaction rate of ammonia synthesis is expressed using the Temkin-Pyzhev equation in an iron catalyst bed as follows [111]:

$$r_{NH_3} = 2k_b\left[K_p^2 f_{N_2}\left(\frac{f_{H_2}^3}{f_{NH_3}^2}\right)^a - \left(\frac{f_{NH_3}^2}{f_{H_2}^3}\right)^{1-a}\right] \qquad \left[\frac{kmol}{m_{catalyst}^3.h}\right] \quad (4.33)$$

In this case, the fugacity, f at equilibrium is related to the fugacity of the pure component f_i^0 at the same pressure and temperature follows Lewis-Randall rule:

$$f_i = x_i \times f_i^0 \quad (4.34)$$

The pure component fugacity as mentioned is found at reactor pressure P and temperature:

$$f_i^0 = \gamma_i \times P \quad (4.35)$$

Also, the equilibrium constant is found using the expression:

$$K_p^2 = \frac{k_f}{k_b} \quad (4.36)$$

The pressure drop across the ammonia reactor is modeled using Ergun correlation [112]:

$$\frac{dP}{dz} = -\frac{\dot{m}_{gas}}{V_{reactor}} \times \frac{1-\left(\frac{V_{gas}}{V_{reactor}}\right)}{\left(\frac{V_{gas}}{V_{reactor}}\right)^3} \times \left[\frac{150\left(1-\frac{V_{gas}}{V_{reactor}}\right)\mu}{D_p} + 1.75\frac{\dot{m}_{gas}}{A}\right] \quad (4.37)$$

4.4 Exergy analysis

Exergy has the characteristic that it is not conserved only when all processes occurring in a system and the environment are irreversible. When an exergy analysis is performed on a chemical processing plant, the thermodynamic imperfections can be quantified as exergy loss and consumption, which represent losses in energy quality or usefulness [108]. In this study, exergy efficiencies are evaluated based on 2 characteristics, the first exergy efficiency is based on the useful exergy products of the system compared to that of the exergy input of the system. However, this takes only into account exergy transformed by the process of synthesizing ammonia and is presented in equation (I). The second exergy definition (II) is used to access the quality of the steam recovered in the process. Since the amount of steam generated is much higher than the produced ammonia, steam recovery becomes important, and the quality of steam shows the irreversibilities in the sub processes where steam can be recovered. Unreacted gases that are in flow or transit, such as methane, argon and excess gas are purged out of the system. The amount of purge affects directly the quality of ammonia produced. Equation (III) is proposed to access the quality of purged gas. If the flow of the purged gas is high the exergy efficiency will go to a 100 % and this is evident from the definition. Thus, accounting for the purged and transit gas flow it is important to take into consideration the irreversibilites due to purging. Considering all three exergy efficiency definitions, the first exergy efficiency definition will give a better understanding of the performance of the overall system. Also, while assuming all the excess gas is converted into ammonia.

Equations I, II and III in Table 4.1 are derived on the consideration that the work generated by the turbine expander and the produced ammonia in line with the expander. So, the approach suggests, recovering work in the form of mechanical work to drive the pumps, compressors and extract heat of produced ammonia directly after synthesis reactor results in decrease total power consumption and increase production rate could be considered as a more attractive way and thus the exergy efficiency of the system is described in terms of expander work and ammonia recovered to that of steam recovered in the process. Although equation (II) reflects the potential for exergy recovery, the main purpose of the system is to produce ammonia. Thus, deviating from comparing the low-quality exergy of steam being produced, equation (I) is derived based on the ammonia

reactor minimum exergy consumption to the actual consumption of syngas and steam going into the system and generated work.

Table 4.1 Exergy efficiency definitions.

Equation	Exergy efficiency
(I) Overall	$\boldsymbol{\psi_1 = \frac{\dot{m}_{NH_3} ex_{NH_3} + W_{net}}{\dot{m}_{syngas} ex_{syngas} + \dot{m}_{steam} ex_{steam} + \dot{m}_{air} ex_{air}}}$
(II) Steam Recovery	$\boldsymbol{\psi_2 = \frac{\dot{m}_{recovered\ steam} ex_{\text{recovered } steam}}{\dot{m}_{syngas} ex_{syngas} + \dot{m}_{air} ex_{air} - \dot{m}_{NH_3} ex_{NH_3} - \dot{W}_{net}}}$
(III) Unreacted gas transit	$\boldsymbol{\psi_3 = \frac{\dot{W}_{net}}{\left(\dot{m}_{syngas} ex_{syngas} + \dot{m}_{steam} ex_{steam}\right) - \dot{m}_{Excess\ gas} ex_{Excess\ gas} - \dot{m}_{NH_3} ex_{NH_3}}}$

CHAPTER 5 : RESULTS AND DISCUSSION

In this chapter, the experimental and mathematical modeling results of the lab scale ammonia synthesis reactor are presented and discussed. In addition, the results of the theoretical integrated energy system for power, steam and ammonia production are also depicted and discussed.

5.1 Experimental results of the lab scale ammonia synthesis reactor

Ammonia is synthesized electrochemically in the presence of EMF using H_2 and N_2 as precursors. The electrolyte KOH and NAOH are mixed and melted at 170 ℃ changing the mixture phase from solid to the eutectic phase with a total volume of 215 ml. The electrolyte is considered highly conductive in eutectic mixture due to the purity of the OH^- ions. To increase the rate of reaction 10 g of Fe_3O_4 nanoparticle iron oxide are injected into the reactor prior to testing. To complete the reactor, the outer circuit is connected to a Galvanometer. EMF is incorporated to the reactor via copper coil connected to the ZVS circuit. Nickel foam with a surface area of 55 cm^2 is connected to the gas carriers on both sides of the electrodes. The working and counter electrodes are nitrogen and hydrogen respectively. Experimental tests on the reactor are repeated multiple times to ensure no anomalies occurring and for the purpose of accuracy.

Effect of current density on the performance of the lab scale ammonia synthesis reactor

As shown in as shown in Figure 5.1, a current density of 6.4 mA/cm^2 is applied for 30 min at a 210 ℃ applied load and the volume flow rate is set to 0.14 L/min and 0.05 L/min for N_2 and H_2 respectively, while the EMF recorded 49 mT. The results show an average voltage of 969.7 mv. At the beginning of the experiment, the reaction between hydrogen and nitrogen is spontaneous thus the graph shows the voltage increase from 945mv to a maximum voltage of 990 mv. When the reaction reaches equilibrium. The reaction then shifts toward the reactant and thus the voltage drops to the initial equilibrium state. When the produced ammonia is transported from the reactor the reaction shifts toward the products and thus the voltage increase showing the electrochemical reaction of ammonia synthesis is taking place. The maximum ammonia mole flow is found to be 10^{-10} $mol/cm^2.s$.

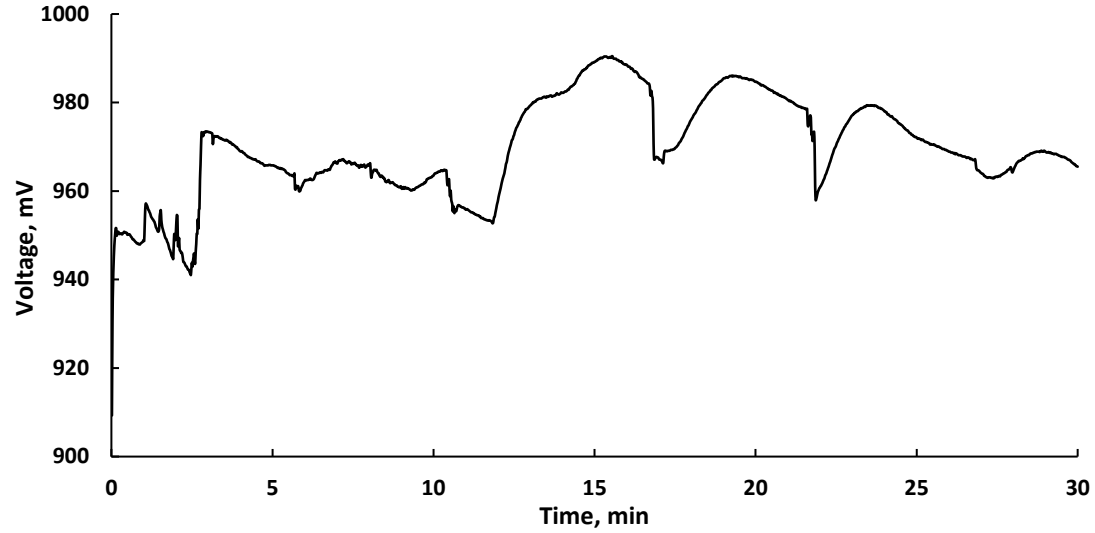

Figure 5.1 Voltage vs time graph for Exp 1. (galvanostatic mode with EMF, current; 0.35A, time; 30 min, applied temperature; 197 ℃, N_2 flow rate; 0.14 L/min, and H_2 flow rate; 0.05 L/min).

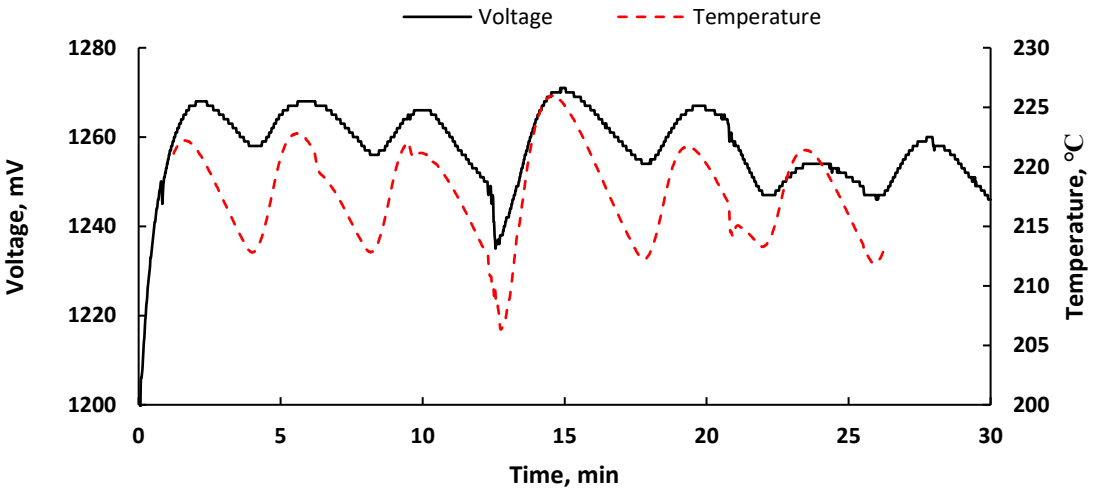

Figure 5.2 Voltage and temperature vs time graph for Exp 2. (galvanostatic mode with EMF, current; 0.5A, time; 30 min, applied temperature; 197 ℃, N_2 flow rate; 0.14 L/min, and H_2 flow rate; 0.05 L/min).

For the following experiment, the current destiny is increased to 9.09 mA/cm^{2,} and the flow of hydrogen and nitrogen remain the same. The temperature inside the reactor is recorded, and the graph is posed to the change in potential as shown in Figure 5.2. It is noticed that the temperature is directly proportional to the ammonia reaction rate. The recorded average potential is 1.258 V, and the mole flow of ammonia is calculated to be 1.21×10^{-10} mol/cm^2.s while 49 mT is recorded by the EMF.

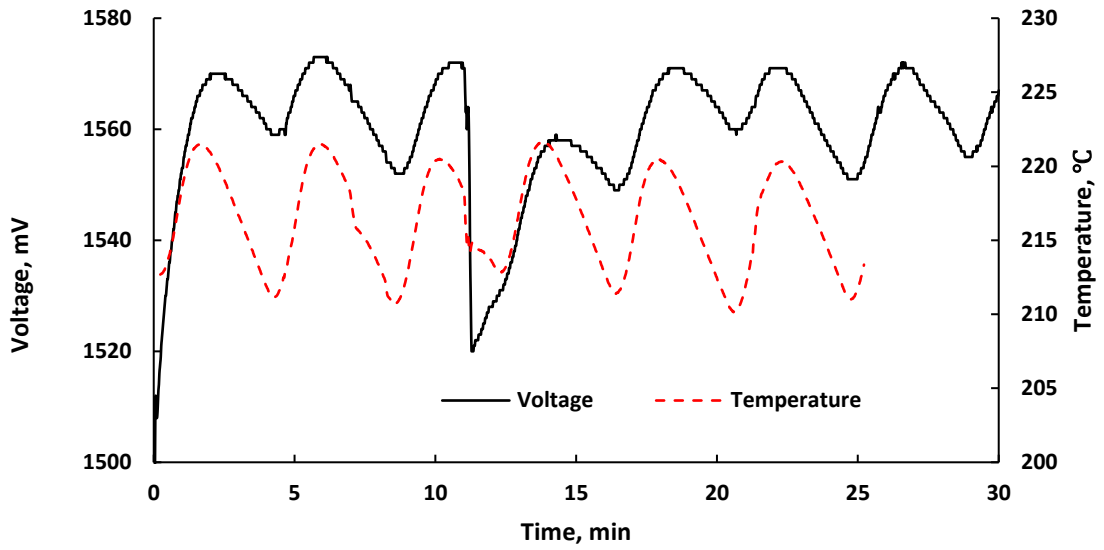

Figure 5.3 Voltage and temperature vs. time graph for Exp 3. (galvanostatic mode with EMF, current; 0.65A, time; 30 min, applied temperature; 197 ℃, N_2 flow rate; 0.14 L/min, and H_2 flow rate; 0.05 L/min).

For this experimental test, the current destiny is increased to 11.82 mA/cm^{2,} and the flow of hydrogen and nitrogen remain the same. The temperature inside the reactor is recorded, and the graph is posed to the change in potential as shown in Figure 5.3. As the potential across the cathode increase, ammonia is synthesized, and the reaction is exothermic thus the temperature increase. The recorded average potential is 1.56 V, and the mole flow of ammonia is calculated to be 1.11×10^{-11} mol/cm^2.s while the EMF is recorded at 59 mT. Interestingly, ammonia is synthesized directly from H_2 and N_2 in the presence of Fe_2O_3 iron oxide nanoparticle catalyst at low voltage consumption and a relatively low temperature. The performed tests are applied in galvanostatic mode. Also, the experiment is repeated to exclude any interference to preserve the integrity of the results. When the applied load temperature is set to 197 ℃ and the flow of H_2 and N_2 are 0.05 and 0.14 L/min respectively it is noted the ammonia flow rate is directly proportional to the temperature and current density. As the current density increase the ammonia rate of formation decrease. This is caused by the over applied potential where the ammonia gas is dissociated back to N_2 and H_2 after reaching the equilibrium state. The maximum Faraday efficiency is calculate to be 5.4 % and the ammonia formation rate is 10^{-10} mol/cm^2.s. The eddy current generated by the EMF is induced into the nickel electrodes, forcing the free electrons to move causing the “Joule” effect. Since the fixation of nitrogen requires high

energy to break the triple bond, the movement of the electrons on the surface of the electrode, through the Fe_2O_3 nano particles is partially causing the N_2 to reduce to $2N_3^-$ by electron excitation and transfer at a frequency of 60 Hz.

Effect of temperature on the performance of the lab scale ammonia synthesis reactor

The second set of experiments show the effect of temperature on the rate of formation of ammonia. It is noted the applied load temperature is set by the controller. However, the real temperature is measured by a thermocouple inside the reactor in sequence with the applied tests (heat transfer caused by thermal and chemical convection, EMF induction). This experiment, the current destiny is increased to 14.54 mA/cm^{2,} and the flow of hydrogen and nitrogen remain the same. The load temperature controller is set to 197 ℃ and the temperature inside the reactor is recorded, and the graph is posed to the change in potential as shown in Figure 5.4. The voltage across shows the minimal change between 0 and 25 min; this is caused by the volume of the products as the reaction reaches an equilibrium state. The change in potential is magnified and recorded to be 50 mV, and the temperature change is recorded to be 8 ℃. The recorded average potential is 1.89 V, and the mole flow of ammonia is calculated to be 7.06×10^{-11} mol/cm^2.s.

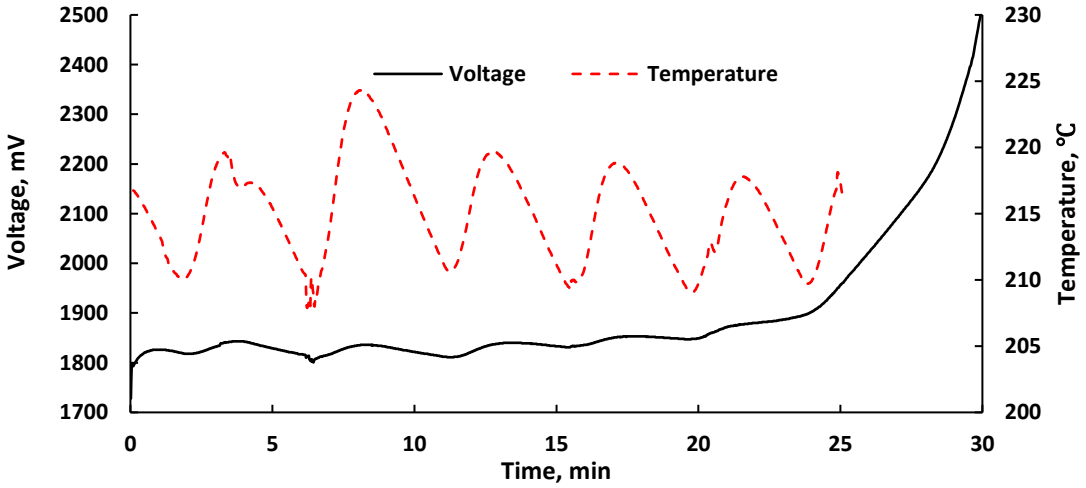

Figure 5.4 Voltage and temperature vs time graph f.or Exp 4. (galvanostatic mode with EMF, current; 0.8 A, time; 30 min, applied temperature; 197 ℃, N_2 flow rate; 0.14 L/min, and H_2 flow rate; 0.05 L/min).

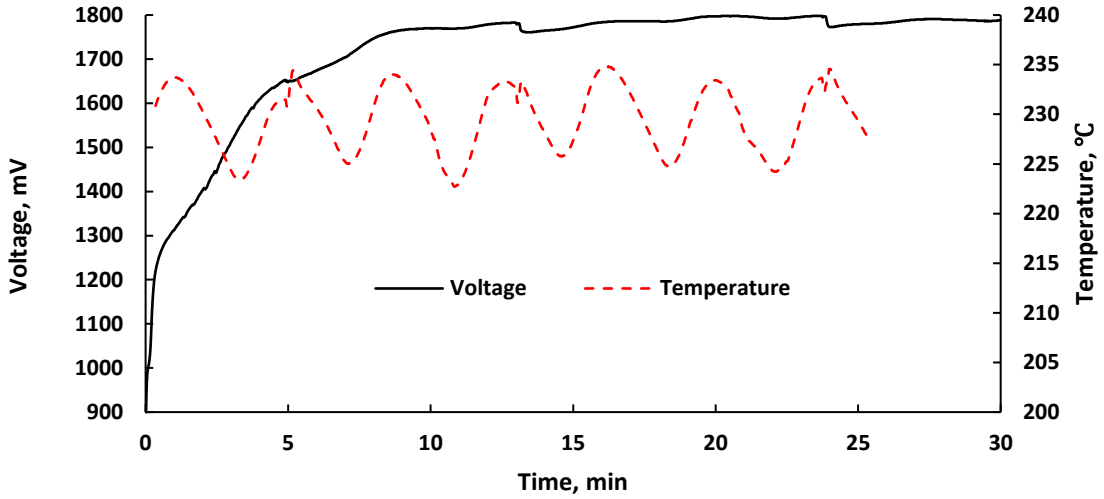

Figure 5.5 Voltage and temperature vs. time graph for Exp 5. (galvanostatic mode with EMF, current; 0.35 A, time; 30 min, applied temperature; 210 ℃, N_2 flow rate; 0.14 L/min, and H_2 flow rate; 0.05 L/min).

Now, the current destiny is set to 6.4 mA/cm^2 and the flow of hydrogen and nitrogen remain the same. The load temperature controller is increased to 210 ℃ and the temperature inside the reactor is recorded and the graph is posed to the change in potential as shown in Figure 5.5. As the temperature of the reactor increase, ammonia synthesis reaction rate decrease. This is caused by the temperature; when the temperature is high, the reaction will shift toward the reactants. The highest temperature recorded at 235 ℃ while the recorded average potential is 1.72 V and the mole flow of ammonia is calculated to 8.06×10^{-11} mol/cm^2.s.

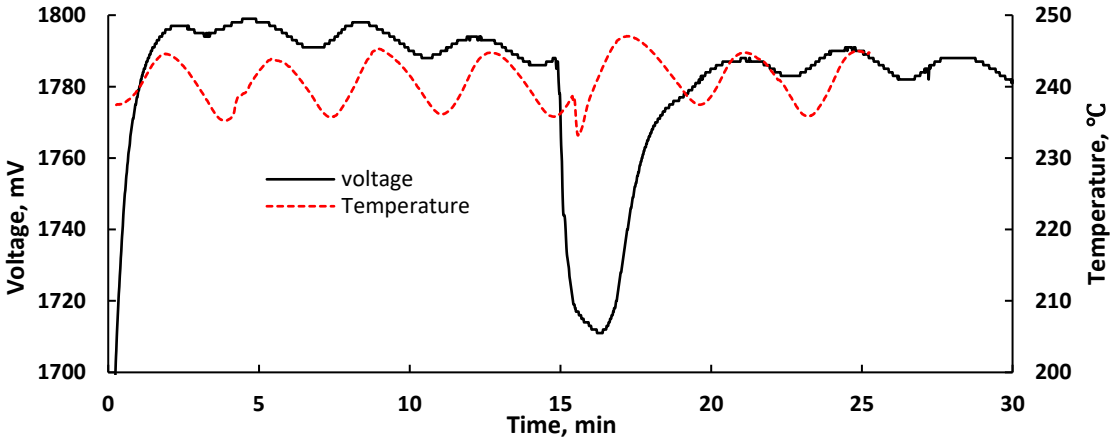

Figure 5.6 Voltage and temperature vs time graph for Exp 6. (galvanostatic mode with EMF, current; 0.35 A, time; 30 min, applied temperature; 230 ℃, N_2 flow rate; 0.14 L/min, and H_2 flow rate; 0.05 L/min).

The last experiment in second set, the current destiny is set to 6.4 mA/cm^2 and the flow of H_2 and N_2 remain the same. The load temperature controller is increased to 230 ℃ and the temperature inside the reactor is recorded and the graph is posed onto the change in potential as shown in Figure 5.6 as the temperature increase, ammonia synthesis reaction rate decrease. This is caused by the temperature; when the temperature is high, the reaction will shift toward the reactants. The sudden drop in temperature is due to the dissociation of ammonia caused by the over potential. The average potential is 1.78 V, and the mole flow of ammonia is calculated to be 8.06×10^{-10} mol/cm^2.s. One can explain, as the current density increase the force on the electrons increase in the direction opposite to the electric field at the same time the electromagnetic field will cause the electron to drift. It is possible that both the electric and magnetic field cause the electron to drift and rotate in a non-uniform motion increasing conductivity in one field and decreasing conductivity in another field contributing to the sinusoidal wave shape. When the crest is formed it is relatively proportional to the reduction of nitrogen and formation of ammonia.

Effect of Volume flow rate on the performance of the electrochemical ammonia reactor in an electromagnetic field

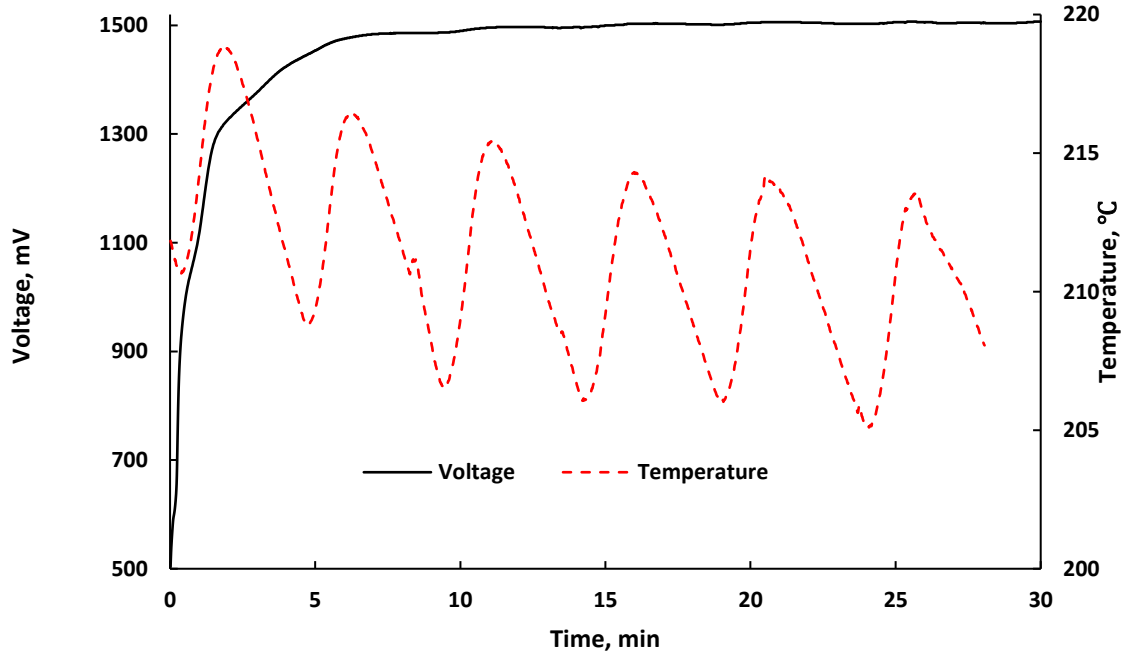

Figure 5.7 Voltage and temperature vs time graph for Exp 7. (galvanostatic mode with EMF, current; 0.2A, time; 30 min, applied temperature; 197 ℃, N_2 flow rate; 0.07 L/min, and H_2 flow rate; 0.05 L/min).

The following experiment the current destiny is decreased to 3.63 mA/cm^2 and the flow of hydrogen is the same while the flow of nitrogen is decreased to 0.07 L/min. The load temperature controller is decreased to 197 ℃ and the temperature inside the reactor is recorded as shown in Figure 5.7. As the volume flow rate of nitrogen decrease the reaction rate also decreases. The recorded average potential is 1.47 V and the mole flow of ammonia is calculated to be$1.92 \times 1.71^{-10}\ mol.cm^{-2}.s^{-1}$. For the eighth experiment the current density is decreased to 1.8 mA/cm^2 and the flow of hydrogen is decreased 0.025 L/min while the flow of nitrogen is increased to 0.14 L/min. The load temperature controller is decreased to 197 ℃ and the temperature inside the reactor is recorded and the graph is posed onto the change in potential as show in Figure 5.8. As the volume flow rate of nitrogen increase the reaction rate also increases. The recorded average potential is 1.12 V and the mole flow of ammonia is calculated to be $6.05 \times 10^{-11}\ mol.cm^{-2}.s^{-1}$.

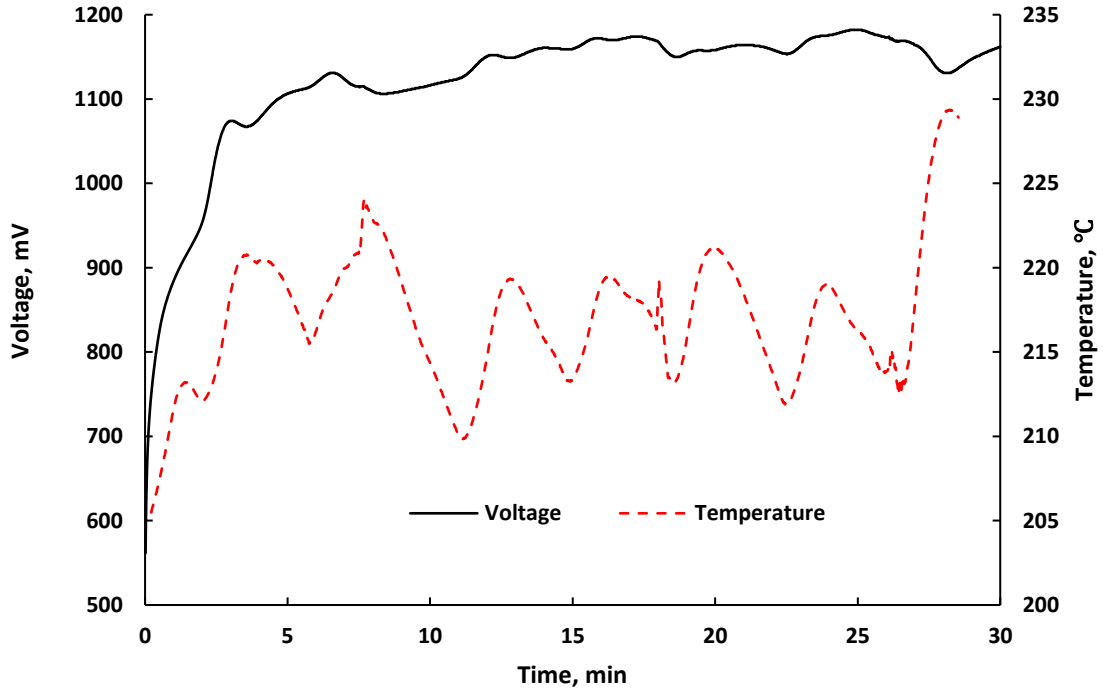

Figure 5.8 Voltage and temperature vs time graph for Exp 8. (galvanostatic mode with EMF, current; 0.1A, time; 30 min, applied temperature; 197 ℃, N_2 flow rate; 0.14 L/min, and H_2 flow rate; 0.025 L/min).

Effect of EMF of the lab scale ammonia synthesis reactor in galvaonstatic and potentiostatic mode

For this experiment, the electrochemistry of the reactor is studied through potentiostatic mode. The applied potential is 1.3 V and the volume flow rate of hydrogen is 0.0025 L/min while the flow of nitrogen is 0.14 L/min. The load temperature controller is increased to 205 ℃ and the temperature inside the reactor is recorded and the graph is posed to the change in current density as shown in Figure 5.9. It is noted that the current density is proportional to the ammonia formation rate. The recorded average current density is 2.7 mA/cm^2 and the mole flow of ammonia is calculated to be 5.04×10^{-10} $mol/cm^2.s$.

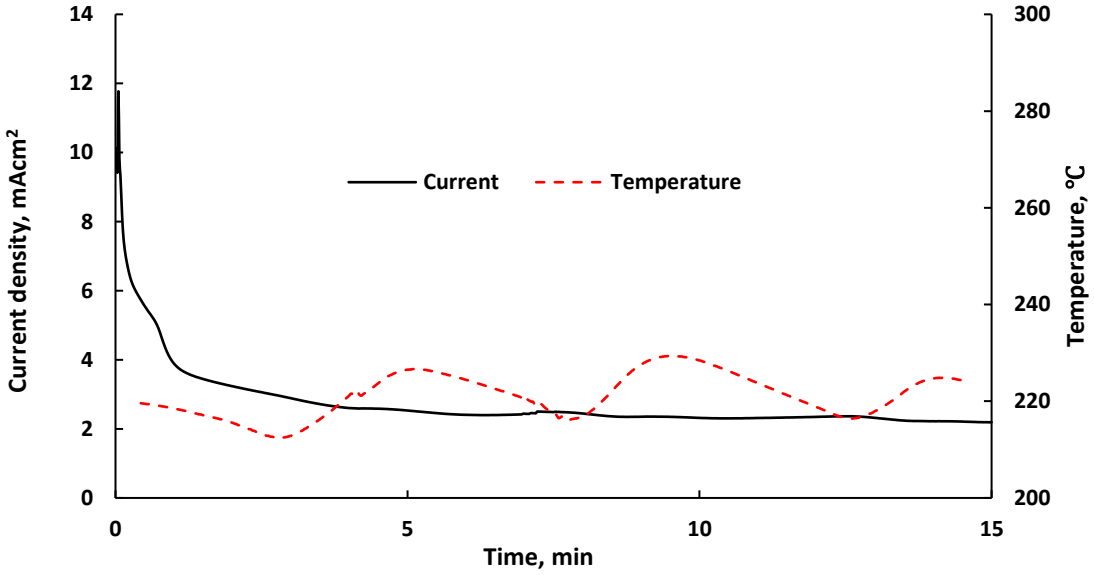

Figure 5.9 Current density and temperature vs time graph for Exp 9. (potentiostatic mode with EMF, time; 15 min, applied temperature; 205 ℃, N_2 flow rate; 0.14 L/min, and H_2 flow rate; 0.025 L/min).

The effect of EMF is confirmed in this experiment. The first part of the experiment is conducted without EMF by turning off the ZVS device. The reactor is set in galvanostatic mode and the applied current density is 6.4 mA/cm^2. The load temperature controller is set to 197 ℃ and the temperature inside the reactor is recorded and the graph is posed to the change in potential. Then, the same conditions mentioned above are repeated but this time the ZVS device is turned on to induce the electromagnetic field and the time is set to 30 min. The experiments were repeated multiple times to ensure no anomalies occurring and for the purpose of accuracy. In the presence of the electromagnetic field, the ammonia formation rate is higher. The chemical kinetics corresponding to reaction rate and catalyst

activity is recorded in Figure 5.10, taking a closer look at the magnified part of the graph, the “with” EMF test recorded higher average potential and faster rate of reaction with an average potential of 1.7 V while the “without” EMF test recorded an average potential of 1.2 V. The results point to the likelihood that the EMF has better reaction rate.

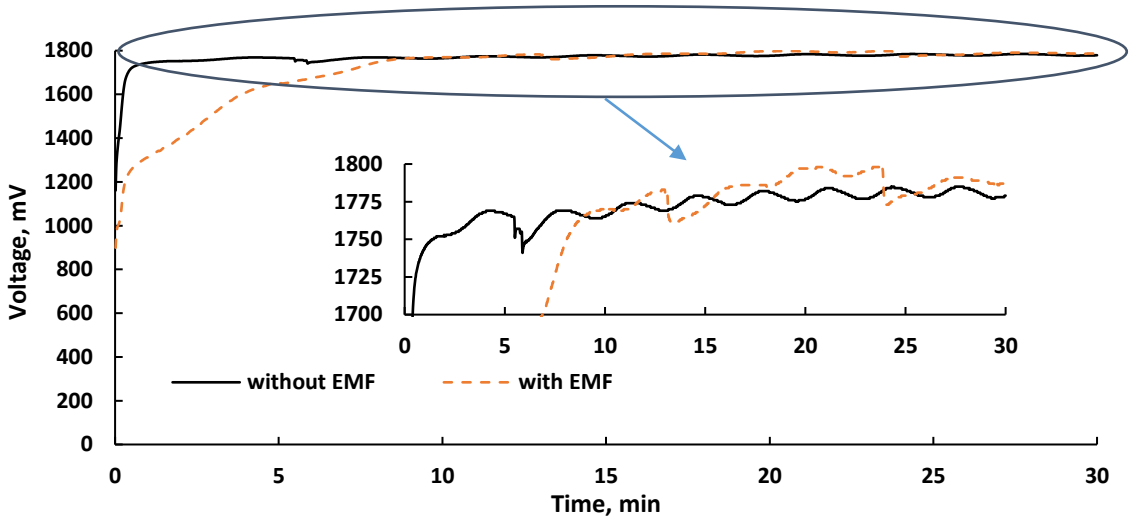

Figure 5.10 Voltage vs. time graph (galvanostatic mode with/without EMF, time; 30 min, applied temperature; 197 ℃, N_2 flow rate; 0.14 L/min, and H_2 flow rate; 0.05 L/min) and 0.3 A applied current.

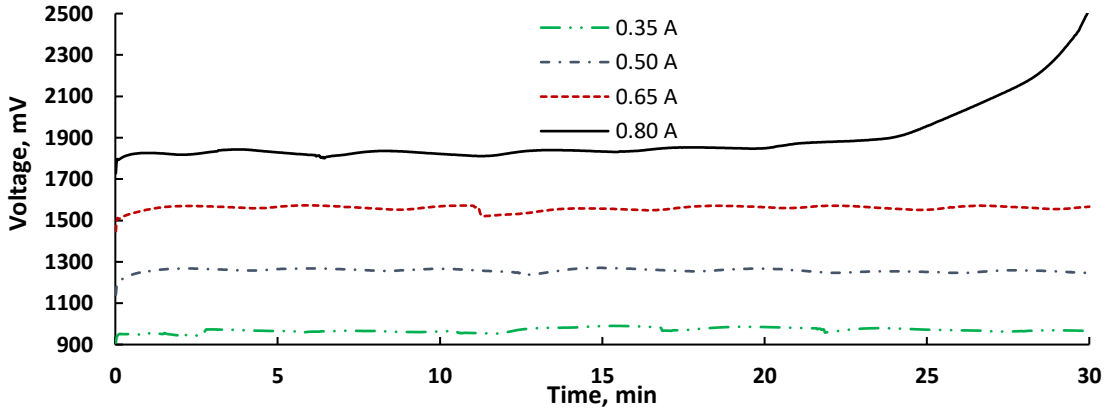

Figure 5.11 Change in current vs potential. The conditions including temperature and volume flow are maintained the same.

The presented graph in Figure 5.11 shows the comparison between different applied current densities and the equivalent recorded potential. Thus, it is concluded that the reaction rate of formation of ammonia is driven by the catalyst. The higher potential is equivalent to slower reaction rate and higher Gibbs free energy, while the lowest potential

recorded is equivalent to the fastest reaction rate and lowest activation energy. Ammonia is a base and due to its solubility, it is easy to trap ammonia in acid. The Titrimetric method is the standard method to measure dissolved ammonia with a lower limit of 20 µg in 100 ml of boric acid. The presented results are titrated multiple times for better accuracy. Thus, the ammonia formation rates presented in this finding are arguably better than some of the formation rate presented in the literature. The Faraday efficiency recorded is found to be 5.4 %, the energy efficiency is found to be 2 % and the exergy efficiency is 1.89 %.

Electrochemical impedance and chronopotentiometry results of the lab scale ammonia synthesis reactor

To investigate the stability of the ammonia synthesis reactor, electrochemical impedance, and chronopotentiometry scan are performed. Firstly, chronopotentiometry test is conducted. The potential is measured averse to the counter electrode for an elapsed time of 200 min by applying a current pulse. It is noted in Figure 5.12, that the eutectic mixture of NaOH and KOH shows stability when the current is stepped between the electrodes. In the beginning, the recorded potential is low due to ohmic losses, accompanied by a gradual change that is caused by overpotenial which is developed as the nitrate and hydrogen is depleted at the electrode surface. When the current is greater than the limiting current, the necessary flux for the current cannot be rendered by diffusion

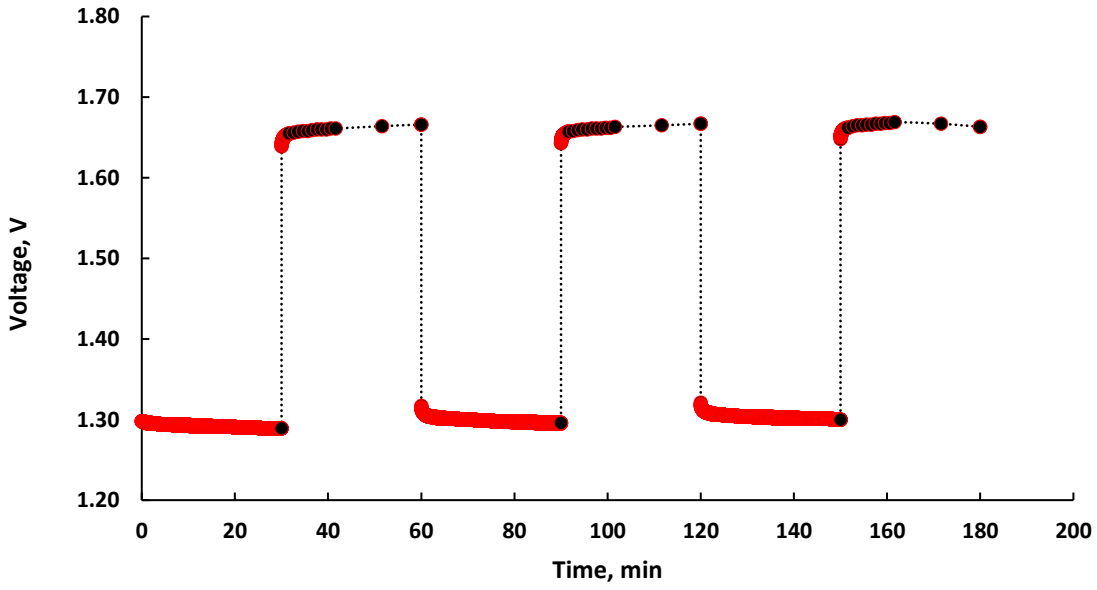

Figure 5.12 Chronopotentiometry graph (temperature; 197 ℃, N_2 flow rate; 0.14 L/min, and H_2 flow rate; 0.05 L/min)

Thus, the potenial across the reactor rises until it exceeds the the electrode potential for the reduction of nitrogen and ammonia formation. The concentrated red dots in Figure 5.12 are due to the developed concentrated over potenial caused by iR loss. Eventually, the equlibrium nickel electrode potenial is achieved and chemical difussion is recorded. For the aforementioned tests, 30 samples are collected. Then, the titration method is applied to calculate the amount of dissolved ammonia in boric acid. The measured sample is equivalent to repeated titration of the sample. In the presence of ammonia, the prepared boric acid changes color to green, this is caused by the mixed indicators. Then the Faraday efficiency is measured and the ammonia formation rate per current density is calculated. Figure 5.13 shows that the electrochemical reactor achieved a Faraday efficiency of 5.14 % and 170 mg of ammonia are synthesized.

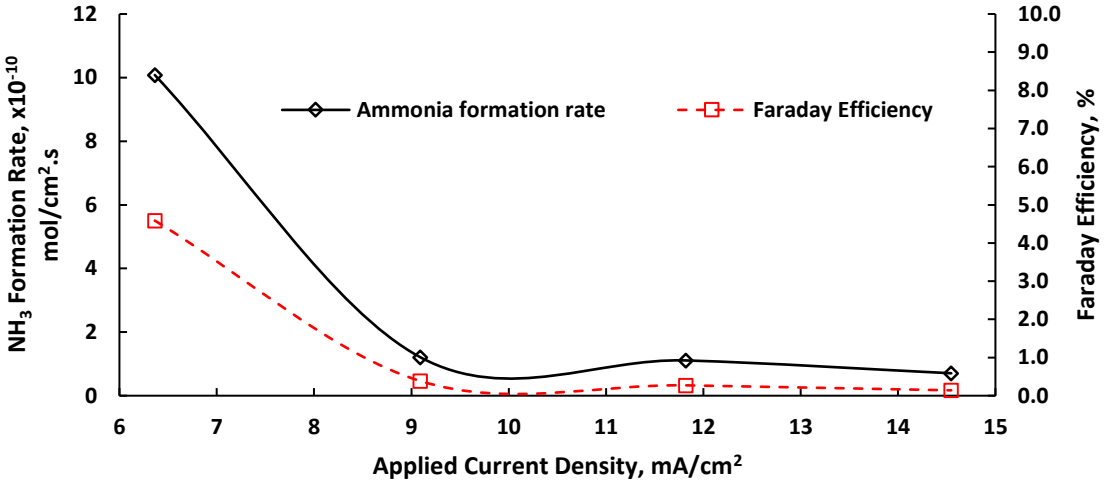

Figure 5.13 Ammonia formation rate and Faradaic efficiency graph with respect to various applied current density.

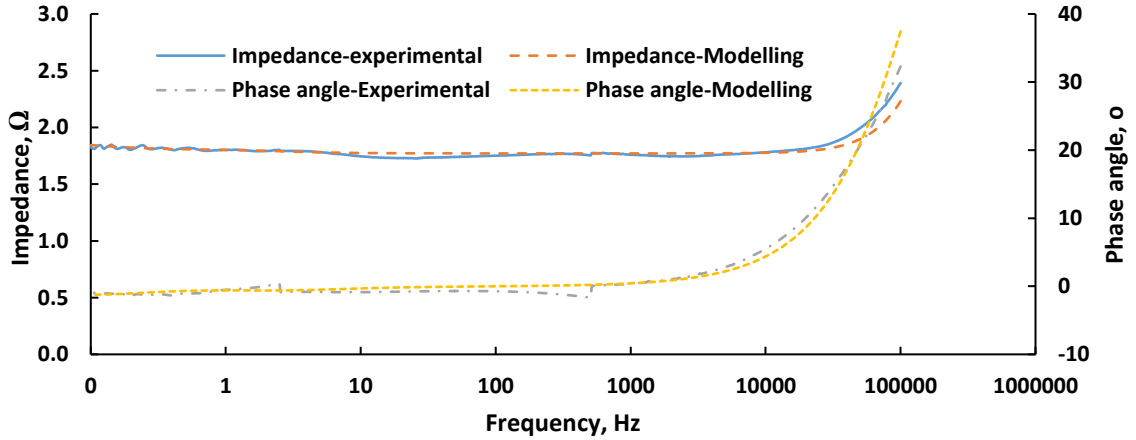

Figure 5.14 Experimental and modeling results of the electrochemical impedance spectroscopy performed on the ammonia synthesis reactor.

The Bode plot results of the EIS study is presented in Figure 5.14. The increase in frequency results in increase in the impedance and phase angle. However, a drastic jump in the impedance values is observed as the frequency is increased higher than 10000 Hz. Furthermore, the EIS circuit model fit is also shown in Figure 5.15. The parameters obtained for the equivalent circuit modelled in Figure 5.15 calculated. The Rs parameter is obtained to be 1.77 Ohms.

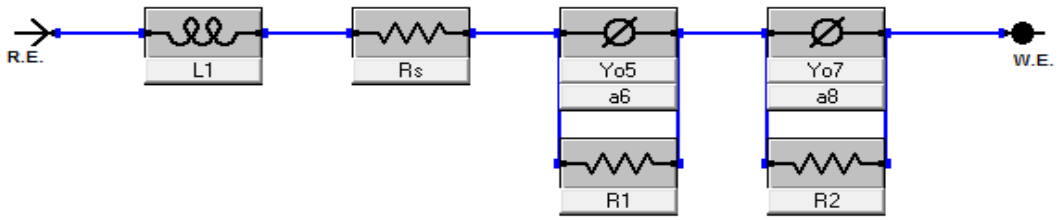

Figure 5.15 Equivalent circuit model for the electrochemical impedance spectroscopy.

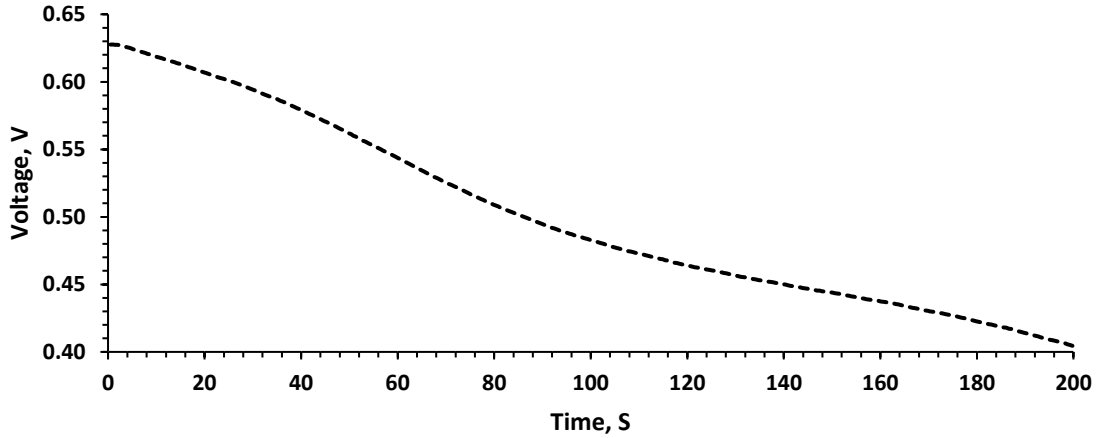

Figure 5.16 Open circuit voltage graph displaying the voltage drop across the reactor at the end of the experiment.

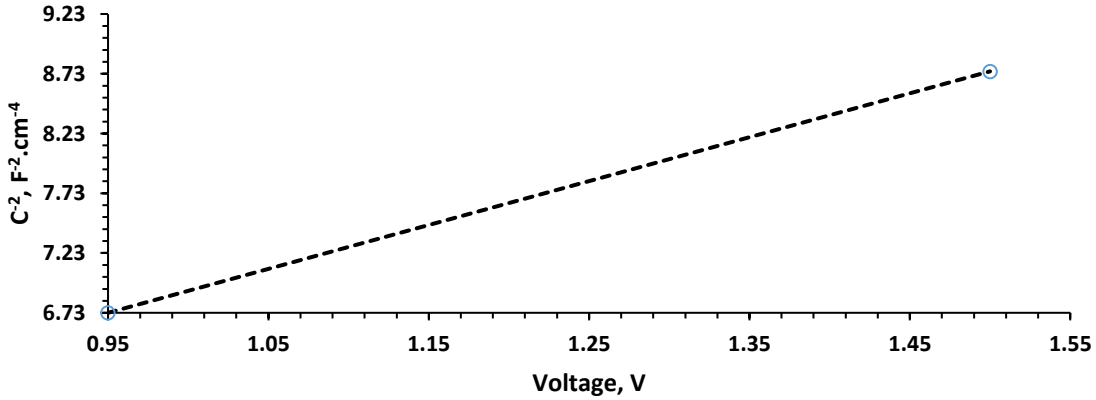

Figure 5.17 Mott-Schottky graph showing the built in potential and conduction band level in the reactor.

5.2 Mathematical modeling results for the lab scale ammonia synthesis reactor

The presented modeling equation of the ammonia synthesis reactor is built in engineering equation solver (EES). The model is set in single dimension analysis. In order to provide and model the ammonia synthesis reactor several input parameters are tabulated and uncertainties are incorporated into the results section to account for the accuracy of the ammonia production rate and consistency. As derived in the literature and analysis section, the ammonia synthesis reaction is derived by three main parameters; temperature, pressure, and volume. However, in this thesis, the ammonia is synthesized electrochemically. Thus the pressure effect is not presented. In order to understand the effect of pressure vs. atmospheric electrochemical ammonia production, the parametric study is integrated with pressure variation and the Faraday, energy, and exergy assessment is concluded. For, this, ammonia dynamic equilibrium is considered optimal when the temperature of the reaction is 200 ℃ and pressure is at 200 atm. If the temperature is increased the equilibrium reaction shifts towards the reactants by absorbing the heat and decreasing the temperature of the reaction and the opposite is true. However, the lower the temperature, the slower the reaction rate is. Thus, finding the suitable temperature and pressure are essential as shown in Figure 5.18, the mole fraction of ammonia is higher at low temperature and much lower at 1000 K.

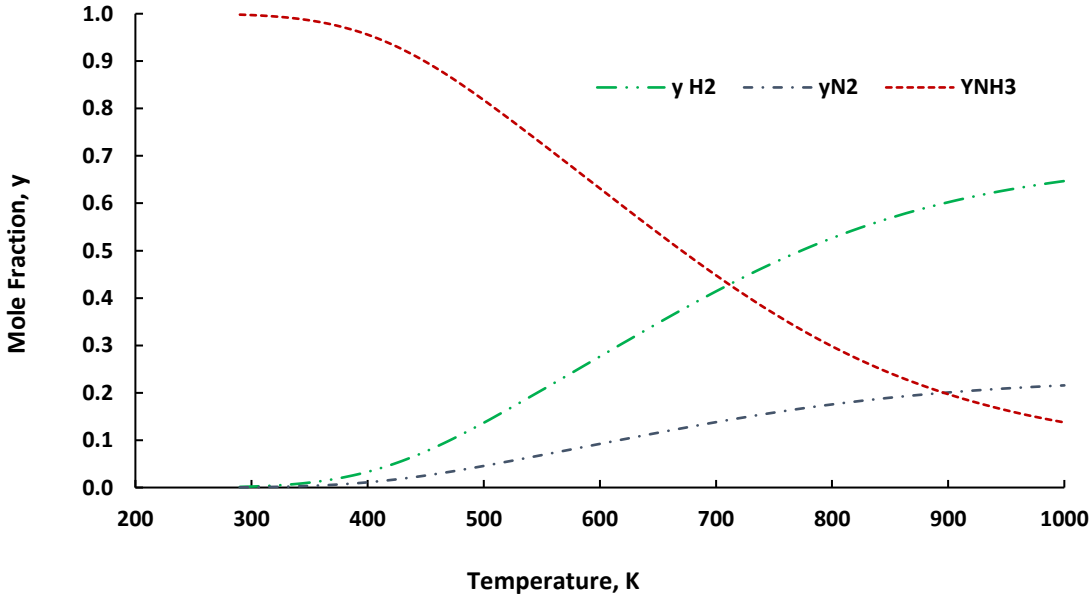

Figure 5.18 The variations of mole fraction as a function of temperature.

Increasing the pressure in the ammonia synthesis reactor cause the reactant to react and reduce the applied pressure and thus the equilibrium reaction shifts toward the products. So, the optimal conversion rate is concluded to be driven by high pressure and low temperature, high production, and maintenance cost and energy consumption. For that, the advantage of developing and investigation of electrochemical reactors is essential since the operational conditions of the reactor to synthesis ammonia is attained at atmospheric pressure as shown in Figure 5.19 the mole fraction of ammonia is 40 % at 200 to 300 bar.

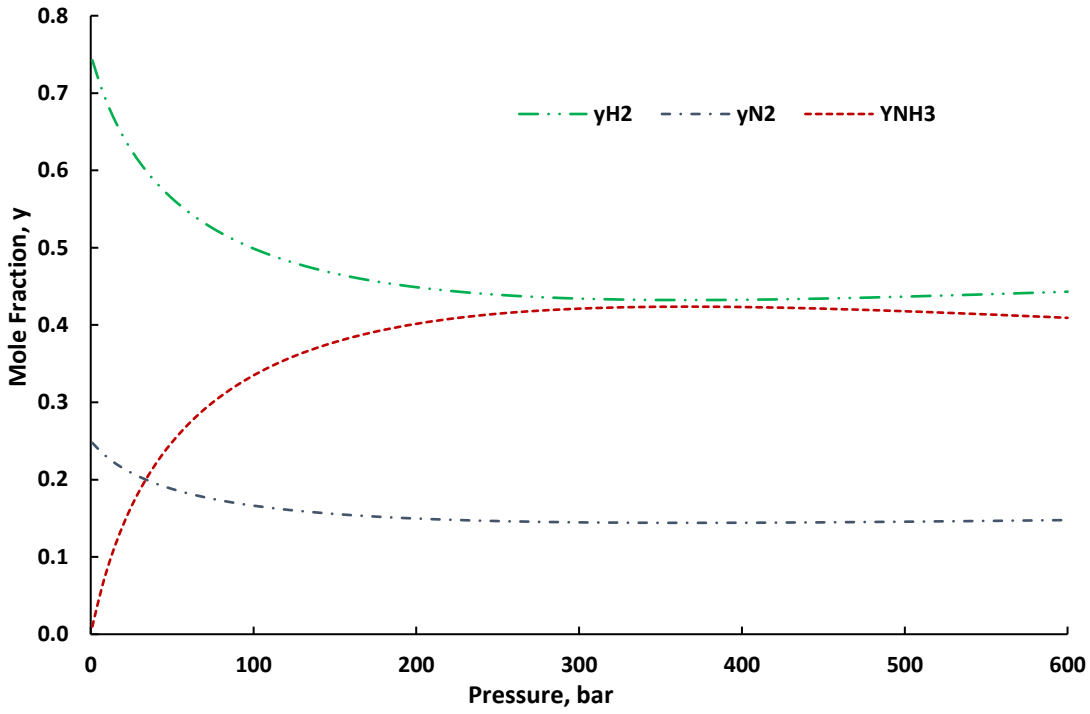

Figure 5.19 Variations of mole fraction as a function of pressure.

Investigating the power consumption for the electrochemical ammonia synthesis reactor, it is convincible that the power consumption based on energy consumption or input is by far much desirable than the energy consumption of high pressure temperature operating the reactor. The illustrated Figure 5.20 and Figure 5.21 show the power consumption of the electrochemical cell used in this thesis has a higher limiting power consumption of 1.4 W and lower limit of 0.3 W. Thus reducing the pressure and having desirable conversion rate in necessary.

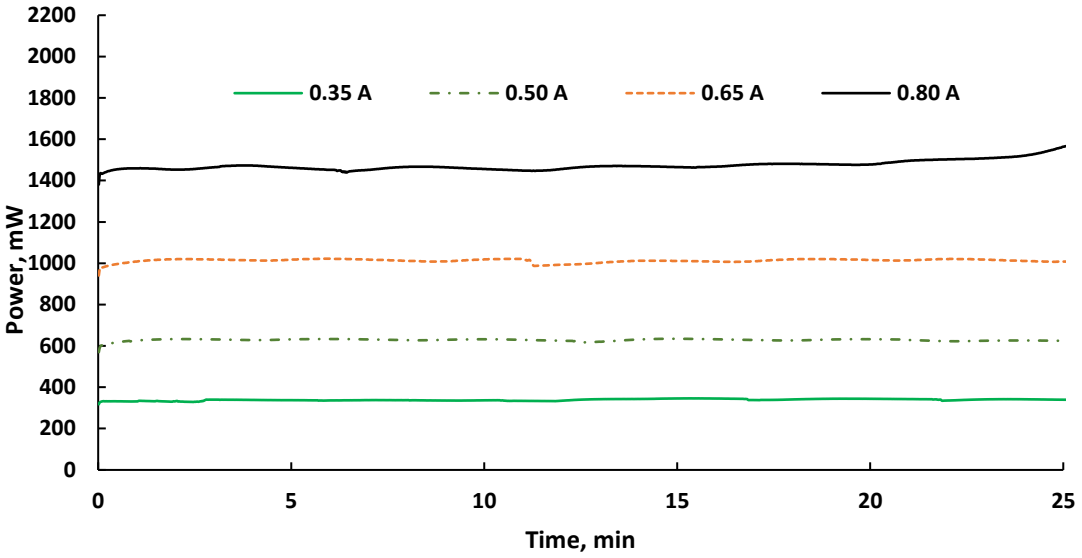

Figure 5.20 Power consumption of the lab scale reactor is desirable and essential for ammonia synthesis.

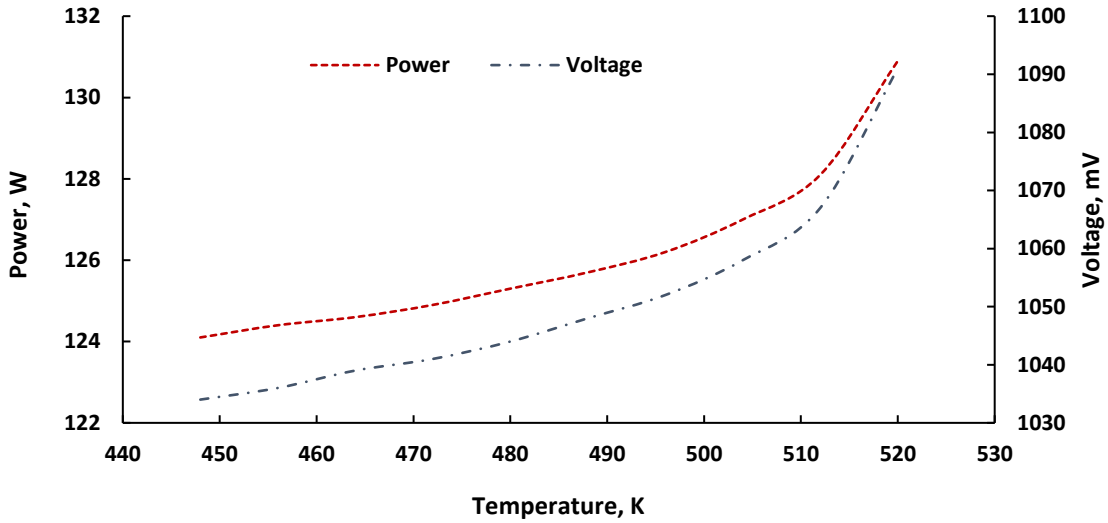

Figure 5.21 Power consumption of the ammonia synthesis reactor and the voltage needed to drive the reaction rate are inversely proportional to current density.

Although the increase in pressure dissipated higher conversion rates. However, the volume flow rate is inversely proportional to the mass flow rate as shown in Figure 5.22. When the volume of the ammonia increase the equilibrium reaction shifts towards the reactant as fewer molecules are favorable to the equilibrium of the reaction. Thus the need to extract ammonia is imperative to the ammonia synthesis rate. Withal, the next chapter argues the integration of a turbine as a means to extract ammonia from the reactor and produce power.

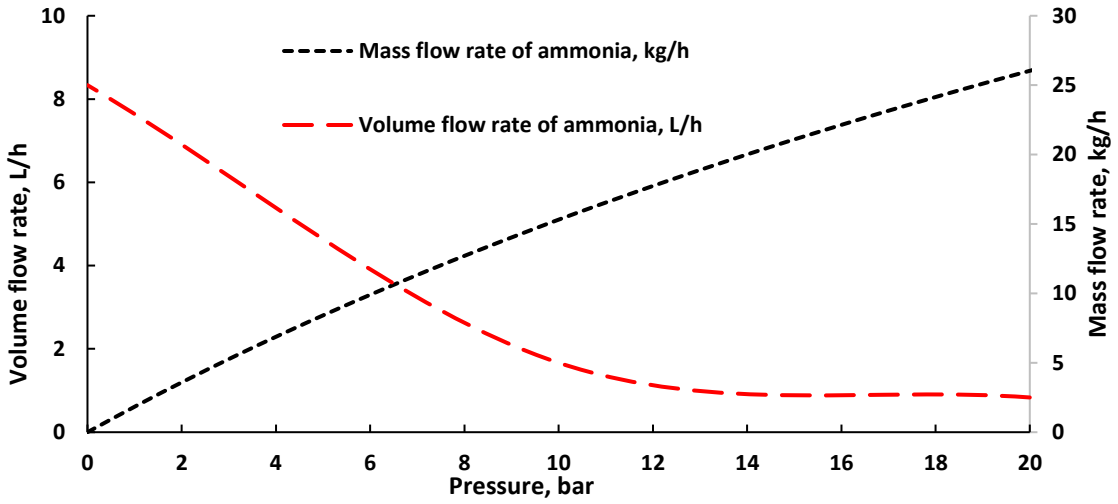

Figure 5.22 The change in pressure is proportional to the mass flow rate and inversely proportional to the volume flow rate.

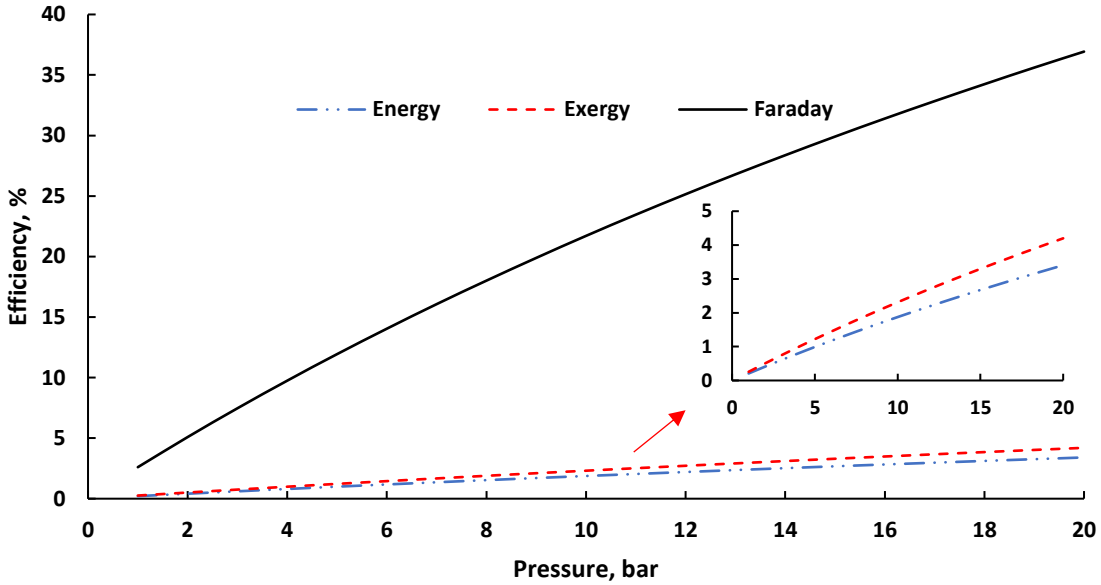

Figure 5.23 Varying the pressure results in high energy, exergy and Faraday efficiency.

Thus, to distinguish between the effects of pressure, temperature, and volume on the ammonia synthesis rate. The parametric study strongly shows that the conversion rate is driven by high pressure low temperature, and volume flow rate which shares a number of similarities in published journals. As a result, increasing the pressure will result in high conversion rate and elevated energy exergy and faraday efficiency as shown in Figure 5.23 for ammonia synthesis. Although it is concluded to attain high Faraday, energy and exergy efficiency, high pressure is required for ammonia synthesis.

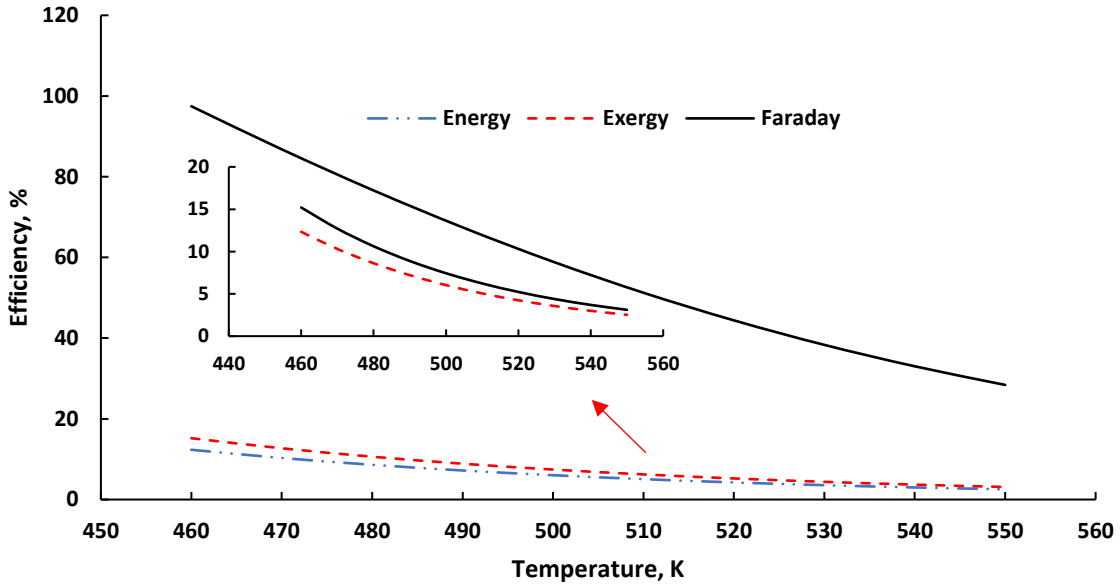

Figure 5.24 Varying the temperature results in low energy, exergy and Faraday efficiency.

The temperature is varied from 460 to 550 K, the efficiency of the system is reduced to 16 %, 18 %, and 98 % for energy, exergy and faraday respectively, to 2 %, 3 %, and 16 % for energy exergy and faraday respectively. Thus, this parametric study verifies that excessive temperatures are not desirable for ammonia production. Furthermore, to compare the conventional parameters; pressure, temperature, and volume flow, on the effect of ammonia synthesis. The following parametric study is built in EES using the electrochemical impedance spectroscopy results from Figure 5.15.

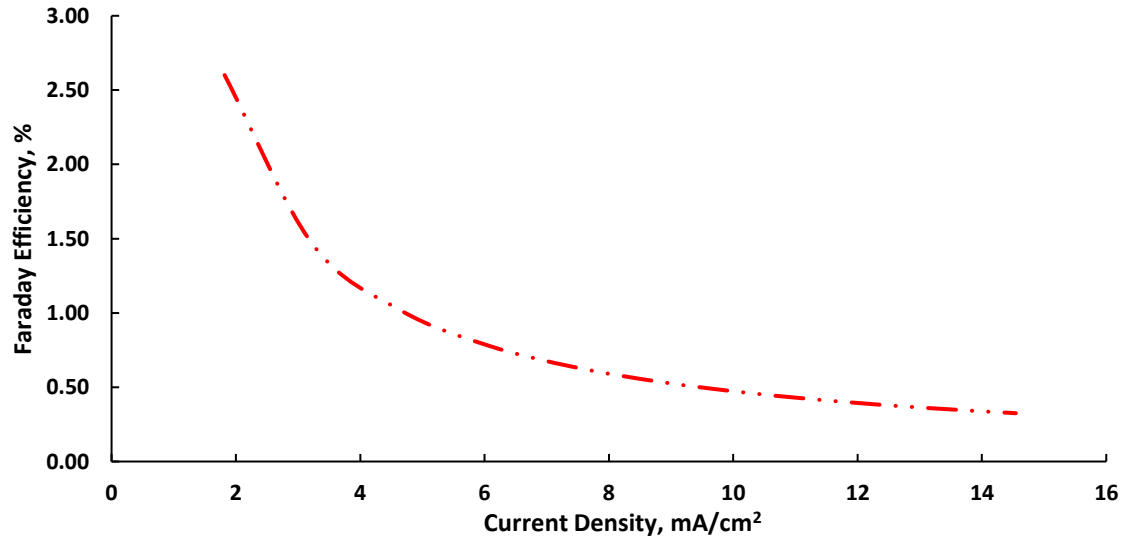

Figure 5.25 Increasing the current density shows desirable Faraday efficiencies.

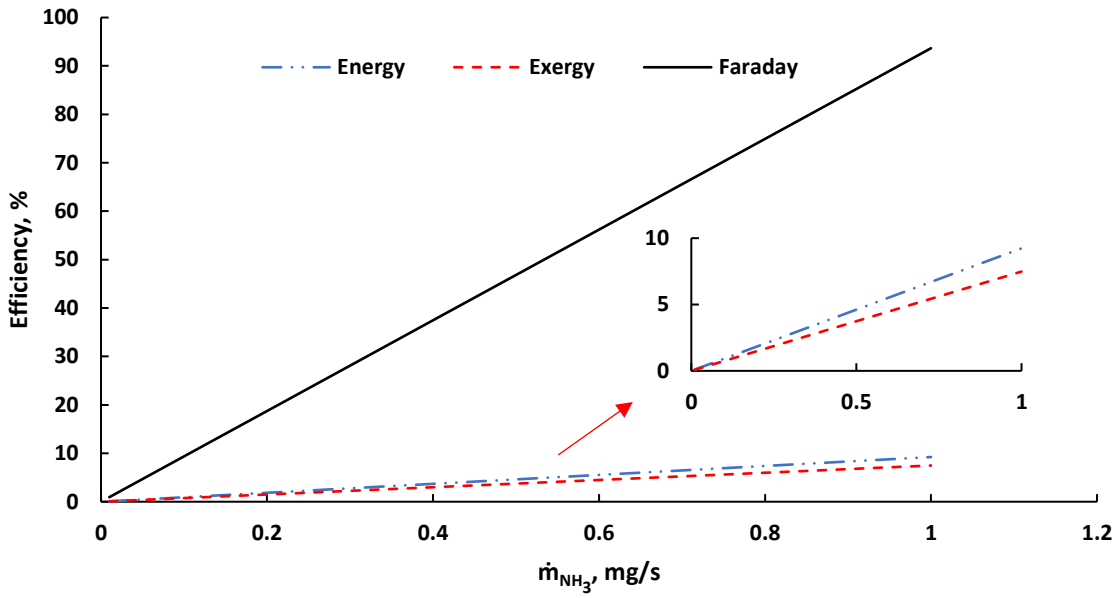

Figure 5.26 Ammonia production rate consistent with high Faraday, exergy, and energy efficiency.

The lab scale electromagnetic induced ammonia synthesis reactor kinetics presented in the analysis section is provided in EES software. The first parametric study suggests that high current densities result in low Faraday efficiency. However, these results should be treated, analyzed with attention. Since the input of the system is driven by an electromagnetic field and none of the published journals provide considerable work in this new field. The results are the input of a square regression and the function is feed to the equations. Withal, increasing the current density show a drop in the overall faraday efficiency to 0.3 % at 13 mA/cm^2. Moreover, when the current density is 1.5 mA/cm^2 the resulting faraday efficiency is 3.23 %. These results confirm the experimental galvanostatic results. The decrease in the Faraday efficiency can be interpreted by the excess of current flowing through the electrodes, iron oxide catalyst and reversing the synthesis reaction to H_2 and N_2. The evidence of the effect of the electromagnetic field on ammonia synthesis is related to current density and not affected by an increase in the volume of the products. Thus this finding validates the usefulness of this data for further investigation. Although, the ammonia synthesis reactor is effected by current density. The assessment of varying the flow of hydrogen on the energy, exergy and faraday efficiency is investigated. In addition, the nitrogen fixation/ reduction is also studied to highlight/validate the

practicality of the electromagnetic induction in ammonia synthesis molten salt electrolyte suspended in nano particles iron oxide Fe_2O_3.

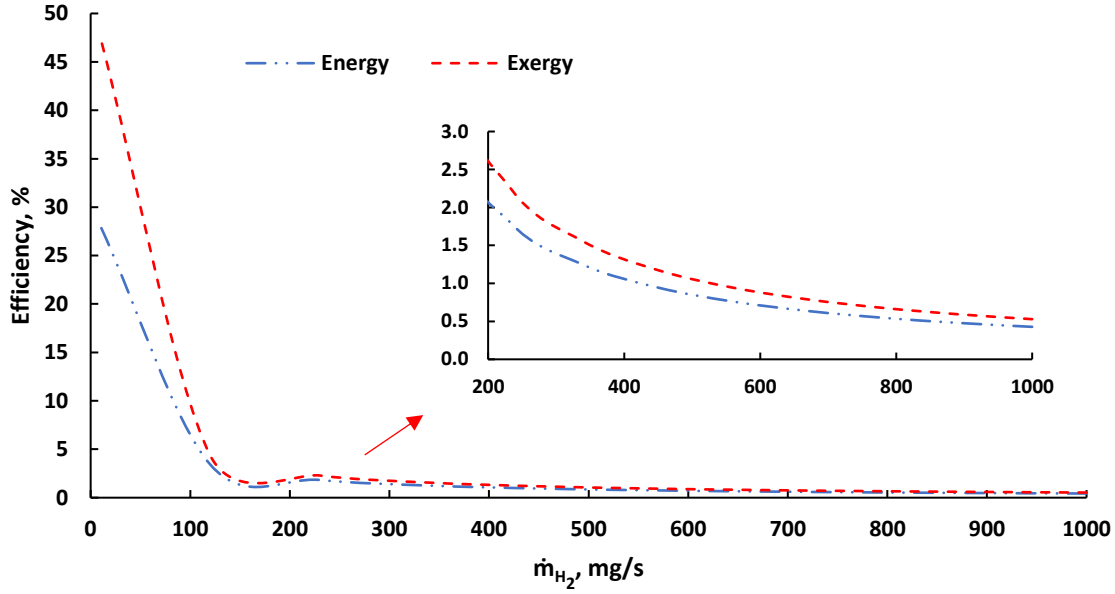

Figure 5.27 Energy, and exergy efficiencies decrease as the mass flow rate of hydrogen increase.

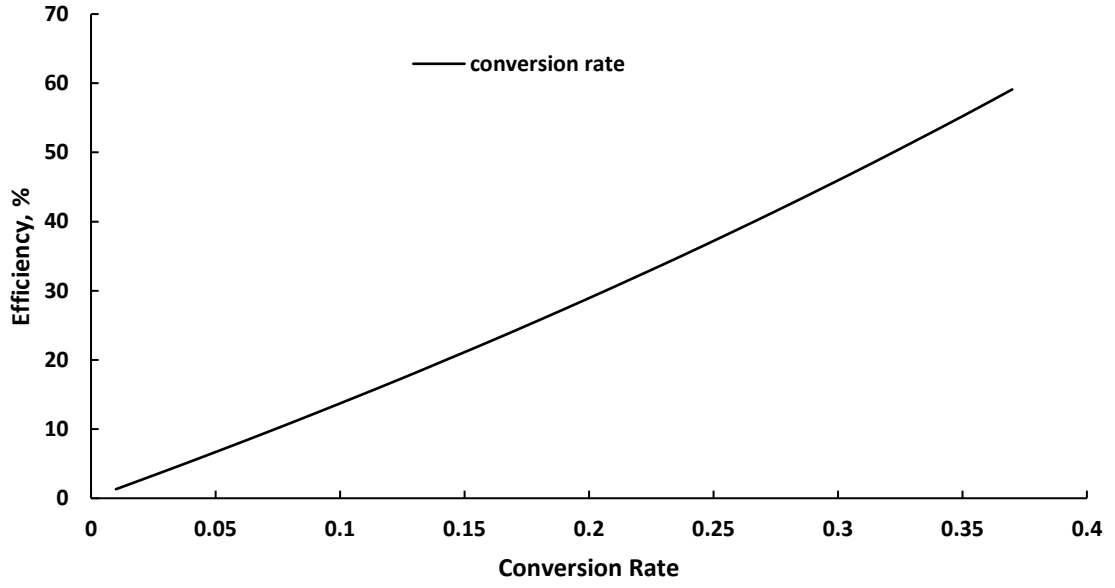

Figure 5.28 Faraday efficiency is linearly proportional to the conversion rate of nitrogen and hydrogen to ammonia.

The parametric study; varying the mass flow of hydrogen, show interesting results on the overall efficiency of the system. As dissipated in the Figure 5.28. The increase in

hydrogen flow rate is not efficient and this can be argued, when the hydrogen volume is maximized inside the reactor the OH^- ions from the NaOH and KOH instead of increasing the ionic conductivity, few are dissolved with hydrogen to form water condensate. This is evident from the water condensation in the tubes developed during the experiments, upon increasing the hydrogen flow rate and thus decreasing the overall efficiency including faraday, energy and exergy efficiency.

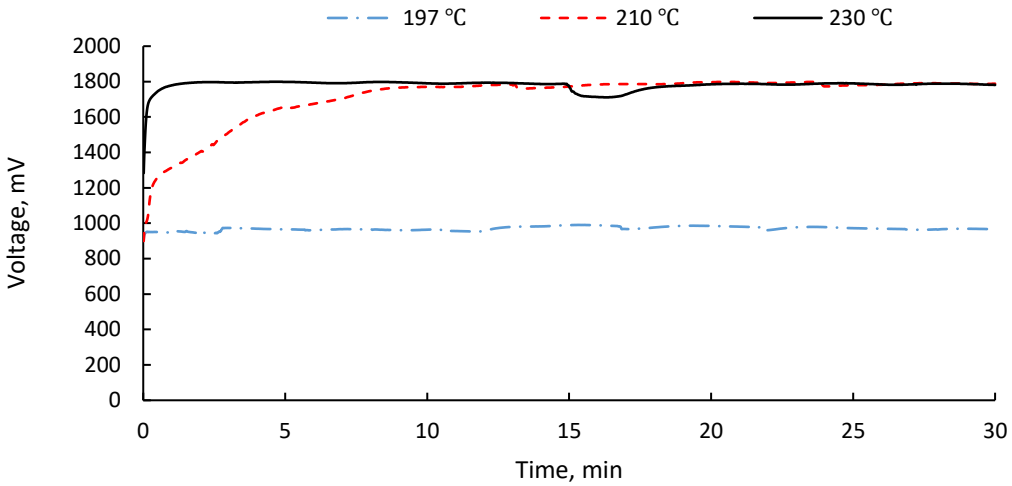

Figure 5.29 Comparison of applied potentials under various operating temperature with the same applied current value; 0.35A.

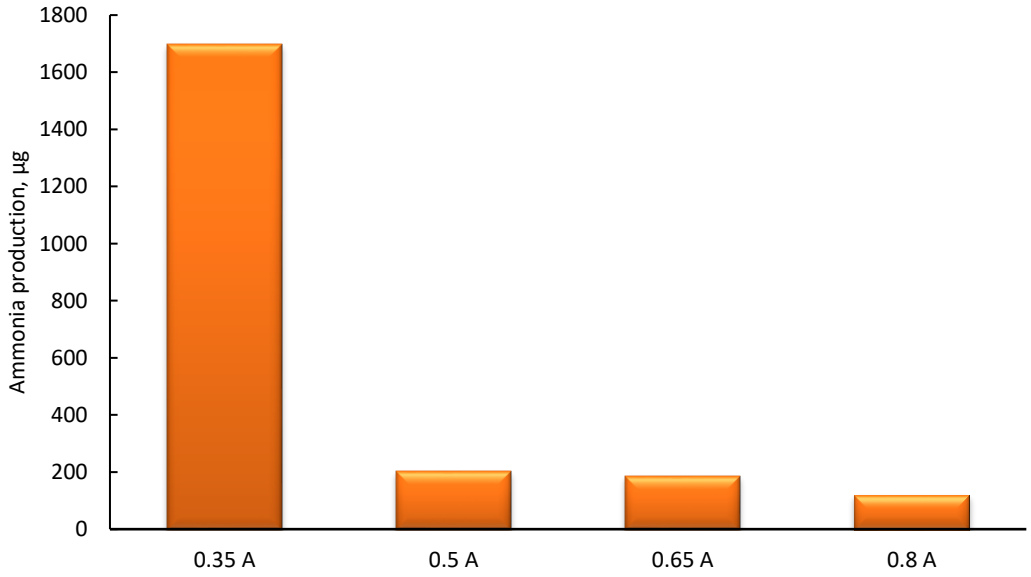

Figure 5.30 Comparison of ammonia production under various operating temperature with the same current value.

5.3 Results of the theoretical integrated energy system

It is evident that the reaction of hydrogen and nitrogen is driven by three main properties: temperature, pressure and volume. Thus, the proposed system characteristics are developed based on the law of Le Chatelier. The overall schematic diagram shown in Figure 5.31 consists of five subsystems, the reformer unit which consists of primary and secondary reforming, the CO conversion unit which consists of a high-temperature-shift reactor and a low temperature-shift reactor, the CO_2 removal unit, methanation, dryer, the ammonia synthesizer, and the integrated 2 stage expander unit.

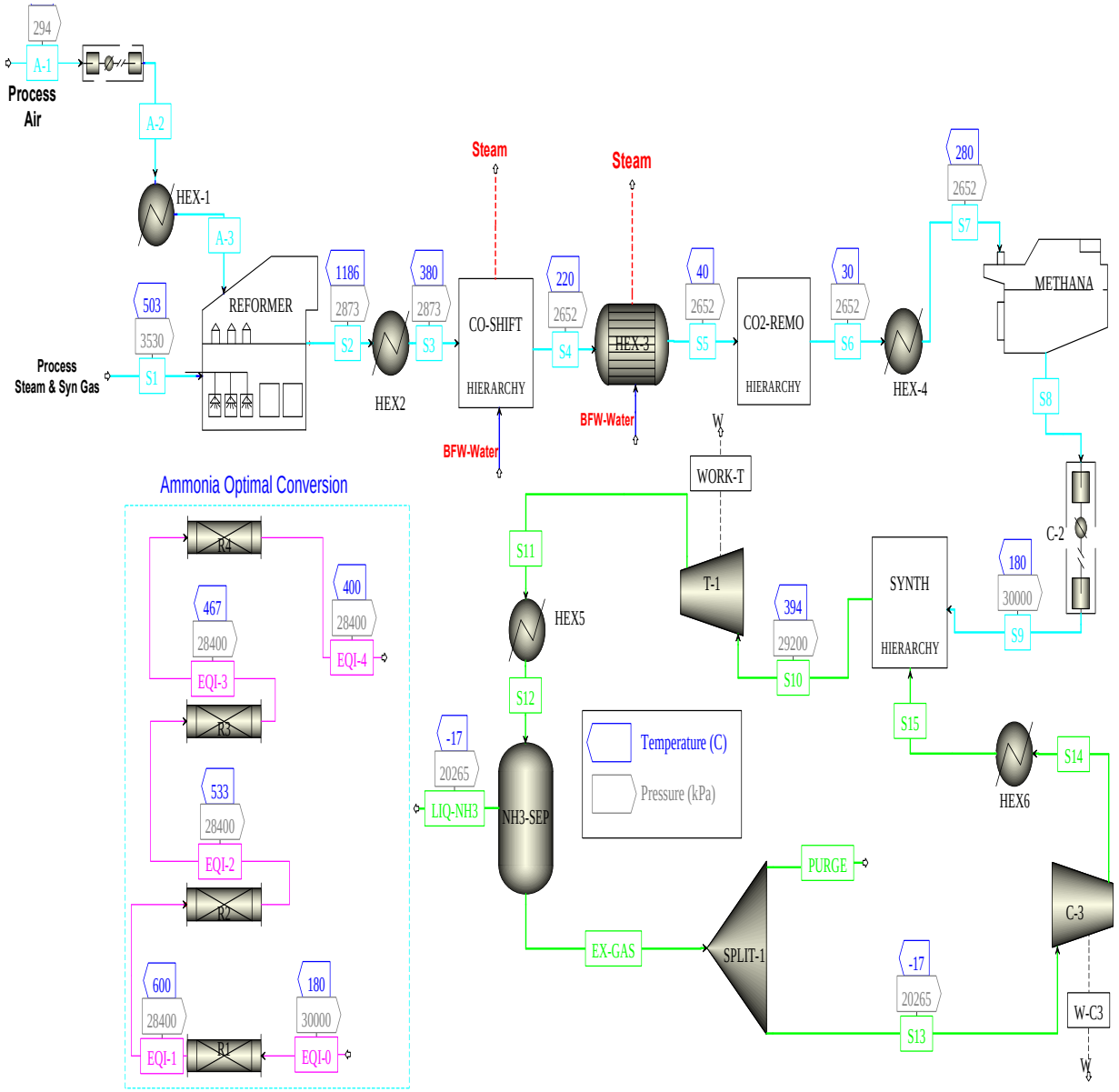

Figure 5.31 Ammonia unit is presented in aspen with temperature and pressure across main reaction unit.

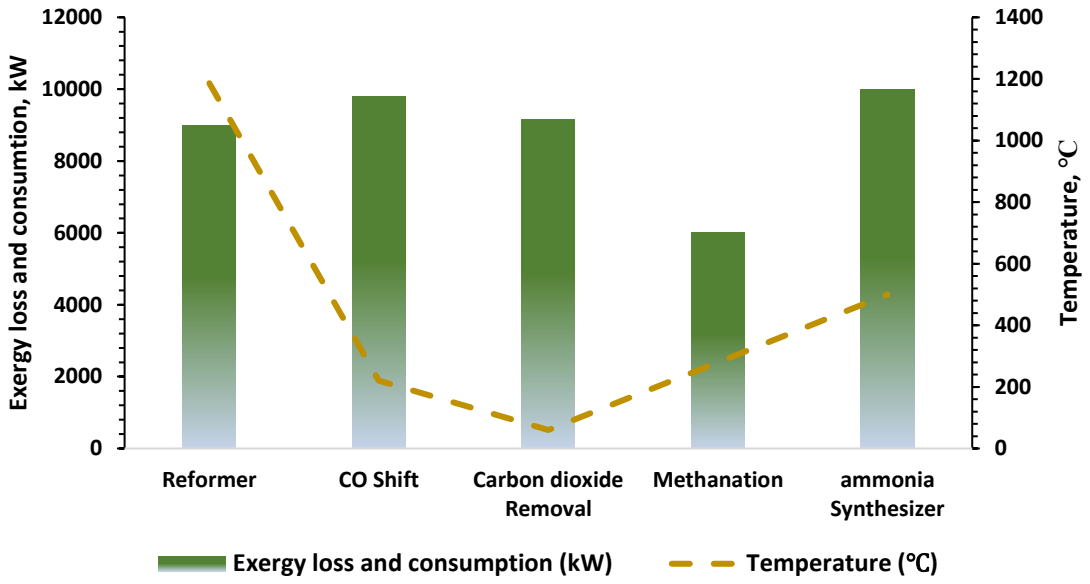

Figure 5.32 Exergy loss and consumption across the main units of the integrated energy system.

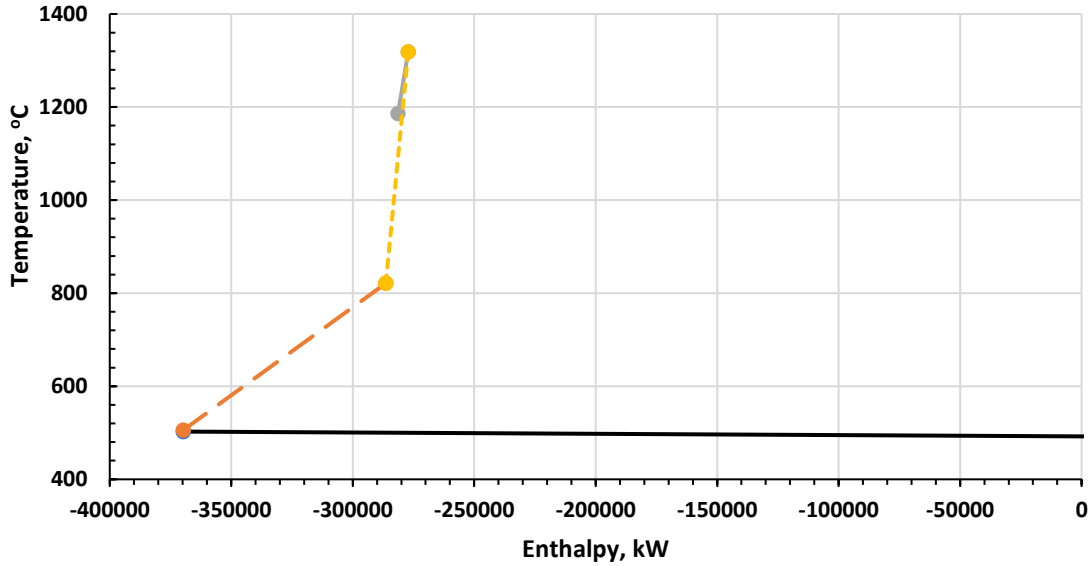

Figure 5.33 The negative enthalpy rate shows that the reaction across the unit is endothermic.

The reformer unit shows an exergy loss and consumption of 9003 kW as dissipated in Figure 5.32 with a temperature of 1186 °C. Taking into consideration that the 3- plug reactors represent the firing zone of a reformer unit and graphing the enthalpy flow versus temperature. It is concluded that reaction in highly endothermic with an enthalpy reaction rate of 35000 kW as shown in Figure 5.33. The carbon to hydrogen ratio is calculated at 0.81 while, the overall exergy efficiency of the reformer unit is 97 % is presented in Figure 5.34. The products of the reformer unit contain carbon monoxide with is poison to the

ammonia synthesis reactor catalyst. Thus, the undesired gas is introduced to the CO shift unit as shown in Figure 5.35. The high-temperature shift conversion unit, achieved an exergy loss and consumption of 2335 kW while the low-temperature shift reactor unit has an exergy rate of 743 kW. The drastic change in the exergy consumption and loss is due to the change in temperature across both reactors this is accomplished by a heat exchanger cooling the system with a high exergy rate of 538 kW and the by-product is superheated steam exiting the system at a temperature of 300 °C. The overall exergy efficiency of the CO shift conversion unit is 93.63 % which is considered moderate when compared to the reactor unit proposed by Marc Rosen [21] with an exergy efficiency of 76 %.

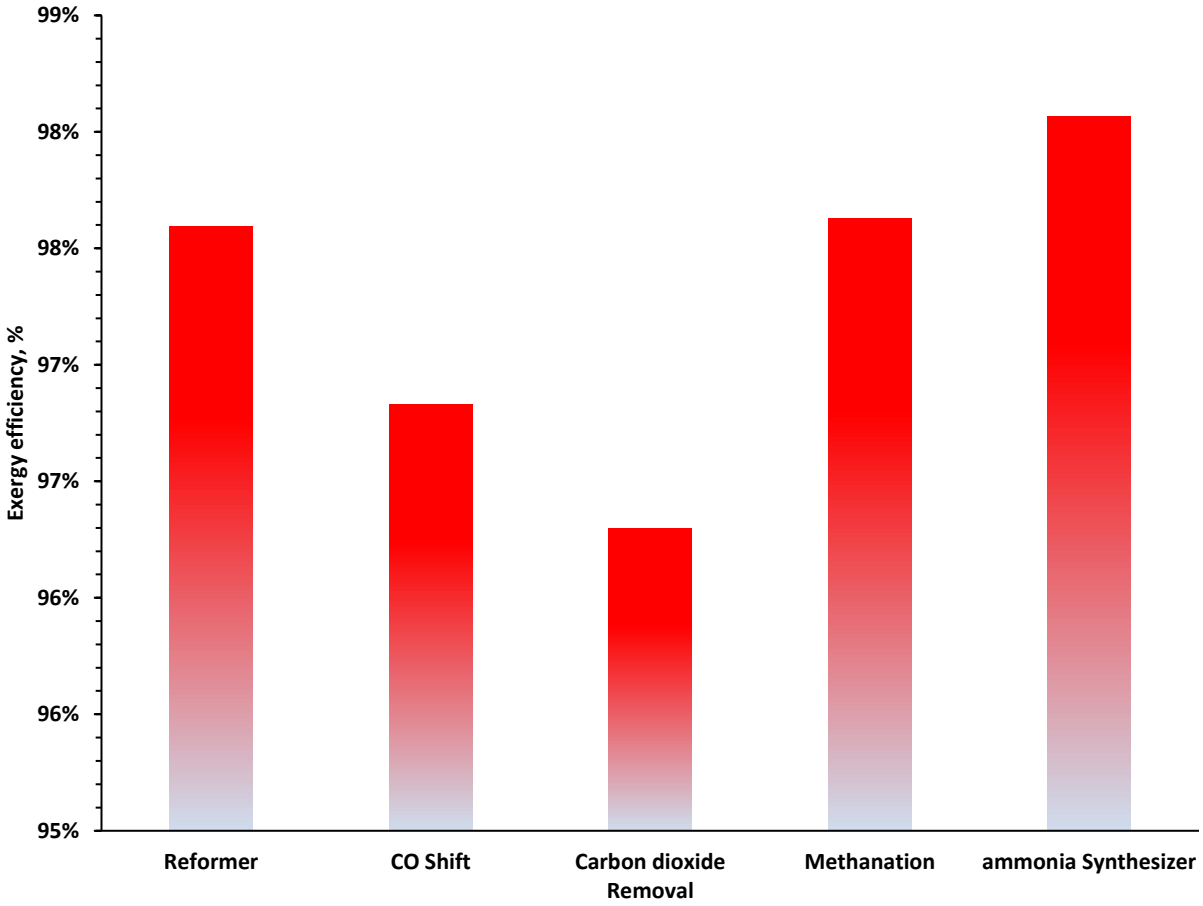

Figure 5.34 The highest exergy efficiency achieved in the ammonia reactor due to the recycle loop.

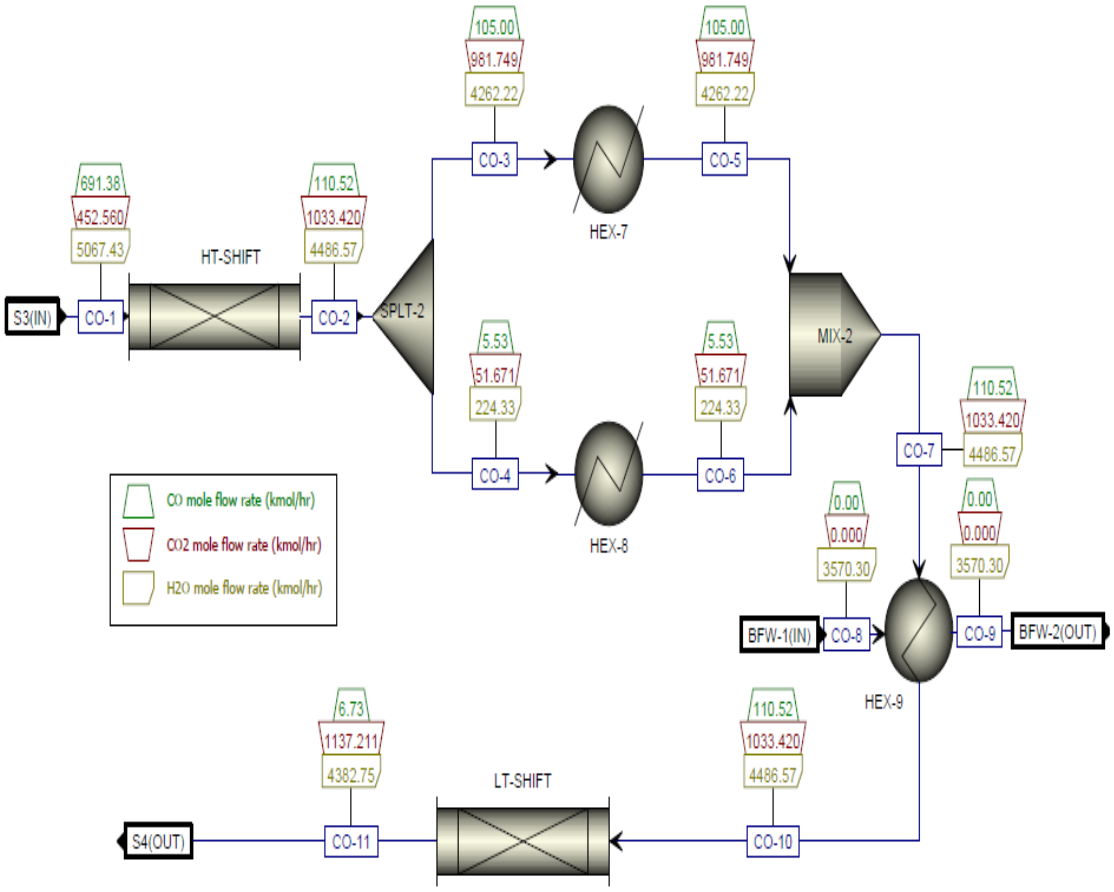

Figure 5.35 CO shift unit presented in Aspen Plus, the unit operates through the high temperature shift and low temperature shift reactor.

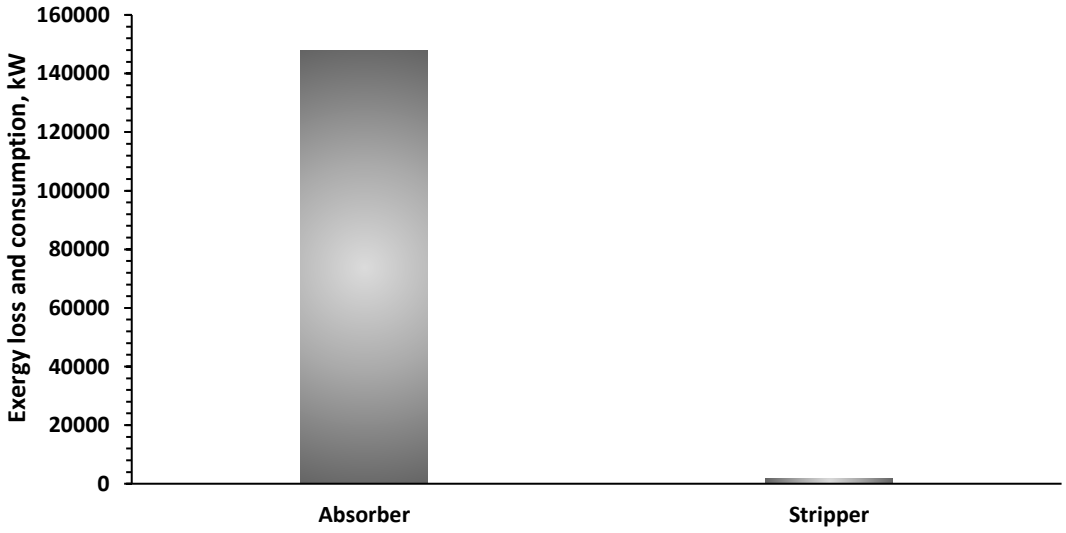

Figure 5.36 Exergy loss and consumption across the CO_2 unit.

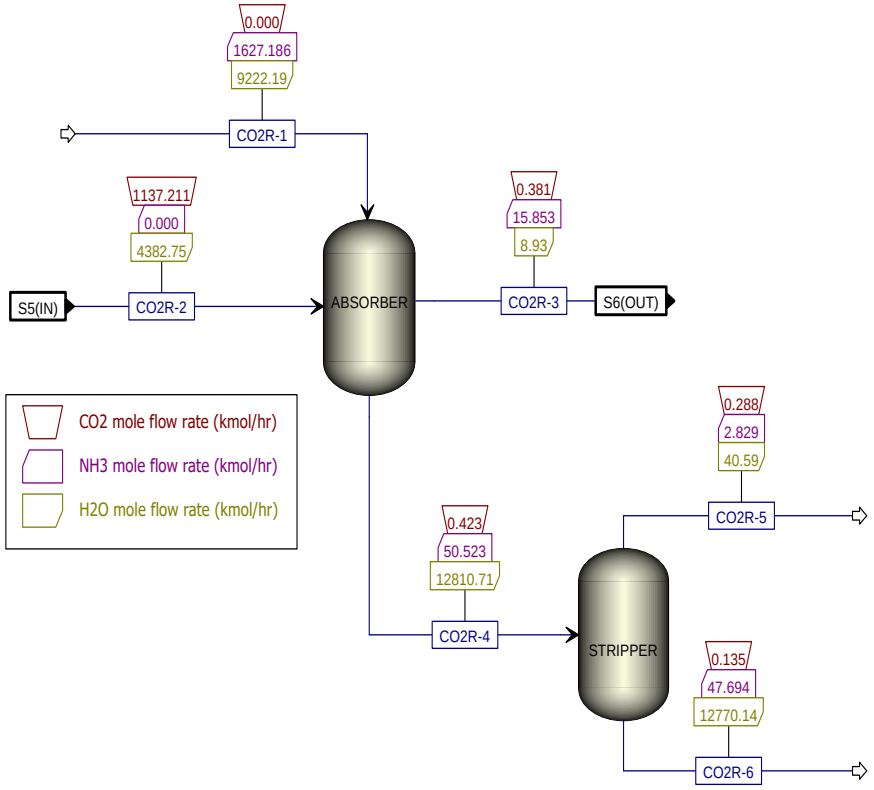

Figure 5.37 CO_2 removal unit in Aspen Plus.

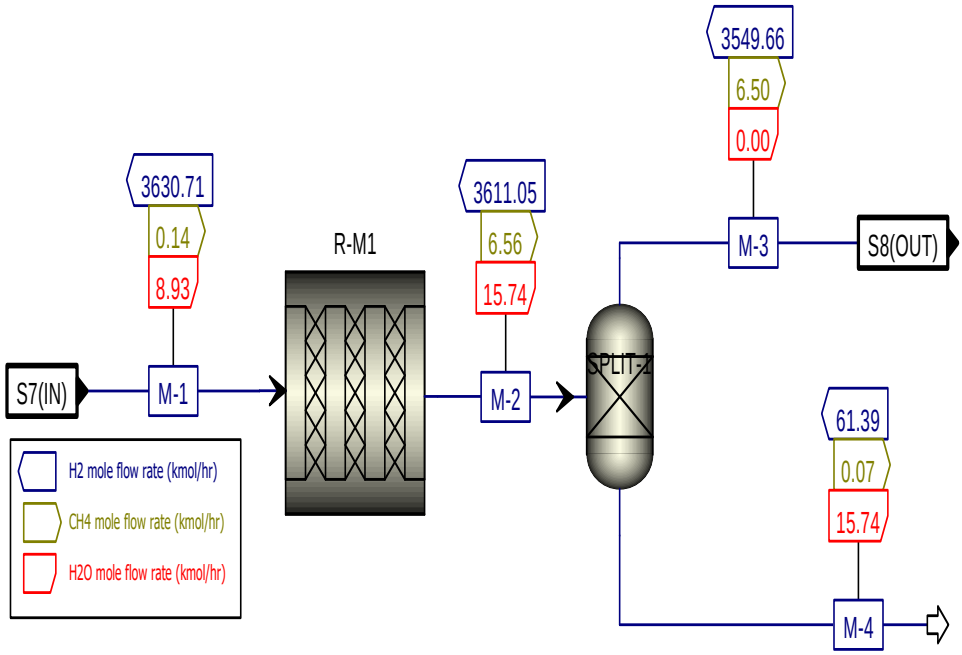

Figure 5.38 Methanation unit developed in Aspen Plus.

In the CO_2 removal unit in Figure 5.37, the absorber reactor absorbs most of the CO_2 in the presence of NH_3, and the by-products are hydrogen carbonate. The overall exergy efficiency of the unit is 96 % while similar operating units described in literature achieved lower exergy rate. Although the CO-shift conversion and CO_2 removal are efficient, small fractions of CO and CO_2 are poison for the ammonia iron catalyst reactor. Thus, they are chemically removed via methanation as shown in Figure 5.38 over a nickel catalyst.

The pressure and temperature and maintained in equilibrium throughout the process. The exergy efficiency of the unit is calculated at 97 % and exergy consumption and loss of 6000 kW. Excess gas purged outside the system is used in the steam reformer unit as fuel. The product of the methanation unit is called synthesis gas made of hydrogen and nitrogen. The stoichiometric ratio is adjusted before the synthesis unit to achieve $3H_2$ for $1N_2$ mole.

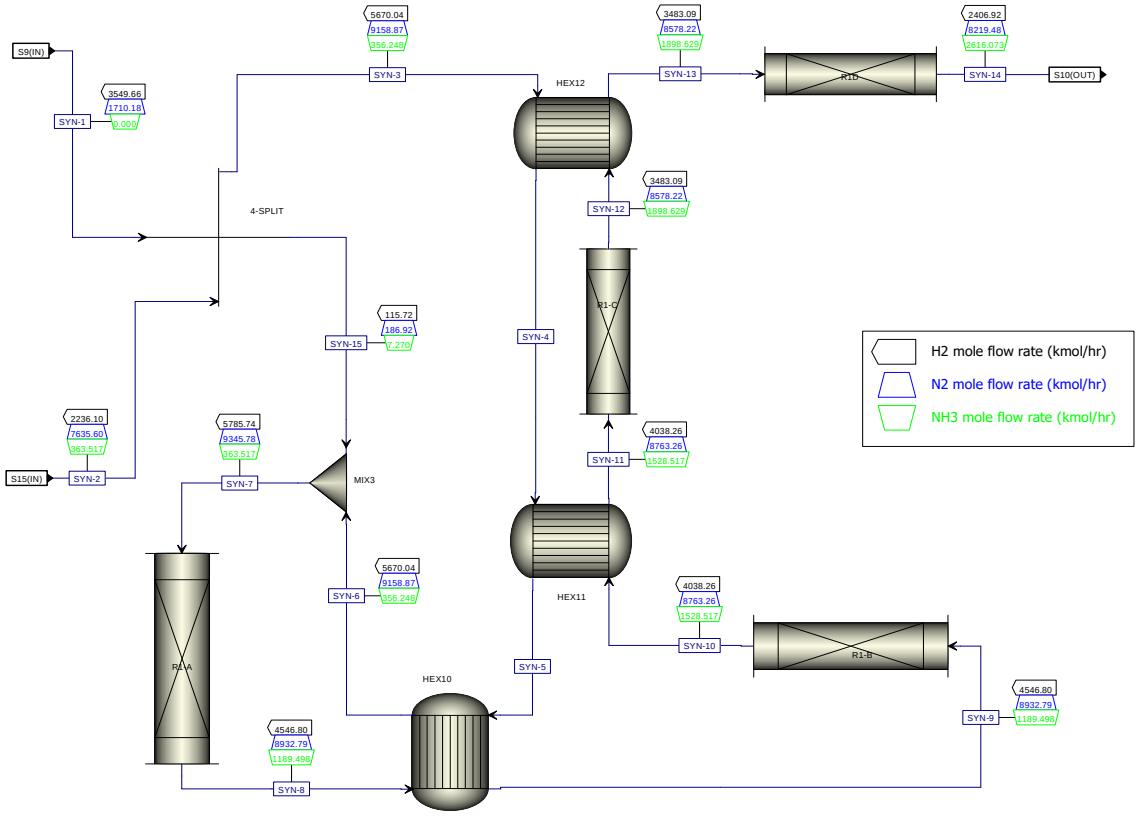

Figure 5.39 Ammonia synthesis unit built in aspen. The unit consists of 3 catalyst reactors and 1 convertor reactor. Syn-2 represents the recycle gas mixture back into the loop to achieve higher conversion rate.

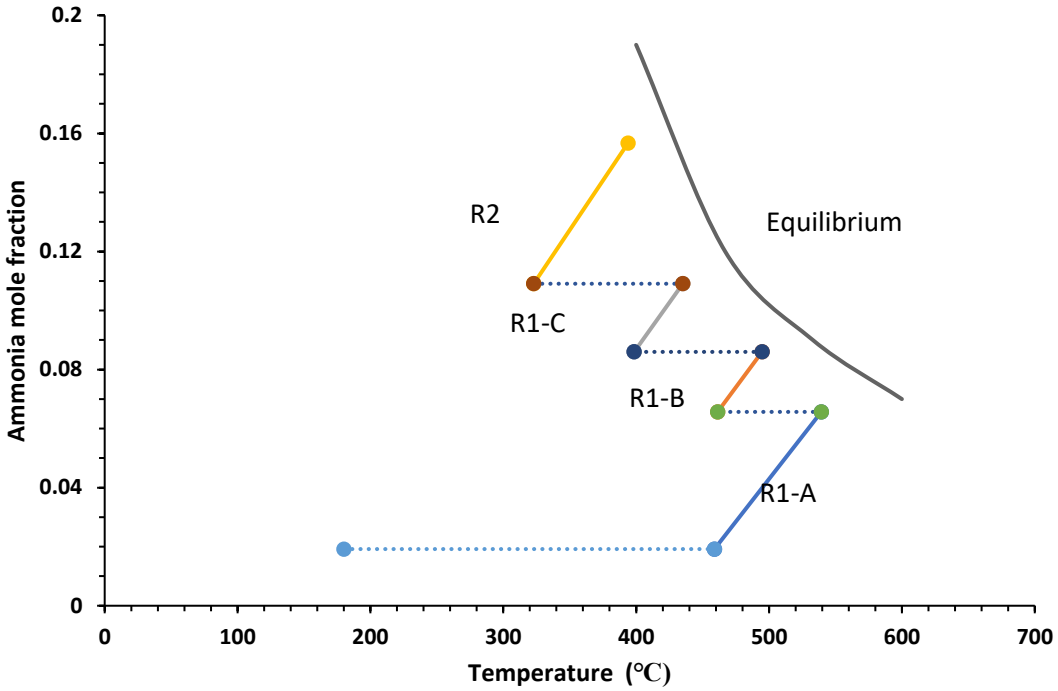

Figure 5.40 Conversion mole fraction in ammonia across each bed. While the equilibrium line shows the optimal conversion rate for ammonia unit.

The synthesis gas is compressed to 300000 kPa and H_2 and N_2 are catalytically converted into NH_3 in the SYNTH as shown in Figure 5.38. The exergy efficiency of the ammonia unit is 98 % and 38 % conversion. This is achieved by implementing a 2-stage expander unit to shift the reaction equilibrium towards the products. The work produced by the expander is used to operate the compressors C-1 and C-2 in Figure 5.31. The enthalpy rate of reaction across the catalyst bed shown in is 35000 kW and is highly exothermic. The ammonia produced is then separated in a separator with an achieved production rate of 2616 kmol/h. Unreacted gas is then compressed and heated up to 180 °C and 30000 kPa. Figure 5.40 shows the conversion ratio of ammonia across R1-A, R1-B, and R1-C catalyst bed and is compared to the optimal equilibrium conversion ratio of 0.19 at 400 °C. The exergy consumption and loss rate of 9991.6 kW, respectively.

CHAPTER 6 : CONCLUSIONS AND RECOMMENDATIONS

In this final chapter, the experimental system; lab scale electromagnetic induced ammonia synthesis reactor, summary is concluded based on the findings presented in the experimental part. Also, the summary of the second theoretical integrated energy system for power, steam and ammonia production is concluded based on the findings simulated through Aspen Plus. Finally, the illustration of future work on both systems and recommendations are provided.

6.1 Conclusions

Ammonia has attracted a lot of attention in recent years anticipated to its increasing demand as a feedstock to produce fertilizers also as an energy carrier due to its low volumetric energy density. In the present thesis study, two novel ammonia production systems are presented. The first experimental system is a lab scale electromagnetic induced ammonia synthesis reactor. The reactor is designed, built and tested under various conditions. The main findings of the fist experimental system are:

- The lab scale ammonia synthesis reactor produced ammonia at a rate of 1.2×10^{-10} mol/cm^2.s with voltage reduction of 1.258 V, while 49 mT is recorded by the EMF at an applied current density of 6.4 mA/cm^2 and equivalent Faraday efficiency of 5.4 %, respectively. The experimental tests on "with" EMF resulted in lower average potential and faster rate of reaction with an average potential of 1.2 V while the "without" EMF test recorded an average potential of 1.7 V. The results point to the likelihood that the EMF has better reaction rate.
- The electrochemical impedance spectroscopy results are related to the diffusion, electron transfer and ohmic resistance in the reactor. The calculated Rs parameter is 1.77 Ω. While increasing frequency it shows an increase in the impedance and phase angle increment.
- The chronopotentiometry test results show the overpotential at an applied current density of 1.82 mA/cm^2 required for nitrogen reduction in an alkaline electrolyte is increased by 370 mV. This enhancement of nitrogen reduction kinetics is due to the rise in electrode temperature and ionic conductivity of the electrolyte.

In addition, the second part of this thesis research is about a conceptually developed theoretical system which is an integrated energy system for power, steam and ammonia

production which is developed, analyzed and simulated through Aspen Plus and assessed thermodynamically through energy and exergy approaches. The system employs a novel ammonia production loop to potentially replace the conventional Haber-Bosch process by integrating an expander/turbine in the ammonia loop. The main findings of this novel integrated system are listed as follows:

- Then integrated energy system produces 2310 kmol/h of liquid ammonia and steam as useful outputs in addition to power generation.
- The exergy losses and consumptions in the processes of the CO shift conversion, CO_2 removal and methanation are insignificant because of the low-quality exergy.
- The overall exergy efficiency of the integrated system is 78 % while the ammonia production unit is 98 % efficient and the turbine exergy efficiency is 91 % under optimum operating conditions with a total power of 6600 kW
- The ammonia conversion rate attained by the integrated energy system is 38 %, respectively.

6.2 Recommendations for further work

This thesis study on ammonia synthesis in particular the first experimental system in which a lab scale ammonia synthesis reactor is developed and tested under various conditions in addition to the second theoretical system where a new integrated energy system for power, steam, and ammonia synthesis developed in Aspen Plus has highlighted a number of topics on which further work would be beneficial:

- There are number of areas for future research which are highlighted by the study of this thesis for the experimental system. These include further investigations of ammonia synthesis characteristics in the presence of an electromagnetic field. The ability to produce ammonia using AC power rather than DC power should be investigated. This would help confirm and quantify ammonia synthesis capacity under electromagnetic induction.
- The level of uncertainty associated with the experimental system for ammonia production might be further investigated using addition data such of human error, and light effect on the electromagnetic spectrum and ammonia synthesis. This would additionally benefit in minimizing and controlling the method of synthesizing ammonia.

- The capacity of ammonia produced is performed in a small reactor vessel. The data obtained from the experimental part could be usefully applied in a large reactor. This would give a better understanding of overall performance of the reactor and ammonia synthesis.
- An exergoeconomic analysis, life cycle assessment and scale-up study of chemical reactor should be conducted in conjunction with the studies on the environmental sustainability of ammonia synthesis and the feasibility of the system.
- This thesis study in particular the second theoretical integrated energy system has investigated the implications of the integrated expander in the ammonia loop. This has demonstrated the importance of extracting heat in the ammonia loop where the conversion rate is important. Similar approaches might be taken to demonstrate how ammonia can be produced a lower pressure and temperature which is significant for industrial ammonia production plants.
- The approach used in the second part of the thesis where the theoretical integrated energy system is developed and simulated in Aspen Plus might be usefully applied in the field of optimization. The objective function of the optimization analysis for the integrated ammonia loop should lower the pressure and increase the power produced by the expander. This will give a correlation in ammonia synthesis with low pressure and how much power can be generated by the expander unit.

REFERENCES

1. Dincer I. 2002. The role of exergy in energy policy making. *Energy Policy*. 30:137–149.
2. Sadorsky P. 2014. The Effect of Urbanization and Industrialization on Energy Use in Emerging Economies: Implications for Sustainable Development. *Am. J. Econ. Sociol.* 73:392–409.
3. Dincer I, Ezzat MF. 2018. 3.6 Geothermal Energy Production. *Compr. Energy Syst.* Elsevier, pp 252–303.
4. Dincer I, Ozcan H. 2018. 1.17 Geothermal Energy. *Compr. Energy Syst.* Elsevier, pp 702–732.
5. Dincer I, Rosen MA, Khalid F. 2018. 3.8 Ocean (Marine) Energy Production. *Compr. Energy Syst.* Elsevier, pp 335–379.
6. Acar C, Dincer I. 2018. 1.30 Future Energy Directions. *Compr. Energy Syst.* Elsevier, pp 1199–1214.
7. Islam S, Dincer I. 2018. 4.1 The Role of Energy Conversion. *Compr. Energy Syst.* Elsevier, pp 1–39.
8. Dincer I, Ezzat MF. 2018. 3.4 Renewable Energy Production. *Compr. Energy Syst.* Elsevier, pp 126–207.
9. Dincer I. 2002. Technical, environmental and exergetic aspects of hydrogen energy systems. *Int. J. Hydrogen Energy*. 27:265–285.
10. Orhan MF, Dincer I, Rosen MA. 2009. Efficiency analysis of a hybrid copper–chlorine (Cu–Cl) cycle for nuclear-based hydrogen production. *Chem. Eng. J.* 155:132–137.
11. Dincer I, Balta MT. 2011. Potential thermochemical and hybrid cycles for nuclear-based hydrogen production. *Int. J. Energy Res.* 35:123–137.
12. Bicer Y, Dincer I, Zamfirescu C. 2016. A holistic approach to thermodynamic analysis of photo-thermo-electrical processes in a photovoltaic cell. *Energy Convers. Manag.* 123:218–231.
13. Naterer GF, Dinçer I, Zamfirescu C. 2013. *Hydrogen production from nuclear energy*. Springer.
14. Dincer I, Zamfirescu C. 2012. Sustainable hydrogen production options and the role of IAHE. *Int. J. Hydrogen Energy*. 37:16266–16286.
15. Acar C, Ghosh S, Dincer I, Zamfirescu C. 2015. Evaluation of a new continuous type hybrid photo-electrochemical system. *Int. J. Hydrogen Energy*. 40:11112–11124.
16. Acar C, Dincer I, Zamfirescu C. 2014. A review on selected heterogeneous photocatalysts for hydrogen production. *Int. J. Energy Res.* 38:1903–1920.
17. Potential Roles of Ammonia in a Hydrogen Economy. Available from https://www.hydrogen.energy.gov/pdfs/nh3_paper.pdf.
18. U.S. Department of Energy Potential Roles of Ammonia in a Hydrogen Economy A Study of Issues Related to the Use Ammonia for On-Board Vehicular Hydrogen Storage 2006.
19. Bicer Y. 2017. Investigation of Novel Ammonia Production Options Using Photoelectrochemical Hydrogen.
20. Smith A., Klosek J. 2001. A review of air separation technologies and their integration with energy conversion processes. *Fuel Process. Technol.* 70:115–134.

21. Rosen MA. 1991. Thermodynamic investigation of hydrogen production by steam-methane reforming. *Int. J. Hydrogen Energy*. 16:207–217.
22. Hammerli M. 1984. When will electrolytic hydrogen become competitive? *Int. J. Hydrogen Energy*. 9:25–51.
23. Siddiqui O, Dincer I. 2017. Analysis and performance assessment of a new solar-based multigeneration system integrated with ammonia fuel cell and solid oxide fuel cell-gas turbine combined cycle. *J. Power Sources*. 370:138–154.
24. Liu C, Sakimoto KK, Colón BC, Silver PA, Nocera DG. 2017. Ambient nitrogen reduction cycle using a hybrid inorganic–biological system. *Proc. Natl. Acad. Sci.* 114:6450–6455.
25. Heidlage MG, Kezar EA, Snow KC, Pfromm PH. 2017. Thermochemical Synthesis of Ammonia and Syngas from Natural Gas at Atmospheric Pressure. *Ind. Eng. Chem. Res.* 56:14014–14024.
26. EFMA. 2000. Production of Ammonia. *Best available Tech. Pollut. Prev. Control Eur. Fertil. Ind.*:158–194.
27. Coulson JM, Richardosn JF, Sinnott RK. 2005. Chemical Engineering.:2011–2014.
28. Bicer Y, Chehade G, Dincer I. 2017. Experimental investigation of various copper oxide electrodeposition conditions on photoelectrochemical hydrogen production. *Int. J. Hydrogen Energy*.:1–12.
29. Bicer Y, Dincer I, Zamfirescu C, Vezina G, Raso F. 2016. Comparative life cycle assessment of various ammonia production methods. *J. Clean. Prod.* 135:1379–1395.
30. Casallas C, Dincer I. 2017. Assessment of an integrated solar hydrogen system for electrochemical synthesis of ammonia. *Int. J. Hydrogen Energy*. 42:21495–21500.
31. Chen C, Lovegrove KM, Sepulveda A, Lavine AS. 2018. Design and optimization of an ammonia synthesis system for ammonia-based solar thermochemical energy storage. *Sol. Energy*. 159:992–1002.
32. Bastidas DM, Tao S, Irvine JTS. 2006. A symmetrical solid oxide fuel cell demonstrating redox stable perovskite electrodes. *J. Mater. Chem.* 16:1603.
33. Yuan Mengyao. *Managing Energy in Fertilizer Production and Use*. Available from http://large.stanford.edu/courses/2014/ph240/yuan2/.
34. Dincer I, Zamfirescu C. 2016. *Sustainable hydrogen production*. Elsevier.
35. Lan R, Irvine JTS, Tao S. 2013. Synthesis of ammonia directly from air and water at ambient temperature and pressure. *Sci. Rep.* 3:1145.
36. Vasileiou E, Kyriakou V, Garagounis I, Vourros A, Manerbino A, Coors WG, Stoukides M. 2016. Electrochemical enhancement of ammonia synthesis in a BaZr0.7Ce0.2Y0.1O2.9 solid electrolyte cell. *Solid State Ionics*. 288:357–362.
37. Zhao X, Jia H, Kim J, Wang P. 2009. Kinetic limitations of a bioelectrochemical electrode using carbon nanotube-attached glucose oxidase for biofuel cells. *Biotechnol. Bioeng.* 104:1068–1074.
38. Price CP, James DR. 1988. Analytical Reviews in Clinical Biochemistry: The Measurement of Urate. *Ann. Clin. Biochem. An Int. J. Biochem. Lab. Med.* 25:484–498.
39. Mateo C, Palomo JM, Fernandez-Lorente G, Guisan JM, Fernandez-Lafuente R. 2007. Improvement of enzyme activity, stability and selectivity via immobilization techniques. *Enzyme Microb. Technol.* 40:1451–1463.

40. Serge Cosnier, Marc Fontecave, Danièle Limosin and, Nivièr V. 1997. A Poly(amphiphilic pyrrole)−Flavin Reductase Electrode for Amperometric Determination of Flavins.
41. Clark DS. 1994. Can immobilization be exploited to modify enzyme activity? *Trends Biotechnol.* 12:439–443.
42. Krajewska B. 2004. Application of chitin- and chitosan-based materials for enzyme immobilizations: a review. *Enzyme Microb. Technol.* 35:126–139.
43. Paschkewitz TM. 2012. Ammonia Production at Ambient Temperature and Pressure: An Electrochemical and Biological Approach. *PhD (Doctor Philos. thesis*.. Available from http://ir.uiowa.edu/etd/4893.
44. Hinnemann B, Nørskov JK. Catalysis by enzymes: the biological ammonia synthesis.
45. P. Avenier,1 M. Taoufik,A. Lesage,2 X. Solans-Monfort,3 A. Baudouin A de M. 2007. Dinitrogen Dissociation on an Isolated Surface Tantalum Atom. *Sience AAAS*. 1.
46. Schomburg D (Dietmar), Stephan D (Dörte). 1994. *Enzyme handbook. Class 1.13-1.97, Oxidoreductases*. Springer-Verlag.
47. Kumar S, Wittmann C, Heinzle E. 2004. Minibioreactors. *Biotechnol. Lett.* 26:1–10.
48. Arechederra R, Minteer SD. 2008. Organelle-based biofuel cells: Immobilized mitochondria on carbon paper electrodes. *Electrochim. Acta*. 53:6698–6703.
49. Klotzbach TL, Watt M, Ansari Y, Minteer SD. 2008. Improving the microenvironment for enzyme immobilization at electrodes by hydrophobically modifying chitosan and Nafion® polymers. *J. Memb. Sci.* 311:81–88.
50. Lan R, Alkhazmi KA, Amar IA, Tao S. 2014. Synthesis of ammonia directly from wet air at intermediate temperature. *Appl. Catal. B Environ.* 152–153:212–217.
51. Modak JM. 2002. Haber process for ammonia synthesis. *Resonance*. 7:69–77.
52. Kandemir T, Schuster ME, Senyshyn A, Behrens M, Schlögl R. 2013. The Haber-Bosch Process Revisited: On the Real Structure and Stability of “Ammonia Iron” under Working Conditions. *Angew. Chemie Int. Ed.* 52:12723–12726.
53. Binous H, Aheed A, Hossain MM. 2016. Haber process and steam-coal gasification: Two standard thermodynamic problems elucidated using two distinct approaches. *Comput. Appl. Eng. Educ.* 24:58–70.
54. Huberty MS, Wagner AL, McCormick A, Cussler E. 2012. Ammonia absorption at haber process conditions. *AIChE J.* 58:3526–3532.
55. Modak JM. 2011. Haber process for ammonia synthesis. *Resonance*. 16:1159–1167.
56. Amar IA, Petit CTG, Zhang L, Lan R, Skabara PJ, Tao S. 2011. Electrochemical synthesis of ammonia based on doped-ceria-carbonate composite electrolyte and perovskite cathode. *Solid State Ionics*. 201:94–100.
57. Casallas C, Dincer I. 2017. Assessment of an integrated solar hydrogen system for electrochemical synthesis of ammonia. *Int. J. Hydrogen Energy*. 42:21495–21500.
58. Bicer Y, Dincer I, Vezina G, Raso F. 2017. Impact Assessment and Environmental Evaluation of Various Ammonia Production Processes. *Environ. Manage.* 59:842–855.
59. Bicer Y, Dincer I. 2017. Life cycle assessment of nuclear-based hydrogen and ammonia production options: A comparative evaluation. *Int. J. Hydrogen Energy*.

42:21559–21570.
60. Bicer Y, Dincer I. 2017. Performance assessment of electrochemical ammonia synthesis using photoelectrochemically produced hydrogen. *Int. J. Energy Res.* 41:1987–2000.
61. Bicer Y, Chehade G, Dincer I. 2017. Experimental investigation of various copper oxide electrodeposition conditions on photoelectrochemical hydrogen production. *Int. J. Hydrogen Energy*. 42:6490–6501.
62. Licht S, Cui B, Wang B, Li F-F, Lau J, Liu S. 2014. Ammonia synthesis by N2 and steam electrolysis in molten hydroxide suspensions of nanoscale Fe2O3. *Science (80-.).* 345:637–640.
63. Li F-F, Licht S. 2014. Advances in Understanding the Mechanism and Improved Stability of the Synthesis of Ammonia from Air and Water in Hydroxide Suspensions of Nanoscale Fe_2O_3. *Inorg. Chem.* 53:10042–10044.
64. Kim K, Yoo C-Y, Kim J-N, Yoon HC, Han J-I. 2016. Electrochemical synthesis of ammonia from water and nitrogen catalyzed by nano-Fe2O3 and CoFe2O4 suspended in a molten LiCl-KCl-CsCl electrolyte. *Korean J. Chem. Eng.* 33:1777–1780.
65. Tsuyoshi Murakami, Tokujiro Nishikiori, Toshiyuki Nohira and, Ito* Y. 2002. Electrolytic Synthesis of Ammonia in Molten Salts under Atmospheric Pressure.
66. Murakami T, Nohira T, Ogata YH, Ito Y. 2005. Electrolytic Ammonia Synthesis in Molten Salts under Atmospheric Pressure Using Methane as a Hydrogen Source. *Electrochem. Solid-State Lett.* 8:D12.
67. Murakami T, Nohira T, Ogata YH, Ito Y. 2005. Electrochemical Synthesis of Ammonia and Coproduction of Metal Sulfides from Hydrogen Sulfide and Nitrogen under Atmospheric Pressure. *J. Electrochem. Soc.* 152:D109.
68. Murakami T, Nishikiori T, Nohira T, Ito Y. 2005. Electrolytic Ammonia Synthesis from Hydrogen Chloride and Nitrogen Gases with Simultaneous Recovery of Chlorine under Atmospheric Pressure. *Electrochem. Solid-State Lett.* 8:D19.
69. Casallas C, Dincer I. 2017. Assessment of an integrated solar hydrogen system for electrochemical synthesis of ammonia. *Int. J. Hydrogen Energy*. 42:21495–21500.
70. Amar IA, Lan R, Petit CTG, Arrighi V, Tao S. 2011. Electrochemical synthesis of ammonia based on a carbonate-oxide composite electrolyte. *Solid State Ionics*. 182:133–138.
71. Amar IA, Lan R, Petit CTG, Tao S. 2015. Electrochemical Synthesis of Ammonia Based on Co3Mo3N Catalyst and LiAlO2–(Li,Na,K)2CO3 Composite Electrolyte. *Electrocatalysis*. 6:286–294.
72. Amar IA, Petit CTG, Zhang L, Lan R, Skabara PJ, Tao S. 2011. Electrochemical synthesis of ammonia based on doped-ceria-carbonate composite electrolyte and perovskite cathode. *Solid State Ionics*. 201:94–100.
73. Amar IA, Petit CTG, Mann G, Lan R, Skabara PJ, Tao S. 2014. Electrochemical synthesis of ammonia from N2 and H2O based on (Li,Na,K)2CO3–Ce0.8Gd0.18Ca0.02O2−δ composite electrolyte and CoFe2O4 cathode. *Int. J. Hydrogen Energy*. 39:4322–4330.
74. Amar IA, Petit CTG, Lan R, Mann G, Tao S. 2014. Electrochemical synthesis of ammonia from wet nitrogen using $La_{0.6}Sr_{0.4}FeO_{3-\delta}$–$Ce_{0.8}Gd_{0.18}Ca_{0.02}O_{2-\delta}$ composite cathode. *RSC Adv.* 4:18749–18754.

75. Lan R, Irvine JTS, Tao S. 2013. Synthesis of ammonia directly from air and water at ambient temperature and pressure. *Sci. Rep.* 3:1145.
76. ZHANG Z, ZHONG Z, LIU R. 2010. Cathode catalysis performance of SmBaCuMO5+δ (M=Fe, Co, Ni) in ammonia synthesis. *J. Rare Earths*. 28:556–559.
77. Renner JN, Greenlee LF, Ayres KE, Herring AM. 2015. Electrochemical Synthesis of Ammonia: A Low Pressure, Low Temperature Approach. *Interface Mag.* 24:51–57.
78. Liu R, Xu G. 2010. Comparison of Electrochemical Synthesis of Ammonia by Using Sulfonated Polysulfone and Nafion Membrane with $Sm_{1.5}Sr_{0.5}NiO_4$. *Chinese J. Chem.* 28:139–142.
79. Xu G, Liu R, Wang J. 2009. Electrochemical synthesis of ammonia using a cell with a Nafion membrane and SmFe0.7Cu0.3−x Ni x O3 (x = 0−0.3) cathode at atmospheric pressure and lower temperature. *Sci. China Ser. B Chem.* 52:1171–1175.
80. Skodra A, Stoukides M. 2009. Electrocatalytic synthesis of ammonia from steam and nitrogen at atmospheric pressure. *Solid State Ionics*. 180:1332–1336.
81. Kordali V, Kyriacou G, Lambrou C. 2000. Electrochemical synthesis of ammonia at atmospheric pressure and low temperature in a solid polymer electrolyte cell. *Chem. Commun.*:1673–1674. doi:10.1039/b004885m.
82. Lan R, Irvine JTS, Tao S. 2013. Synthesis of ammonia directly from air and water at ambient temperature and pressure. *Sci. Rep.* 3:1145.
83. Li Z, Liu R, Wang J, Xu Z, Xie Y, Wang B. 2007. Preparation of double-doped $BaCeO_3$ and its application in the synthesis of ammonia at atmospheric pressure. *Sci. Technol. Adv. Mater.* 8:566–570.
84. Guilin Ma , Feng Zhang, Jianli Zhu and, MengG. 2006. Proton Conduction in La0.9Sr0.1Ga0.8Mg0.2O3-α.
85. Xie Y-H, Wang J-D, Liu R-Q, Su X-T, Sun Z-P, Li Z-J. 2004. Preparation of La1.9Ca0.1Zr2O6.95 with pyrochlore structure and its application in synthesis of ammonia at atmospheric pressure. *Solid State Ionics*. 168:117–121.
86. Zhang F, Yang Q, Pan B, Xu R, Wang H, Ma G. 2007. Proton conduction in La0.9Sr0.1Ga0.8Mg0.2O3−α ceramic prepared via microemulsion method and its application in ammonia synthesis at atmospheric pressure. *Mater. Lett.* 61:4144–4148.
87. Li Z, Liu R, Xie Y, Feng S, Wang J. 2005. A novel method for preparation of doped Ba3(Ca1.18Nb1.82)O9−δ: Application to ammonia synthesis at atmospheric pressure. *Solid State Ionics*. 176:1063–1066.
88. Marnellos G. 1998. Ammonia Synthesis at Atmospheric Pressure. *Science (80-.).* 282:98–100.
89. Wang WB, Liu JW, Li YD, Wang HT, Zhang F, Ma GL. 2010. Microstructures and proton conduction behaviors of Dy-doped BaCeO3 ceramics at intermediate temperature. *Solid State Ionics*. 181:667–671.
90. Liu J, Li Y, Wang W, Wang H, Zhang F, Ma G. 2010. Proton conduction at intermediate temperature and its application in ammonia synthesis at atmospheric pressure of BaCe1−x Ca x O3−α. *J. Mater. Sci.* 45:5860–5864.
91. Chen C-H, Chang S-J, Chang S-P, Li M-J, Chen I-C, Hsueh T-J, Hsu C-L. 2009.

Novel fabrication of UV photodetector based on ZnO nanowire/p-GaN heterojunction. *Chem. Phys. Lett.* 476:69–72.
92. Wang H, Liu M, Kong H, Hao Y. 2018. Thermodynamic Analysis on Mid/low Temperature Solar Methane Steam Reforming with Hydrogen Permeation Membrane Reactors. *Appl. Therm. Eng.*
93. Flórez-Orrego D, de Oliveira Junior S. 2017. Modeling and optimization of an industrial ammonia synthesis unit: An exergy approach. *Energy*. 137:234–250.
94. García-Martín J, Gómez-Gil J, Vázquez-Sánchez E. 2011. Non-Destructive Techniques Based on Eddy Current Testing. *Sensors*. 11:2525–2565.
95. Forest F, Laboure E, Costa F, Gaspard JY. 2000. Principle of a multi-load/single converter system for low power induction heating. *IEEE Trans. Power Electron.* 15:223–230.
96. Principle of high frequency induction heater-Induction Heating Equipment,induction brazing machine. Available from https://www.dw-inductionheating.com/Technology/Principle-of-high-frequency-induction-heater-484.html.
97. Zero Voltage Switching Resonant Power Conversion.mAvailable from http://www.ti.com/lit/ml/slup089/slup089.pdf.
98. Gamry Reference 3000 Potentiostat/Galvanostat/ZRA. Available from https://www.gamry.com/potentiostats/reference-3000/.
99. NI-9203 - National Instruments. Available from http://www.ni.com/en-ca/support/model.ni-9203.html.
100. Thermocouples Probes with Miniature Connectors. Available from https://www.omega.com/pptst/JMQSS.html.
101. Pressure Relief Valves | McMaster-Carr. nAvailable from https://www.mcmaster.com/#pressure-relief-valves/=1dbyffs.
102. Mantle-Minder™ II, Automatic Temperature Controller, Glas-Col® | VWR. Available from https://us.vwr.com/store/product/4563183/mantle-minder-ii-automatic-temperature-controller-glas-col.
103. Corning® pH/ISE/mV/T meters Model 450, AC/DC input 120 V AC | Sigma-Aldrich. Available from https://www.sigmaaldrich.com/catalog/product/aldrich/z283096?lang=en&region=US.
104. Small, fixed-mounted USB infrared camera: optris PI160. [cited 17 June 2018]. Available from https://www.optris.com/thermal-imager-pi160.
105. Standard Methods for the Examination of Water and Wastewater. Available from https://www.mwa.co.th/download/file_upload/SMWW_4000-6000.pdf.
106. Dincer I, Rosen MA. 2013. Chemical Exergy. *Exergy*. Elsevier, pp 31–49.
107. Alatiqi IM, Meziou AM, Gasmelseed GA. 1989. Static and Dynamic Simulation of Steam Methane Reformers., pp 535–550.
108. Dincer I, Zamfirescu C. 2014. Energy, Environment, and Sustainable Development. *Adv. Power Gener. Syst.* Elsevier, pp 55–93.
109. Sehested J, Dahl S, Jacobsen J, Rostrup-Nielsen JR. 2005. Methanation of CO over Nickel: Mechanism and Kinetics at High H_2 /CO Ratios †. *J. Phys. Chem. B.* 109:2432–2438.
110. Bonalumi D, Lillia S, Valenti G, Fosbøl PL, Thomsen K. 2017. Kinetic study of a

Layout for the Carbon Capture with Aqueous Ammonia without Salt Precipitation. *Energy Procedia*. 114:1352–1359.
111. Coker AK. 2001. *Modeling of Chemical Kinetics and Reactor Design*. *Technology*. 13.
112. Ukpaka, Izonowei. 2017. International Scientific Orgnization. *Chem. Int.* 3:46–57.